

UNIVERSITAT POLITÈCNICA DE VALÈNCIA

DOCTORADO EN INGENIERÍA Y PRODUCCIÓN INDUSTRIAL



UNIVERSITAT
POLITÈCNICA
DE VALÈNCIA

DOCTORAL DISSERTATION

“Halloysite nanotubes/hydroxyapatite nanocomposites as hard tissue substitutes: effect on the morphology, thermomechanical behavior and biological development of aliphatic polyesters and polymethacrylates”

Author:

Elena Torres Roca

Thesis directed by:

Prof. Ana Vallés Luch

Ph.D. Vicent Fombuena Borrás

June 2019

UNIVERSITAT POLITÈCNICA DE VALÈNCIA

DOCTORADO EN INGENIERÍA Y PRODUCCIÓN INDUSTRIAL



UNIVERSITAT
POLITÈCNICA
DE VALÈNCIA

DOCTORAL DISSERTATION

“Halloysite nanotubes/hydroxyapatite nanocomposites as hard tissue substitutes: effect on the morphology, thermomechanical behavior and biological development of aliphatic polyesters and polymethacrylates”

Elena Torres Roca

AGRADECIMIENTOS

En primer lugar, quiero agradecer el esfuerzo y la ilusión transmitida por mi directora de tesis Ana Vallés, quien arrojó un rayito de luz cuando parecía estar todo perdido y me transmitió confianza para no tirar la toalla. Gran defensora de las causas perdidas y de la investigación como filosofía de vida, se ha convertido en mi referente tanto en la vida profesional como en la personal. En segundo lugar, agradecer el esfuerzo de mi co-director de tesis Vicent Fombuena, quien desde el principio ha estado ahí apoyándome y contagiándome de optimismo, aunque la situación no fuese la más idónea.

A su vez, agradezco la oportunidad que me brindó el profesor Tim Oswald y el profesor Lih-Sheng Turng al poder realizar parte de mi trabajo experimental en el laboratorio BIONATES Universidad de Wisconsin, Madison. Durante esta etapa en UW Madison he aprendido a trabajar con completa autonomía, con la ayuda de Tom Elingham y Brett Napiwocki quienes me han acompañado tanto en el laboratorio como fuera de él. Esta etapa me ha transformado y me ha hecho crecer, definiéndome como la persona que soy hoy en día.

Agradezco sobre todo los mensajes de ánimos transmitidos por mi familia, en especial a mi madre que aun estando a 7.000 Km de distancia me hacía sentir como en casa. Las llamadas de Skype de mis hermanas Ana e Irene durante mi larga estancia en el extranjero, que fortaleció nuestra relación aún si poder abrazarnos. Y, por último, y no menos importante, a mi padre, quien siempre ha estado presente tanto en los momentos fáciles como en los difíciles, y quien me ha transmitido ese sentimiento de superación que provoca que todo aquello que me proponga lo haga desde el corazón.

Con la culminación de este trabajo se cierra un capítulo de mi vida que me ha moldeado y definido como persona y como trabajadora, amante de la ciencia y de la investigación.

*Haz de tu vida un sueño y
de tu sueño una realidad*

ABSTRACT

“Haloysite nanotubes/hydroxyapatite nanocomposites as hard tissue substitutes: effect on the morphology, thermomechanical behavior and biological development of aliphatic polyesters and polymethacrylates”

Bone pathology entails physical disability to a large extent, bone tissue regeneration being therefore one of the most actively researched fields in Tissue Engineering. Accordingly, large efforts are focused on the research of novel bioabsorbable materials as prostheses with stiffness values similar to that of the host tissue capable of fulfilling the requirements for bone fracture remodelling. This work is focused on studying mechanical properties and cell interaction as a function of the chemical structure and hydrophobicity of different bioabsorbable polymers compared with non-absorbable polymers, all of them proposed for the regeneration of hard tissues. Hydroxyapatite (HA) and Haloysite nanotubes (HNTs) were used as fillers in order to improve better cell attachment, proliferation and differentiation along with hydrophobicity behaviour.

For this end, it was aimed to firstly monitor the effects of bioactive fillers on the structural properties of bioabsorbable polycaprolactone (PCL). Thus, mechanical and thermal properties of PCL were studied by modifying the additivation percentage of the bioactive fillers HA and HNTs. This preliminary study allowed to understand the synergistic effect among the polymeric matrix and the functional groups present on the additives chemical structure by establishing the additivation threshold and optimizing the additivation rate. In general terms, a noticeable improvement of mechanical properties was achieved with the simultaneous addition of the two fillers. Additionally, taking advantage of the HNTs nano-tubular shape, those were studied as drug carrier structures and their loading and release ability with curcumin was monitored.

Knowing on the one side that HA promotes the formation of a layer of new bone composed of biological apatite and collagen, and in the other side, that HA and HNTs alter hydrophobicity behaviour, morphological properties supplied by both fillers were studied and compared on different pairs of polymers with similar chemical natures but different hydrophobicity. Accordingly, the hydrophobic polyester PCL was modified by its blending with polylactic acid (PLA) and combined with HA nanoparticles and HNTs. On

the other hand, the hydrophilic poly(2-hydroxyethyl methacrylate) (PHEMA) was copolymerized with ethyl methacrylate (EMA) and also combined with HA and HNTs.

Thus, the effect of both fillers on Hydroxyapatite nucleation, distribution of the fillers into the polymeric matrices and PCL/PLA degradation rate was studied. Therefore, it was observed that introduction of HA in polymers with moderately hydrophilic character induces a higher rate of hydroxyapatite nucleation and a faster degradation rate. However, HNTs tend to form large aggregates when the hydrophilic character increases, driving to crack initiation sites and failure of the material.

The completion of this study was accomplished by means of monitoring cell viability, proliferation, and morphology on the two pairs of polymers varying the polymer's chemical surface by blending hydrophilic and hydrophobic polymers, copolymerizing monomers of opposite nature, and/or loading the polymer matrix with nanoparticles such as HA or HNTs. Polymer surface wettability is known to affect cell attachment and can be enhanced by modifying the polymer with HA and HNTs. In this way, improvement in cell viability with the addition of HA and HNTs was observed due to the generation of new reactive sites with Ca^{2+} and PO_4^{3-} groups present in HA, and silanol groups (Si-OH) located at the surfaces of HNTs. Thus, it was concluded that on hydrophobic materials, due to a faster arrival rate of proteins, those compete for surface absorption driving to low interaction sites between cells and polymer surface showing a round shape. However, on hydrophilic materials, the highly solvated surface at initial stage limits protein arrival and allowed protein rearrangement and spreading over the surface promoting cell adhesion and proliferation with better cytoskeleton spreading.

RESUMEN

“Nanocompuestos de nanotubos de haloisita/hidroxiapatita como sustitutos de tejidos duros: efecto en la morfología, comportamiento termomecánico y desarrollo biológico de poliésteres alifáticos y polimetacrilatos”

Las patologías óseas provocan en gran medida discapacidad física, siendo la regeneración de tejidos vivos uno de los campos más avanzados en Ingeniería de Tejidos. Consecuentemente, se focalizan grandes esfuerzos en el estudio de nuevos materiales bioabsorbibles para tratar remodelaciones de fracturas óseas. Es por ello que este trabajo se centra en estudiar las propiedades mecánicas y la interacción de las células en función de la hidrofobicidad y la química de diferentes polímeros bioabsorbibles comparados con polímeros no-bioabsorbibles, todos ellos comúnmente utilizados en la regeneración de tejidos óseos. Por otro lado, se utilizaron cargas como Hidroxiapatita (HA) y Nanotubos de Haloisita (HNTs) para mejorar la afinidad, interacción y proliferación de células junto con el comportamiento hidrófobo de los materiales.

Para ello, inicialmente se monitorizó el efecto de las cargas inorgánicas en las propiedades estructurales del polímero bioabsorbible policaprolactona (PCL). Por lo tanto, se estudiaron las variaciones de propiedades térmicas y mecánicas de la PCL provocadas por la adición de HA y HNTs. Este estudio preliminar permitió entender el efecto sinérgico entre el polímero y los grupos funcionales de las cargas inorgánicas, estableciendo el umbral de carga y optimizando la ratio de aditivación. En términos generales, se observó una mejora de las propiedades mecánicas cuando las dos cargas se utilizan simultáneamente. Asimismo, aprovechando la forma tubular de los HNTs, estos fueron utilizados como portadores de fármacos, estudiándose su capacidad de ser cargados con curcumina y su habilidad para liberarla después en un ambiente fisiológico.

Conociendo por una parte la habilidad del HA de promover la formación de hueso nuevo compuesto por apatita y colágeno, y, por otra parte, que la HA y los HNTs alteran el comportamiento hidrofóbico de los polímeros, se estudiaron los cambios morfológicos provocados por la adición de HA y HNTs en dos familias de polímeros con químicas similares pero diferente hidrofobicidad. Por consiguiente, el poliéster hidrofóbico PCL se mezcló con ácido poliláctico (PLA) y se combinó con nanopartículas de HA y HNTs. Por

otra parte, el altamente hidrofóbico poli(etil metacrilato) (EMA) se copolimerizó con 2-hidroxietil metacrilato (HEMA) y se aditivó con HA y HNTs. Por lo tanto, se estudió la dispersión de cargas inorgánicas en las matrices poliméricas, además de la formación de hidroxiapatita en la superficie del polímero, y la velocidad de degradación del PCL/PLA. Se observó que la introducción de HA en polímeros con carácter hidrófilo induce la nucleación de hidroxiapatita y la degradación de los polímeros bioabsorbibles. Sin embargo, los HNTs tienden a formar grandes agregados cuando el carácter hidrófilo del polímero aumenta, dando lugar a puntos de inicio de grietas y fallo del material.

La culminación de este estudio se alcanzó mediante la monitorización de la viabilidad celular, proliferación y morfología celular como efecto de la superficie química de los polímeros. La hidrofobicidad de la superficie del polímero afecta a la interacción de las células y esta se puede mejorar mediante la modificación del polímero con HA y HNTs. De ese modo, la mejora de la viabilidad celular con la adición de las dos cargas inorgánicas es inducida por la generación de nuevos centros reactivos de Ca^{2+} y PO_4^{3-} presentes en la HA, y los grupos silanol (Si-OH) situados en la superficie de los HNTs. Así, se observó que, en superficies hidrófobas, debido a la más fácil adsorción de proteínas, estas compiten por el espacio dando lugar a interacciones pobres entre células y polímero mostrando una geometría celular redondeada. Sin embargo, en superficies más hidrófilas, al hallarse altamente solvatadas, las proteínas inicialmente encuentran mayor dificultad para llegar a la superficie, y con ello disponen de mayor espacio para organizarse y anclarse a la superficie, dando lugar a una mayor adhesión y proliferación de las células con una mejor organización del citoesqueleto.

RESUM

“Nanocompòsits de nanotubs haloisites/hidroxiapatites com a substituents del teixit dur: efecte sobre la morfologia, comportament termomecànic i desenvolupament biològic de polièsters i polimetacrilats alifàtics”

Les patologies òssies provoquen en gran mesura discapacitat física, sent la regeneració de teixits vius un dels camps més avançats en Enginyeria de Teixits. Per consegüent, es focalitzen grans esforços en l'estudi de nous materials bioabsorbibles per a tractar remodelacions de fractures òssies. És per això que aquest treball es focalitza a estudiar les propietats mecàniques i la interacció de les cèl·lules en funció de la hidrofobicitat i la química de diferents polímers bioabsorbibles comparats amb polímers no-absorbibles, tots ells comunament utilitzats en la regeneració de teixits ossis. D'altra banda, càrregues com Hidroxiapatita (HA) i Nano-tubs d'Hal·loisita (HNTs) es van utilitzar per a millorar l'afinitat, interacció i proliferació de cèl·lules junt amb el comportament hidrofòbic dels materials.

Per aquest motiu, inicialment es va monitoritzar l'efecte de les càrregues inorgàniques amb les propietats estructurals del polímer bioabsorbible policaprolactona (PCL). Per tant, es van estudiar les variacions de propietats tèrmiques i mecàniques de PCL provocades per l'addició de HA i HNTs. Aquest estudi preliminar va permetre entendre l'efecte sinèrgic entre el polímer i els grups funcionals de les càrregues inorgàniques, establint el límit de càrrega i optimitzant la ràtio d'aditivació. En termes generals, es va observar una millora de les propietats mecàniques quan les dues càrregues s'utilitzen simultàniament. Així mateix, aprofitant la forma tubular dels HNTs, aquests van ser utilitzats com a portadors de fàrmacs, estudiant la seva habilitat per a ser carregats amb cúrcuma i la seva habilitat per a alliberar-la en un ambient fisiològic.

Coneixent d'una banda l'habilitat de l'HA de promoure la formació d'os nou compost per apatita i col·lagen, i, d'altra banda, que l'HA i els HNTs alteren el comportament hidrofòbic dels polímers, es van estudiar els canvis morfològics provocats per l'addició de HA i HNTs en dues famílies de polímers amb químiques semblants però diferent hidrofobicitat. Per consegüent, el polièster hidrofòbic PCL es va mesclar amb àcid polilàctic (PLA) i es va combinar amb nanopartícules de HA i HNTs. D'altra banda, l'altament hidrofòbic poli (etil metacrilat (PEMA) és va copolimeritzar amb 2-hidroxietil metacrilat (HEMA) i s'aditivà amb HA i HNTs. A continuació, la dispersió de càrregues

inorgàniques en les matrius polimèrica va ser estudiada, a més de la formació d'hidroxiapatita en la superfície del polímer, i la velocitat de degradació del PCL/PLA. Es va observar que la introducció de HA en polímers amb caràcter hidrofílic induïx la nucleació de hidroxiapatita i la degradació dels polímers bioabsorbibles. No obstant això, els HNTs tendeixen a formar grans agregats quan el caràcter hidrofílic del polímer augmenta, donant lloc a punts d'inici de clavills i fallada del material.

La culminació d'aquest estudi es va aconseguir per mitjà del monitoratge de la viabilitat cel·lular, proliferació i morfologia de les cèl·lules com a efecte de la superfície química dels polímers. La hidrofobicitat de la superfície del polímer afecta la interacció de les cèl·lules i aquesta es pot millorar per mitjà de la modificació del polímer amb HA i HNTs. D'aquesta manera, l'increment de la viabilitat cel·lular amb l'addició de les dues càrregues inorgàniques és induït per la generació de nous centres reactius de Ca^{2+} i PO_4^{3-} presents en l'HA, i els grups silanol (Si-OH) situats en la superfície dels HNTs. Per tant, es va observar que en superfícies hidrofòbiques, a causa d'un alt grau d'arribada de proteïnes, aquestes competeixen per l'espai donant lloc a interaccions pobres entre cèl·lules i polímer mostrant una geometria cel·lular arrodonida. No obstant això, en superfícies hidròfiles, al trobar-se altament solvatades, les proteïnes inicialment troben més dificultat per a arribar a la superfície, i amb això disposen de major espai per a organitzar-se i ancorar-se a la superfície, donant lloc a una major adhesió i proliferació de les cèl·lules amb una millor organització del citoesquelet.

CONTENTS

ABBREVIATIONS AND TERMS.....	19
1 INTRODUCTION.....	21
1.1 Tissue Engineering.....	23
1.1.1 Bone tissue regeneration.....	24
1.2 Aliphatic polyesters.....	27
1.2.1 PCL: Poly(ϵ -caprolactone).....	28
1.2.2 PLA: Poly(lactic acid).....	29
1.2.3 PCL/PLA copolymers.....	31
1.2.4 PGA: Polyglycolic acid.....	31
1.2.5 PHAs: Polyhydroxyalkanoates (PHB, PHBV, P4HB, PHBHHx, PHO).....	32
1.3 Biodegradation of aliphatic polyesters.....	33
1.3.1 Biodegradation process for aliphatic polyesters [71].....	33
1.3.2 Biodegradation rate of PCL, PLA and PGA.....	35
1.3.3 Inflammatory response of polyesters.....	37
1.4 Polymethacrylates.....	39
1.4.1 Inflammatory response of polymethacrylates.....	39
1.5 Bioactive composites.....	40
1.5.1 Hydroxyapatite (HA).....	40
1.5.2 Halloysite nanotubes (HNTs).....	43
1.5.3 Curcumin.....	45
2 OBJECTIVES.....	47
3 EXPERIMENTAL SECTION.....	51
3.1 First chapter – Study of the improvement of PCL thermal and mechanical properties through the addition of HA and HNTs.....	53
3.1.1 Preparation of the PCL-based hybrids.....	53
3.1.2 Thermal characterization.....	55
3.1.3 Mechanical characterization.....	58
3.1.4 Optimization of the HNTs loading with curcumin.....	59
3.1.5 Curcumin delivery rate.....	61

3.2	Second chapter - Study of the influence of the addition of HA and HNTs on the morphological properties of PCL- and PHEMA-based polymers	62
3.2.1	PCL/PLA-based hybrid samples.....	62
3.2.2	PHEMA and P(HEMA-co-EMA)-based hybrids.....	63
3.2.3	Structural properties	64
3.2.4	Hydroxyapatite nucleation	65
3.2.5	Degradation of PCL and PCL/PLA based hybrids.....	66
3.3	Third chapter - Influence of the hydrophobic–hydrophilic nature of PCL- and PHEMA-based polymers and their nanocomposites on their <i>in vitro</i> biological development.....	66
3.3.1	Contact Angle Measurements	68
3.3.2	Cell Viability and Morphology	69
3.3.3	Organization of Cell Cytoskeleton	71
4	RESULTS AND DISCUSSION.....	73
4.1	First chapter – Study of the improvement of PCL thermal and mechanical properties through the addition of HA and HNTs.....	75
4.1.1	Thermal characterization	75
4.1.2	Mechanical characterization	80
4.1.3	General observations: Improvement of PCL mechanical properties with HA and HNTs 89	
4.1.4	Optimization of the HNTs loading with curcumin.....	91
4.1.5	Curcumin delivery rate.....	96
4.1.6	General Observations: Loading HNTs with curcumin and delivery rate.....	97
4.2	Second chapter - Study of the influence of the addition of HA and HNTs on the morphological properties of PCL- and PHEMA-based polymers	99
4.2.1	Structural properties	99
4.2.2	Hydroxyapatite nucleation	101
4.2.3	Degradation of PCL and PCL/PLA based hybrids.....	111
4.2.4	General observations: Influence of the addition of HA and HNTs on the morphological properties of PCL- and PHEMA-based polymers	114
4.3	Third chapter - Influence of the hydrophobic–hydrophilic nature of PCL- and PHEMA-based polymers and their nanocomposites on their <i>in vitro</i> biological development.....	115
4.3.1	Contact Angle Measurements	115
4.3.2	Cell Viability and Morphology	116
4.3.3	Organization of Cell Cytoskeleton	120

4.3.4	General observations for cell interaction influenced by the hydrophobic–hydrophilic nature	124
5	CONCLUSIONS.....	131
5.1	First chapter – Study of the improvement of PCL thermal and mechanical properties through the addition of HA and HNTs	133
5.2	Second chapter - Study of the influence of the addition of HA and HNTs on the morphological properties of PCL- and PHEMA-based polymers	134
5.3	Third chapter - Influence of the hydrophobic–hydrophilic nature of PCL- and PHEMA-based polymers and their nanocomposites on their <i>in vitro</i> biological development.....	135
6	LIST OF CONTRIBUTIONS.....	137
7	FIGURE CAPTIONS	141
8	TABLE CAPTIONS.....	145
9	REFERENCES.....	149

ABBREVIATIONS AND TERMS.

Adenosine Triphosphate	(ATP)
Average Value	(\bar{X})
Copolymers of 3-Hydroxybutyrate and 3-Hydroxyhexanoate	(PHBHH _x)
Crystallization Temperature	(T _c)
D,L-Lactide	(PDLLA)
Decomposition Temperature	(T _d)
Differential Scanning Calorimetry	(DSC)
D-Lactide	(PDLA)
Dulbecco's Phosphate Buffered Saline	(DPBS)
Dynamic Mechanical Analysis	(DMA)
Dynamic Mechanical Thermal Analyses	(DMTA)
Energy-Dispersive X-Ray Spectroscopy	(EDS)
Enthalpy	(ΔH)
Ethyl Methacrylate	(EMA)
Ethyldiaminotetra Acetic Acid	(EDTA)
Ethylene Glycol Dimethacrylate	(EGDMA)
Glass Transition Temperature	(T _g)
Halloysite Nanotubes	(HNTS)
Heat Adsorbed per Mass Unit	(Δh_m)
Heat Deflection Temperature Tests	(HDT)
Hydroxyapatite	(HA)
Hydroxyl-2-Ethyl Methacrylate	(HEMA)
L-Lactide	(PLLA)

Melting Temperature	(T _m)
Phosphate Buffered Saline	(PBS)
Poly 4-Hydroxybutyrate	(P ₄ HB)
3-Hydroxybutyrate And 3-Hydroxyvalerate	(PHBV)
Poly(2-Hydroxyethyl Methacrylate)	(PHEMA)
Poly(2-Hydroxyethyl Methacrylate) and Ethyl Methacrylate blend	P(HEMA-Co-EMA)
Poly(Dioxanone)	(PDO)
Poly(Lactic Acid)	(PLA)
Poly(Lactic-Co-Glycolic Acid)	(PLGA)
Poly(ϵ -Caprolactone)	(PCL)
Polyglycolic Acid	(PGA)
Polyhydroxyalkanoates	(PHAS)
Polyhydroxybutyrate	(PHB)
Polyhydroxyoctanoate	(PHO)
Scanning Electron Microscopy	(SEM)
Simulated Body Fluid	(SBF)
Softening Point	(T _{vicat})
Standard Deviation	(s)
Stereocomplex	(Scpla)
Storage Modulus	(G')
Temperature at the Melting Onset	(T _{Onset})
Temperature at the Peak Maximum	(T _{mPeak})
Thermogravimetric Analysis	(TGA)
Maximum Stress	(Σ max)
Water Contact Angles	(WCA)

1 Introduction

1.1 Tissue Engineering

Tissue Engineering was defined in 2009 by D.F. Williams as “*the creation of new tissue for the therapeutic reconstruction of the human body, by the deliberate and controlled stimulation of selected target cells through a systematic combination of molecular and mechanical signals*” [1]. Tissue Engineering has been exploring new methods to treat or replace missing or malfunctioning human tissues and organs through biomaterials-based scaffolds. Scaffolds are usually engineered to drive cell growth and proliferation and provide shape to the creation of the new tissue and facilitate the delivery of those molecular and mechanical signals.

Biomaterial is a term which involves different connotations since it could either imply something derived from life or something used to the benefit of life. Therefore, it is very important to state a valid definition. The first attempt to define the concept “Biomaterial” was not until the Consensus Conference on Definitions in Biomaterials Science, in 1987 of the European Society for Biomaterials. Biomaterial was defined as “*a non-viable material used in a medical device, intended to interact with biological systems*” [2] being debated overtime and finally accepted in 1999 as “*a material intended to interface with biological systems to evaluate, treat, augment or replace any tissue, organ or function of the body*” considering the scope of the definition in the field of health care [1]. Up to now, biomaterials have been widely used in skin [3, 4], cartilage [5] bone [6, 7] tendons [8] vessels [9, 10] nerves [11], bladder [12] and liver [13] tissue engineering. Among all the biomaterials used for Tissue Engineering, polymers are the dominant scaffolding materials [14] due to their special characteristics, comprising a great processing flexibility and biodegradability, which enable to meet the required structural designs [15]. However, different issues should be taken in consideration when engineering a polymeric scaffold. Material selection is a key factor, since it should satisfy the following criteria [16]:

- Biocompatibility, capability of being integrated in the organism without immune response, cytotoxic or genotoxic effects.
- Biodegradability/bioabsorbability with a controllable degradation and resorption rate to match cell/tissue growth in *vitro/vivo*.
- Suitable surface chemistry and hydrophobicity for cell attachment, proliferation, and differentiation [17].

- Three-dimensional and highly porous structure with an interconnected porous network for cell growth, flow transport of nutrients, and metabolic wastes.
- It should mimic mechanical properties to match the tissues at the site of implantation [18].

1.1.1 Bone tissue regeneration

Bone tissue regeneration is one of the most actively researched fields in Tissue Engineering, because of the critical functions of the involved tissues in the daily life [19]. Recently, bone implant materials have been described by Ikada [20], Meyer [21] and Barrere [22] as materials which, besides the characteristics mentioned above, should have the following properties:

- **Osteoinductivity:** process whereby mesenchymal stem cells are stimulated by the chemical environment to differentiate into pre-osteoblasts, driving to the acceleration of new bone formation.
- **Osteoconductivity:** the growth of bony tissue into the structure of an implant or graft. This process should be coupled with the biodegradability rate because the scaffold material should be absorbed to provide space to the new tissue while mechanical properties are maintained.

When talking about bone regeneration, there are certain aspects that determine whether metal prostheses, autologous bone grafts or biopolymers should be used in each particular case, as discussed below:

Metal prostheses

Bone pathology entails an important average of physical disability; metal prostheses, plates and screws are often used for long term applications with no need of being bioabsorbable. Defective bone often needs to be surgically removed and replaced by a graft or scaffold in order to restore the bone functionality [23]. Considering that bone implants were originally designed to support mechanical effort of the injured bone while healing, materials used for these applications include metallic materials, such as stainless steel and titanium alloys. However, the use of bioabsorbable polymers acting as a prostheses, scaffolds, plates and screws is increasing. Metal prostheses have the

advantage of being biocompatible and highly resistant to break; nevertheless, they present numerous disadvantages:

- are heavy and expensive,
- are neither biodegradable nor bioabsorbable,
- do not promote bone regeneration,
- impose a second surgical intervention to remove the device once the fractured bone is healed, entailing higher costs, extended recuperation processes and promotion of infections,
- induce shielding effect: this effect is caused by large load stress supported by the prosthesis instead of the bone, inducing a poor bone regeneration with a decrease in bone mass and an increase in bone porosity (bone atrophy) [24].

For the purpose of obtaining a desirable tissue remodelling and avoid the shield effect, the design of bioabsorbable prostheses with stiffness values similar to that of the host tissue appears to be the best option. Thus, development of economic low-modulus biodegradable polymers will prevent the aforementioned drawbacks presented by metal prostheses.

Autologous bone graft

The autologous bone graft is the most popular treatment currently used. The bone graft is harvested from the patient's own body, usually from the iliac crest, the fibula, the ribs, the mandible and sometimes from parts of the skull. However, it implies several drawbacks compared with other techniques [25]:

- Need of additional surgery to harvest the patient's bone to obtain the graft, entailing increased surgery times.
- Donor site morbidity and greater scar formation.
- High probability of pain, infection and bleeding increasing probability of donor-site morbidity at the harvesting site [26].
- Limitation on quantity and geometry of the harvested bone.

- Low reproducibility of the patient's feature due to the challenge of precise tailoring of the graft's shape.

A study review of the effects after cranioplasty comparing autologous bone graft with synthetic materials was developed in 2015 using the medical records of 100 cranioplasty patients cases from Turku University Hospital during the period of 2002-2012 [27]. The authors observed that the healing process for re-implanted autografts was complicated in 60% of the cases, and 40% of the patients needed removal of the implanted autograft after cranioplasty. Those results were in consistency with more recent publications [28, 29]. On the other hand, patients with cranioplasty using synthetic materials shown fewer complications and the best outcomes compared with autografts. Following the observations of that review, nowadays, the interest for developing bioactive implants with porous structures with the ability of accelerating bone ingrowth is increasing. The general advantages of using biomaterials include no donor-site morbidity, shortening of operation time, hence shortening of hospital stay.

Biopolymers

Biopolymers have been intensively studied to replace both metal prostheses as well as autologous bone grafts. As an example, some authors have tested poly(ϵ -caprolactone) (PCL) composites as internal fixation systems, such as Lowry *et al.* [30], whose results revealed a higher strength for PCL/bone complex compared with bony humerus healed with a stainless-steel implant. As such, craniofacial repair fixations appear to be a plausible application for PCL, as it has also been studied by Rudd and co-workers for the last decade [31-35]. *In-vivo* studies using poly(lactic acid) (PLA) as plates and screw were also performed by Bos *et al.* [36], who monitored the mandibular bone regeneration of six dogs. Kaan C. *et al.* [37] also followed bone fracture remodelling of twenty-two patients, reporting satisfactory results for PLA plates and screws. Boeree *et al.* [38] studied the efficiency of Polyhydroxybutirate (PHB) injected moulded composites to be used in orthopaedic surgery obtaining good results. Biopolymers are preferable over metal prostheses because they make possible to partly avoid second surgery to remove the metal prosthesis once the fractured bone is healed, which prolongates the recovery process and eventual infections, corrosion and metal toxicity [39]. The shield effect is also suppressed because stiffness values of the scaffold are similar to those of the host tissues [40, 41], resulting in a desirable tissue remodelling.

On the other hand, biopolymers are also preferable over autologous bone grafts since donor bone is not needed, additional surgeries and co-morbidities are eliminated [25],

and rates of infections and implant rejection are lower [27]. All these facts imply shortening of hospital stay; hence, economizing the public health system. Bioabsorbable aliphatic polyesters are the most commonly studied biopolymers for this purpose, e.g., poly(ϵ -caprolactone) (PCL) [40, 41], poly(lactic acid) (PLA) [42], and polyglycolic acid (PGA) [43] due to their low cost, high reproducibility, and good resistance to physical aging and biological attacks. Osteogenic biopolymers offer the virtue of easy processability to achieve a desired geometry. In addition, osteogenic biopolymers also offer the possibility of controlling their physicochemical properties to mimic and accelerate the native tissue remodelling by serving as graft to guide the infiltration of host cells while the biopolymer is reabsorbed by the body. These biopolymers allow the *in vitro* evaluation of the effects of cell-seeding density, culture period and mineralization, demonstrating the feasibility of modulating osteogenesis [44].

It is for these reasons that this work is focused on studying mechanical properties and cell interaction as a function of the chemical structure and hydrophobicity of different bioabsorbable polymers compared with non-absorbable polymers, all of them proposed for the regeneration of hard tissues. For this purpose, the hydrophobic polyester PCL is modified by blending with the more hydrophilic PLA, and the hydrophilic acrylate poly(2-hydroxyethyl methacrylate) (PHEMA) is copolymerized with its hydrophobic counterpart ethyl methacrylate (EMA) at a ratio of 50/50 wt.%. Neat resins (PCL, PLA, PCL/PLA, HEMA, EMA and P(HEMA-co-EMA)) have been used as a control material, and resins combined with hydroxyapatite (HA) nanoparticles and halloysite nanotubes (HNTs) have been studied to enhance cell attachment and mechanical properties [17].

1.2 Aliphatic polyesters

Aliphatic polyesters are a category of polymers that contain the ester functional group in their main chain, providing properties such as biodegradability and biocompatibility. The degradation process of aliphatic polyesters prevents the accumulation of degraded products in the body, reducing the risk of long-term toxicity. Among all the polymers used in Tissue Engineering, PCL, PLA, PHB, PGA, poly(lactic-co-glycolic acid) (PLGA), and poly(dioxanone)s (PDO) are the most studied. Among them, PCL, PLA, PGA, and PHB (Figure 1) are the most used due to their easy processability into tissue engineered scaffolds, and their properties tunability regarding crystallinity, thermal transitions, mechanical strength, through alteration of its molecular weight, or addition of substituents to the polymer backbones [19, 45]. In general, polymers can be biodegraded via

hydrolysis or selective enzymes; however, enzymes are codified to specially attack a specific polymer and are present only if the right cells are present. Consequently, in the early 1960s, PGA was the first artificial degradable polymer developed as suturing material due to the fact that it does not require an enzyme to be degraded in the human body [46].

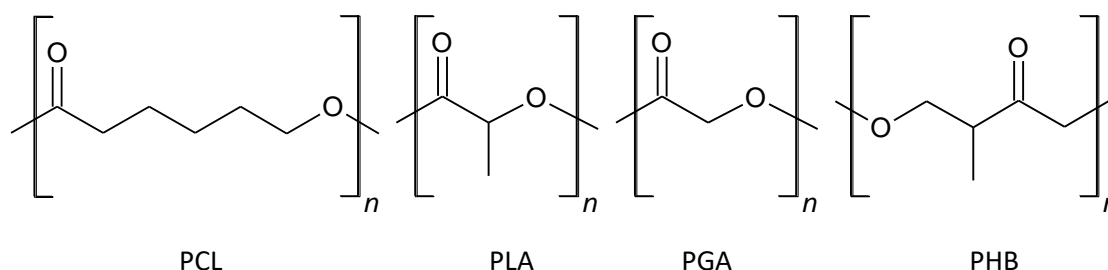
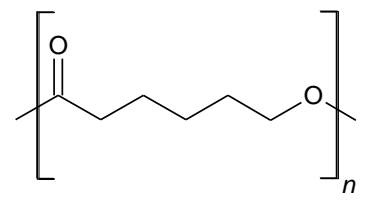


Figure 1 Aliphatic polyesters typically used in Tissue Engineering.

Although this study is focused on PCL, PLA and PCL/PLA blends due to their biocompatibility, biodegradability, low infection rate and their common use as scaffold and fixation elements for hard tissues regeneration, it seems interesting at this point to introduce the characteristics of the most important bio-absorbable polymers of the polyester family. In such a way, PCL, PLA, PGA and PHB are briefly explained in the following section.

1.2.1 PCL: Poly(ϵ -caprolactone)

Table 1 PCL thermal, mechanical properties and degradation rate.

	Tg (°C)	Tm (°C)	Tensile strength (MPa)	Degradation rate	Cost (€/Kg)
	-60	60	23.30±1.39	> 50 weeks (1 year)	7,60
	[39]	[39]	[39]	[47]	

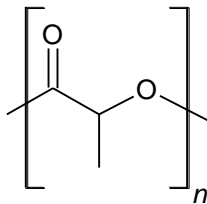
Tg (°C): Glass transition temperature
Tm (°C): Melting temperature

In the early 1930s PCL was synthesized by the Carothers group (DuPont) [48] and became commercialized because of its biodegradability. PCL can be obtained through ring-opening polymerization of ϵ -caprolactone or via free-radical ring-opening polymerization of 2-methylen-1-3dioxepane [49]. PCL is a biopolymer approved by the

US Food and Drug Administration extensively used for drug delivery devices due to its good bio-resorbability, slow degradation rate, cellular biocompatibility, and non-immunogenicity [49]. Accordingly, studies are focused on the use of this biopolymer as a Tissue Engineering scaffold and internal fixation systems. However, its low mechanical properties limit its use; thus, an appropriate addition of fillers or blends to the polymeric matrix could provide an adequate mechanical stiffness to resist *in vivo* stresses and prevent new-tissue deformation [50].

1.2.2 PLA: Poly(lactic acid)

Table 2 PLA thermal, mechanical properties and degradation rate.

	Tg (°C)	Tm (°C)	Tensile strength (MPa)	Degradation rate	Cost (€/Kg)
		55–65	160–170	40	12 months (1 year)
	[51]	[51]	[52]	[53]	-

Tg (°C): Glass transition temperature

Tm (°C): Melting temperature

PLA is a bio-polymer derived 100% from renewable sources [54, 55], which was discovered in 1932 by Carothers (DuPont). Because of its biodegradability, biocompatibility, and non-toxicity, PLA has been approved by the US Food and Drug Administration and is extensively used in biomedical applications. Ring-opening polymerization can result in three stereoisomers of L D-lactide (PDLA), L-lactide (PLLA) (Figure 2) and racemic mixture of D,L-lactide (PDLLA), giving the building block of PLA units isotactic, syndiotactic or atactic/heterotactic PLA primary structures (Figure 3). The stereoisomers PDLA and PLLA present enhanced physical and thermal properties, as well as hydrolytic stability compared with the parent polymers [56].

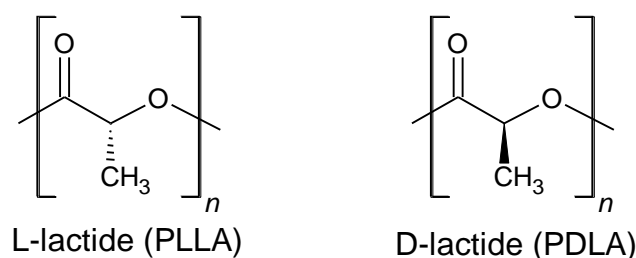


Figure 2 PLA stereoisomers: L-lactide (PLLA) on the left and D-lactide (PDLA) on the right.

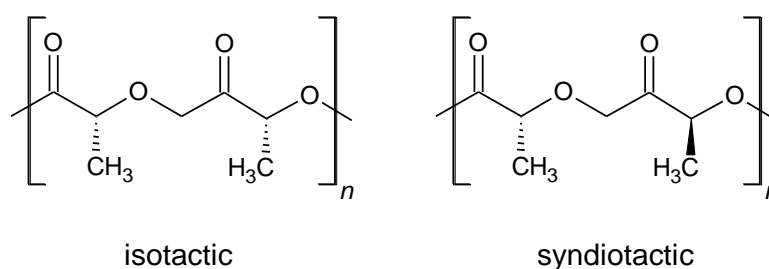


Figure 3 PLA Tacticity. Relative stereochemistry of adjacent PLA chiral centres.

The mechanical properties of PLA depend on the polymer enantiomeric purity, the stereospecificity, and the molecular packing, which will drive to a high crystallinity. Generally, the vast majority of the commercial amorphous PLA is a mixture of L and D lactic copolymers, due to the synthesis process usually leading to impurities. PLA stereocomplex (scPLA), prepared by the equimolecular mixture of PLLA and PDLA (1:1), has been recently studied because of its improved mechanical and thermal properties, rising 60°C its melt temperature. The improvement of scPLA properties is ascribed to the formation of a stereoregular crystal lattice with van der Waals interactions between L-lactic unit sequences and D-lactic units [57].

Table 3 Crystallinity, elongation and thermal properties of the different PLA stereoisomers.

Polymer	Crystallinity (%)	T _m (°C)	T _g (°C)	T (VICAT) (°C)	elongation at break (%)
PLLA	Semi-crystalline 45% [51]	160-180	55-65°C	55-65°C	3-5%
PDLA	Semi-crystalline 37% [51]	170°C	55°C	60-70°C	50-200%
PDLLA	Amorphous	160–170°C	55–65 °C	50-70°C	9%
scPLA	Semi-crystalline 67%	220-230°C	60°C	190°C	3-5%

T_g (°C): Glass transition temperature
T_m (°C): Melting temperature
T (VICAT) (°C): Softening point

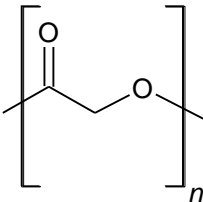
1.2.3 PCL/PLA copolymers

PLA is a rigid polymer with good mechanical properties with its brittleness as the main drawback. On the other hand, PCL is a very flexible polymer with a slow degradation rate. Upon mixing PLA and PCL, a synergic effect leads to retain the merits of each polymer, making the mixture more flexible, hydrophobic, and crystalline compared to neat PLA, which is translated into a slower degradation ratio (ranging from months to years) [58]. The PCL crosslinking factor (crystallinity) limits chains mobility; thus, it decreases the degradation velocity due to the difficult accessibility for the enzymes inside the polymer matrix. The modification on hydrophobicity, inferred by the mixture of both polymers, strongly improves the bioactivity of the blend [17]. Since both polymers are immiscible, PCL/PLA blends have attracted less attention than PCL/PLA copolymers. Although blends prepared through solvent evaporation showed smaller phase separation but worse mechanical properties [59]. and lower crystalline structure because the extrusion process comprises a slow cooling enabling the formation of crystalline regions [59]. PCL/PLA 1:1wt ratio was chosen to proceed with this experimental with the aim of transferring the highest mechanical properties to the PCL without losing its intrinsic characteristics. Therefore, PCL/PLA blends will exhibit the following desired properties:

- Improvement of PCL mechanical properties due to the high mechanical properties of PLA.
- To infer hydrophilic character to the PCL/PLA matrix due to the hydrophilic character of PLA, which will enhance cell attachment and proliferation.
- Accelerate the degradation process of PCL due to the amorphous and hydrophilic character of PLA.

1.2.4 PGA: Polyglycolic acid

Table 4 PGA thermal, mechanical properties and degradation rate.

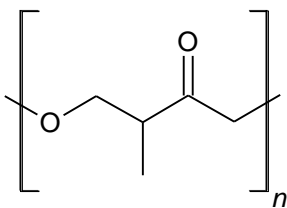
	Tg (°C)	Tm (°C)	Tensile strength (MPa)	Degradation rate
	35-40	225-230	340–920 (fibre)	6 weeks
	[60]	[60]	[61]	[62]

Tg (°C): Glass transition temperature
Tm (°C): Melting temperature

PGA was one of the initial, degradable polymers researched for biomedical application, first synthesized in 1954 [63]. PGA has been commercially available since 1970 [63] and the American Cyanamid Co developed in 1962 the first synthetic absorbable suture of PGA under the name of Dexon [63]. However, its sensitivity to hydrolysis and fast biodegradation rate made it difficult to be used compared with other synthetic polymers. PGA can be obtained through both, polycondensation or ring-opening polymerization of the monomer [63]. PGA is approved by the U.S. Food and Drug Administration for human clinical applications. PGA has high crystallinity because of its chain-structural regularity, it degrades rapidly in aqueous solutions and loses its mechanical integrity between 2 and 4 weeks, depending on the molecular weight.

1.2.5 PHAs: Polyhydroxyalkanoates (PHB, PHBV, P4HB, PHBHHx, PHO)

Table 5 PHB thermal, mechanical properties and degradation rate.

	Tg (°C)	Tm (°C)	tensile strength (MPa)	Degradation rate	Cost (€/Kg)
	2	175	37,5	24-30 months	19,70
	[64]	[64]	[64]	[65]	

Tg (°C): Glass transition temperature
Tm (°C): Melting temperature

Polyhydroxyalkanoates (PHAs) are a family of biodegradable polyesters produced by microorganisms through bacterial fermentation of sugar or lipids. PHAs are semicrystalline bioabsorbable polyesters with excellent biocompatibility and viability. About 150 different congeners of PHAs have been reported [66] and can be combined to obtain several copolymers of polyhydroxyalkanoates, including poly 3-hydroxybutyrate (PHB), copolymers of 3-hydroxybutyrate and 3-hydroxyvalerate (PHBV), poly 4-hydroxybutyrate (P4HB), copolymers of 3-hydroxybutyrate and 3-hydroxyhexanoate (PHBHHx) and polyhydroxyoctanoate (PHO). PHA was first discovered by Lemoigne in *Bacillus megaterium* in the form of poly (3-hydroxybutyrate) (PHB) in 1925 [52]. PHAs can be classified according their chain length: short (scl), with less than 5 carbon atoms,

medium (mcl), between 5-14 carbon atoms, or long (lcl), with more than 14 carbon atoms, but are uncommon [67].

Among all the mentioned PHAs, PHB has attracted the attention for applications in biomedical areas, such as in the production of scaffolds for Tissue Engineering due to its biocompatibility and biodegradability [68]. PHB bio-resorption shows long degradation times [69], displaying slower rates compared with other biodegradable biomaterials.. Although polymers obtained from renewable sources have advantage over conventional petroleum-based polymers, the principal drawback associated to PHB is its high cost production process through fermentation, dependent on high cost carbon sources [67].

1.3 Biodegradation of aliphatic polyesters

Biomedical polymers, especially those introduced above, after implantation or when in contact with biological fluids undergo significant changes regarding mechanical properties influenced by their degradation process. Considering that 75% of the human body is composed by water, 65% of which is located within cells, hydrolytic degradation of aliphatic polyesters is an interesting feature for Tissue Engineering materials. Bone remodelling field implies time-limited applications, which requires the elimination of the biopolymer after use to restore the surrounding living medium. It is important to differentiate the terms biodegradation and bioresorption. Biodegradation entails biological agents that cause the chemical breakdown of the implanted material, while bioresorption entails removal of polymer degradation products by cellular activity through metabolic processes or natural pathways in a biological environment. Thus, aliphatic polyesters able to biodegrade and bioresorb show the highest potential for replacing biostable polymers, such as polyacrylates, in time-limited applications [70].

1.3.1 Biodegradation process for aliphatic polyesters [71]

Biodegradation of aliphatic polyesters in aqueous medium, both *in vitro* and *in vivo*, occurs through disintegration of the polymer chain in small polymeric segments, which are consequently bioresorbed, thus reintegrated into the carbon cycle by assimilation and mineralisation in the media. Biodegradation entails three main stages:

1. **Deterioration**

Water molecules penetrate into the polymer matrix, attacking first the amorphous phase, and the hydrolytic cleavage of ester bonds and carbonate groups start generating

carboxylic acid end groups, as schematized in Figure 4, which later induce autocatalysis [47, 72]. In the initial stages, the partially degraded macromolecules remain insoluble in the surrounding aqueous medium while the autocatalysis process continues. When the molecular weight of partially degraded macromolecules decreases (oligomers) to allow dissolution in the surrounding aqueous medium, the diffusion of these oligomers to the surface of the polymer starts [70]. The rates of degradation at the surface and the interior of the matrix depend on the combination of diffusion, chemical reaction, and dissolution phenomena of the polymeric matrix [73]. During the degradation of the amorphous phase, there is a decrease of molecular weight without loss of physical properties since the material matrix is supported by the crystal phase. Once the amorphous phase is consumed, the crystalline phase degradation begins. In porous systems, due to the higher surface area and easier release of soluble by-products, the degradation rate is slower compared with plain structures. The deterioration effect could proceed through bulk or surface erosion [74]. Thus, matter is lost without a relevant change in the molar mass.

Aliphatic polyesters degrade, roughly speaking, through a bulk hydrolysis process. Fragments are lost from the polymer mass by diffusion, which occurs faster than the cleavage of polymer bonds, and the molar mass decreases due to bond cleavage. Bulk degradation rate is enhanced by autocatalysis due to carboxylic acid end groups, as shown in Figure 4. However, there is some difference between PCL and PLA, because the CH_2/COO^- ratio is greater in the first, that is, is more hydrophobic, and thus, degradation is not purely a bulk one but some surface erosion occurs as well, due to hydrolysis of COO^- groups at the surface.

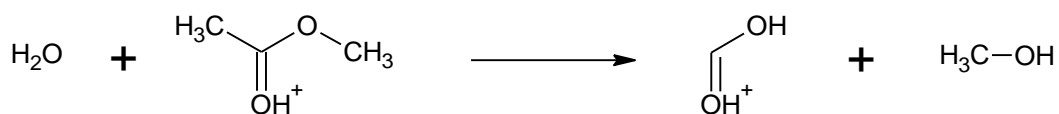


Figure 4 Hydrolytic cleavage of ester bonds generating carboxylic acid end groups.

2. Fragmentation

The fragmentation is a decomposition phenomenon leading to low molecular weight molecules [74] that will, subsequently, be assimilated into the surrounding environment through an electron transfer process.

3. Assimilation

The assimilation consists on the integration of atoms from the degraded polymer inside cells [75, 76]. Inside the cells, the integrated molecules are usually oxidised through catabolic pathways producing adenosine triphosphate (ATP), thus providing the necessary sources of energy for the formation of the cell structure.

1.3.2 Biodegradation rate of PCL, PLA and PGA

Biopolymers used as scaffolds for tissue engineering applications need to accomplish two significant challenges. First of all, the biodegradation process should be controlled. Secondly, the material should maintain its structural and mechanical properties to avoid malformation of the new regenerated bone while healing [77]. Biodegradation rate will be affected by hydrophobicity, crystallinity and acidity of the polymer.

As the amorphous phase is the first to be affected by the hydrolysis of ester bonds, it implies a loss in molecular weight without losing physical properties, since the material matrix is supported by the crystal phase [61]. Thus, the polymer crystallinity influences the degradation rate. Hydrophobicity also has an impact in the degradation rate. A lower water absorption capacity reduces the accessibility of water molecules and enzymes to the polymer bulk [78], fact that restricts the rate of chain scission. Acidity of the polymer influences degradation rate, as mentioned before, because hydrolysis of the remaining ester bonds is catalysed by carboxyl end groups formed after chain cleavage [79]. When soluble oligomeric compounds are generated in the matrix, those which are near the surface can escape before total degradation, while those located inside the matrix can hardly diffuse out of the matrix. Thus, the oligomer compounds released to the aqueous medium are neutralized by the phosphate buffered medium (pH= 7,4) in the case of an *in vitro* study, contributing to decrease the surface acidity. However, the entrapped oligomer molecules inside the polymer matrix catalyse hydrolysis of the neighbouring ester bonds, accelerating the degradation. Although degradation of polymers depends of several factors, it is reasonable to think that acid amorphous and hydrophilic polymers will degrade faster than basic crystalline polymers as shown in Table 6.

Table 6 Comparison among PCL, PLA, PGA and PHB polyesters regarding crystallinity, hydrophobicity and degradation rate.

Polymer	Crystallinity	Hydrophobicity	Degradation rate
PCL	50.4% [80]	hydrophobic	12-24 months [47]
PLA	Amorphous	moderately hydrophobic	12 months [53]
PGA	45-50%	hydrophilic	6 weeks [62]
PHB	highly crystalline 70% [65]		24-30 months [65]

Craniofacial fractures can demand implants to maintain their structural properties between 6 and 52 weeks [32]. Considering resorption kinetics and degradation, *in vivo* studies reported rates of PHA items from 2 to 2.5 years, possibly because of its high crystallinity (70%) [65]. However, due to its low biodegradable rate and expensive obtention process, PHB is uncommonly used in biomedical applications. On the other hand, although PCL shows a notable slow rate of resorption (>24 months) [45], it is resorbed faster than PHB, due to its lower crystallinity degree (50,4%) [80]. PCL is known to persist *in vivo* for more than one year [81, 82] fulfilling the implantation time requirement. PLA, being a moderately hydrophobic and amorphous polymer, remained intact for 6 weeks displaying a lower mechanical performance *in vivo* than PCL [83]. Much more hydrophilic PGA, though crystalline, loses practically all its strength within 6 weeks [62]. Thus, PGA biodegradation period is notably shorter than the 50 weeks exhibited by PCL, making PGA ineffective for fulfilling the requirements needed for treating craniofacial fractures.

In view of the aforementioned facts, the degradation rates decrease in the following order [61]:

PGA>PDLLA>PLLA>PCL>PHB

Aiming to investigate in this thesis the biodegradation and cell interaction on PCL surface when varying its hydrophobicity through blending with PLA and additivating it with HA and HNTs, special attention is placed herein on PCL and PLA degradation studies *in vitro* and *in vivo*. Pego *et al.* [47] studied the *in vitro* degradation of PCL copolymers (90

mol%) and loss of molecular weight over a 52-week period. The results confirmed that PCL copolymers retained a constant strength during the first 50 weeks (around one year) of degradation. However, the mechanical properties were affected during the second year, the values of stress (σ_{max}) decreasing linearly with the decrease of molecular weight. Congruent results were obtained by Kweon *et al.* [80], who analysed mass loss over a 6-week period. Hong Fan Sun *et al.* [78] studied the *in vivo* degradation of PCL in rats for 3 years, finding that PCL structures remained intact during 2-year implantation. However, after 30 months of implantation, they broke into low molecular weight pieces completely losing their mechanical strength. Hong Fan Sun also studied resorption of PCL, concluding that after 135 days 92% of the implanted PCL was excreted from feces and urine, avoiding the accumulation of PCL in body tissue. Results are in agreement with those of Pitt *et al.* [84], who also studied *in vivo* adsorption of PCL at cellular level and concluded that PCL was ingested and digested ultimately by phagocyte and giant cell. Pitt exposed that PCL degradation first involves a decrease in molecular weight without mass loss and deformation, and then the molecular weight drops producing a failure of the material into pieces driving a mass loss. PLA (mixture of L and D lactic copolymers) is an amorphous and moderately hydrophobic polymer due to its methyl groups [61], and needs at least 1 year for completely absorption [53]. However, ring-opening polymerization results in three stereoisomers with different crystallinities depending on the packing of the polymeric units. Thus, degradation takes longer for PLLA (45% of crystallinity), more specifically more than 5 years for total absorption [53].

1.3.3 Inflammatory response of polyesters

When selecting a biopolymer to be used in biomedicine as scaffolding material or internal fixation, the inflammatory response caused in the surrounding living tissue should be considered. When a material is implanted into living tissue, it induces foreign body reactions that take place at the interface between the biomaterial and the host tissue. Understanding the mechanism of biodegradation and the biodegraded products released to the physiological environment will help to design optimum scaffolding materials [85]. PCL, PLA PGA and PHB degradation products are non-toxic and usually metabolized and eliminated through natural pathways [86]; furthermore, the pH equal to 7.4 of phosphate buffer helps to solubilize the degradation by-products, as for example the carboxylate form RCOO^- of organic acids being more hydrophilic than the carboxylic acid form RCOOH [79]. Nonetheless, acidic degradation products and crystalline by-products released during PCL, PLA and PGA degradation can cause inflammatory response [61], as opposed to PHB, which keeps a neutral pH during degradation and hence a higher

tolerance of cells [69]. There are alternatives to minimize inflammation by stabilizing the pH of the environment surroundings. For example, incorporating basic compounds (such as bioactive glasses and calcium phosphates) to the polymeric matrix has been reported to minimize inflammatory reaction [61]. Breakdown products as lactide from PLA degradation, 6-hydroxyhexanoic acid from PCL degradation, and glycol from PGA degradation are excreted from the body by physiological processes (e.g., the Krebs cycle) [87, 88]. While some of them can induce a minimal inflammatory response, they do not induce cytotoxic effects [89, 90]. For instance, PCL degradation product (6-hydroxyhexanoic acid) is transformed by microsomal ω -oxidation to adipic acid, a natural occurring metabolite [91], or excreted through urine [78, 92].

PCL exhibits several advantages over PLA, PGA and PHB. Examining the inflammatory response, Lowry *et al.* [30] stated that the use of PGA and PLA induces a foreign body reaction that has not been seen with PCL implants. Lowry founded his observations on two studies carried out by Bostmant *et al.* [93] and Mannien *et al.* [94] who used PGA screws to maintain a transverse distal femoral osteomy in rabbits femur and self-reinforced PLLA rods to fix cortical femoral rabbit bone for reduction of a transverse osteotomy, respectively. Both studies show foreign-body reaction with the absorption of the PGA screw and occurrence of giant cells and foam cells on the surface of the PLLA rods, as well as around the connective tissue surrounding the rod. More recent studies support Lowry's suggestions [95, 96]. Ceonzo *et al.* [96] studied the inflammatory response following implantation of PGA, concluding that degraded PGA induced an acute peritonitis. Lowry's statements suggest that the use of PCL results in a lower inflammatory response. Gogolewski *et al.* [97] compared tissue response and polymer degradation of PLA and PHB implants in mice. Results showed that the number of inflammatory cells increased with the content of valerate units in the PHB within the three first months of implantation, however, PHB biodegraded products do not change the local pH of the surrounding area [98]. After six months of implantation, PHB degraded less (15%) than PLA. PHB is uncommonly used as biomedical fixation or scaffolds due to low degradation rate and its challenging and expensive purification for medical degree application [99].

Because PCL induces a lower inflammatory response and retains its mechanical properties for the desired amount of time compared to PLA, PGA and PHB; PCL was chosen herein to study mechanical properties and cell viability, proliferation, and surface morphology varying hydrophobicity and acidity of the compounds. To this end, PCL and

PCL/PLA blends were additivated with HA and HNTs and compared with non-biodegradable poly-methacrylate at the same conditions.

1.4 Polymethacrylates

This work aims to study aliphatic polyesters able to biodegrade in order to replace biostable polymers, such as polyacrylates, in time-limited applications [70]. Thus, cell interaction depending on chemical structure and hydrophobicity of different bio-absorbable polymers is compared with non-absorbable polymethacrylates. As non-absorbable polymethacrylate, the hydrophilic acrylate poly(2-hydroxyethyl methacrylate) (PHEMA) copolymerized with ethyl methacrylate (EMA) at a ratio of 50/50 wt.%. PHEMA and P(HEMA-co-EMA) will be used as neat resins or combined with HA nanoparticles and HNTs to enhance cell attachment and mechanical properties.

Crosslinked HEMA hydrogel was first synthesized by Wichterle and Lim in 1960 [100], and is one of the most studied synthetic hydrogels and commonly used in ophthalmic uses as contact lenses and drug delivery applications [101]. HEMA is considered of great importance because of its hydrophilic character and biocompatibility and is extensively used in Tissue Engineering. Hydrogels are hydrophilic polymer networks with the capability of absorbing from 10% to thousand times their dry weight in water. Some hydrogels can be degraded and consequently disintegrate and dissolved; however, HEMA and EMA are chemically stable. When crosslinked hydrogels are placed in aqueous solution, reach an equilibrium swelling which, together with permeability and hydrophilicity, depends mainly on the crosslink density. Water molecules attack the hydrogel surface penetrating into the polymer network and hydrate the most polar and hydrophilic groups. Water interactions produce an expansion of the network allowing other water molecules to penetrate within the hydrogel network. Thus, the swollen network exposes hydrophobic groups, which also interact with water molecules [101]. Hydrogels used in Tissue Engineering will be working in the aqueous physiological environment, thus may never be in their dry (xerogel) state.

1.4.1 Inflammatory response of polymethacrylates

Crosslinked PHEMA and PEMA, which have very similar chemical structures, have been chosen in this study to compare with aliphatic polyesters because of their demonstrated biocompatibility and non-toxicity [101]. However, PHEMA implants have shown inflammatory response in some cases, as for example in the work of Belkas *et al.* [102]

who synthesized poly(2-hydroxyethyl methacrylate-co-methyl methacrylate) (PHEMA-MMA) porous tubes and studied their efficacy *in vivo* in rat sciatic nerves. The study showed collapse of the tube's walls after 16 weeks of implantation and chronic inflammation. Results were in consistency with other authors such as Jeyanthi *et al.* [103], who implanted collagen-PHEMA hydrogels in rats, finding acute and then a chronic inflammatory response after 6 months; and Smetana *et al.* [104], who implanted PHEMA hydrogel in chinchilla rabbits and observed foreign body giant multinucleate cells on the implant surface after 6 months of implantation. Although PHEMA implants induce inflammatory response, no adverse tissue reactions were observed at the implant site, denoting good biocompatibility and non-toxicity of the implanted PHEMA matrix.

1.5 Bioactive composites

Generally, the biopolymers introduced in the previous section show poor mechanical properties, which do not meet the structural demands of the host tissue. Although they show good bioactivity, the new bone formed does not bond tightly to the polymer surface. This problem can be addressed by the introduction of bioceramics, which grant new functionalities such as higher bioactivity and enhancement of mechanical strength [105]. Thus, polymer/inorganic composites are a common practice reviewed intensively in the literature [61, 68]. Aiming to improve mechanical and biological properties of different polymeric matrices, as well as to study cell interaction as consequence of hydrophobicity modification, this study has focused on the use of hydroxyapatite (HA) and halloysite nanotubes (HNTs), both of which are well demonstrated biocompatible fillers [61, 106].

1.5.1 Hydroxyapatite (HA)

Apatite term was used for the first time to refer ores in 1788 by the German geologist William Alexander Deer [107], but the first attempt to establish the hydroxyapatite composition by chemical analysis began in the second half of the 18th century by the Swedish chemist Jöns Jacob Berzelius [108]. Currently, this term is referred to a crystal family of materials related to the formula $M_{10}(RO_4)_6X_2$, where M refers to calcium (Ca^{2+}), R to Phosphorus (PO_4^{3-}) and X to a hydroxide (OH^-) or another halogen compound such as fluorine (F^-). Hydroxyapatite (HA) is one of the most common and inexpensive fillers broadly used in Tissue Engineering field [109-111] due to its osteoconductive properties, low inflammatory response, and very low toxicity in humans [112, 113]. The biological properties exhibited by HA are based on the fact that the mineral phase of the human bone is composed principally (around 60 wt.%) of HA [114, 115], which was determined

in 1926 by X-ray diffraction technique exposing that it was apatite [116]. HA is an apatite composed essentially of phosphorous and calcium with the chemical formula $\text{Ca}_{10}(\text{PO}_4)_6(\text{OH})_2$. The atomic ratio CA/P is 1.67 with 39% by weight of Ca, 18.5% P and 3.38% of OH [117]. Although several materials have been designed as hydroxyapatite by diverse researchers, actually the Ca/P rate shown could be variable with a range of 1.3 to 2.0. Nevertheless, the American Society for Testing and Materials (1987) determined the reference patterns both for hydroxyapatite and tricalcium phosphates, in order to control and determine the purity of these compounds [116].

It is well known that introduction of HA to a polymer matrix induce apatite layer formation on the scaffold surface. The formed apatite layer is composed of nano-crystals of carbonate-ion with very similar characteristics of the mineral phase in bone, thus, cells proliferate and differentiate forming a layer of biological apatite and collagen [118]. The apatite deposition mechanism involves the extraction of Ca^{2+} ions out of the HA crystal by exchange with protons from the SBF solution. The increasing concentration of Ca^{2+} ions in the SBF medium accelerates the apatite precipitation [119]. Silanol groups Si-OH present in the HNTs would provide favourable sites for apatite nucleation; although this mechanism is not totally clear yet, it is speculated that electrostatic interactions drive the formation of calcium silicates [120]. With the precipitation of the Ca^{2+} ions the surface acquires a positive charge and interacts electrostatically with the negatively charged phosphate ions in the SBF, leading to the formation of an amorphous calcium phosphate. Once the apatite nuclei are formed, they grow spontaneously by consuming the calcium and phosphate ions from the SBF solution. Specific surface functional groups can act as effective sites for apatite nucleation even with Ca and P absent from the composition. Phosphate, carboxy, hydroxy and amine groups have been found to induce calcium phosphate nucleation [121, 122]. The introduction of HA to a polymer matrix has also been demonstrated to support enzyme activity [123] and improve cell attachment by generating new reactive sites where proteins can interact by electrostatic forces and hydrogen bonds [124]. These interactions are the result of Ca^{2+} and PO_4^{3-} groups present in HA and are available for binding respectively with negative carboxylate (COO^-) and positive amino groups (NH_3^+), present in the proteins structure [125-128]. After protein interaction on the scaffold surface, protein unfolds and spreads over the polymer; consequently, cells will interact with the unfold protein. It has been demonstrated that HA induce the differentiation of mesenchymal cells into osteoblasts, which accelerates bone formation [61, 129].

Besides its biological properties previously mentioned, the addition of a polymer matrix with HA is a common practice to achieve prostheses stiffness values similar to that of the host tissue, resulting in a desirable tissue remodelling [40, 41]. Considering the polymers studied in this work, different authors have observed both mechanical and biological improvement on biopolymers matrix. For example, Biqiong Chen and Kang Sun [130] studied reinforcement of PCL with different amounts of HA (0 wt.%, 20 wt.%, 40 wt.% and 60 wt.%) and correlated the improvement of mechanical properties with the added hydroxyapatite amount. The composite melting temperature (T_m) and crystallization temperature (T_c) increased by the presence of HA, suggesting slight interactions between PCL and HA, facilitating the crystallization of PCL under cooling, HA acting as nucleating agent. The study reported an enhancement of mechanical properties, reaching the greatest strength value when the concentration of HA was 20%. Nevertheless, when the content of HA increased over 20%, the strength of the compound decreased significantly. Results are in consistency with Heo *et al.* [131] who compared addition of nano-HA and micro-HA to the PCL matrix. Mechanical testing revealed an increase in the Young's modulus of the compound from 193 MPa of the neat PCL to 665 MPa with the addition of 50 wt.% of nano-HA to the PCL matrix. Heo also stated the growth of MSCs and guided their osteogenic differentiation on PCL/HA composites maintaining cell viability. Reviewing PLA bibliography, it was found that Hong *et al.* [132] prepared PLLA/HA composites as potential bone substitute material, and observed that at HA content of 4 wt.%, the composite showed a maximum in tensile strength (74 MPa). Zangh *et al.* [133] also reported greatly enhanced Young's modulus for nano-HA-PLLA nanocomposites, reaching values of 3,6 GPa at 20 wt.%. Regarding improvement of bioactivity, Hong [132], Ronca *et al.* [134] and Abdal *et al.* [135] observed higher cell ingrowth and proliferation of MC3T3 osteoblasts on PLA/HA scaffolds. Studies on PHB/HA composites suitable for medical applications and proved that new bone grows highly organised close to the material, and structural strength was maintained during the *in vivo* implantation period [64]. When talking about polyacrylate biopolymers, few studies have tested the enhancement of mechanical properties with the introduction of HA. Song *et al.* [136] designed synthetic bone grafts based on PHEMA/HA composites, showing excellent structural integration between the filler and the matrix, fact that derived to an improvement of stiffness and the ability to withstand compressive stress. The PHEMA/HA synthetic bone grafts were implanted subcutaneously in rats supporting osteoblastic differentiation of the bone marrow stromal cells pre-seeded on the graft. Huang *et al.* [137] prepared nanoHA-PHEMA/PCL porous nanocomposite scaffolds and studied their bioactivity *in vitro*, observing the formation of a bone-like apatite layer after

immersion in simulated body fluid. Growth and proliferation of primary human osteoblast cells was also observed. In a similar study developed by Juhasz *et al* [138], a nano-HA filler content of 10 wt.% was found to enhance the bioactivity and biocompatibility of the PHEMA/PCL matrix. The fabricated hydrogel was able to retain its ability to swell, while allowing the material to be stabilized *in vivo* and have improved mechanical properties due to the addition of ceramic nanoparticles. The human osteoblast cells were able to differentiate and proliferate on the hydrogel surface.

1.5.2 Halloysite nanotubes (HNTs)

Halloysite nanotubes (HNTs) are a biocompatible clay material found as a raw mineral in natural deposits, fact that makes halloysite economically viable [139] for polymer additivation. HNTs present nanotubular structure where the outer surface can be compared to silica with oxygen atoms, making the surface predominantly negative over most of the physiologically relevant range (pH 6-7) [140], while the inner surface is composed of alumina with hydroxyl groups, giving a positive charge surface below pH equal to 8.5 [141] (Figure 5). Is for their biocompatibility, abundance in nature and tubular shape that HNTs have been extensively used in biomedicine for drug release and Tissue Engineering [141] through polymer additivation. For example, mechanical properties of PCL/HNTs nanocomposites have been studied by Kang-Suk Lee *et al.* [142] reporting an improvement of tensile strength with the inclusion of HNTs, attributed to the formation of strong hydrogen bonds between the hydroxyl groups ($-OH$) present on the HNTs inner surfaces and the carbonyl ($C=O$) of the ester linkages in the PCL molecular chains [143]. However, care must be taken when a matrix is loaded, due to the limitation of the molecular chains movement in the matrix. Indeed, exceeding the amount of the fillers can generate agglomerates, acting as weak points and failure initiation sites [143, 144]. For example, Liu *et al.* [143] and Prashantha *et al.* [144] detected a decrease in flexural properties when exceeding 7.5 wt.% of HNTs, generated by an overloading. The development of PLA matrices reinforced with HNTs was studied by Rangika Thilan De Silva *et al.* [145], who concluded that the percentage of loading with the highest mechanical properties was 5% of HNTs, obtaining an increase of 22% in Young modulus. Stoclet and Sclavons [146] prepared PLA nanocomposites, concluding that the mixture with best mechanical properties was obtained with an 8 wt.% of HNTs additivation. Kalappa [147] and Garrasi *et al.* [148] obtained comparative results with the additivation of 6 wt.% of HNTs to the PLA matrix; they observed, separately, an increase of tensile modulus (15%) and Young modulus (18%). Enhancement of mechanical properties was stated to be induced by hydrogen bonding between the carbonyl groups of PLA and the

hydroxyl groups in HNTs according to Liu *et al.* [149], who used infrared spectroscopy to confirm these observations. Additionally, OH⁻ groups of PLA could also interact with the Si-O-Si groups present in HNTs [150, 151].

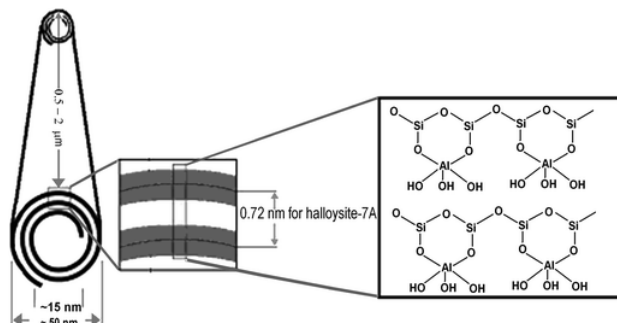


Figure 5 Scheme of an halloysite nanotube [152].

The HNTs cylindrical structure results of a natural process which takes millions of years [152], caused by the hydration of alumina and silica layers, which creates a packing disorder resulting in the curvature of the sheets and rolling its selvages giving a multilayer tube [139]. Their biocompatibility properties and tubular shape make HNTs a perfect material to be used for loading, storage, and controlled release of drugs to be used as a delivery system [139, 153], with a small inner diameter of 15 nm and outer diameter of 50 nm [154-156]. The first relevant study using HNTs as a nanocontainer was carried out by Price *et al.* [155], demonstrating that HNTs are viable nanocontainers for encapsulation of biologically active molecules. It has been demonstrated that the release rate of a drug entrapped in HNTs lumen takes from 30 to 100 times longer than the drug alone, and this rate is increased when the HNTs is coated or embedded in a polymer matrix [157]. The entrapment of a drug in HNTs can be performed in different ways, including adsorption to the external and internal walls of the tubes [158, 159], intercalation [160-165] and loading of the substances into the lumen [166]. The addition of HNTs to the polymeric matrix has proven to favour cell adhesion due to surface nano-roughness acting as an anchoring framework [167] and the presence of silicate ions [168]. The formation of hydrogen bonds between HNTs and proteins are led by silanol groups (Si-OH) located on the surfaces of HNTs [169], especially on their crystal edges [106]. Protein molecules contain hydroxyl and amino groups with which they interact with Si-OH through hydrogen bonds [170].

Due to the HNTs double benefit introduced above, we have investigated the enhancement of mechanical properties and drug delivery capacity of a specific drug previously entrapped in the HNTs lumen.

1.5.3 Curcumin

In such a way, curcumin has been selected as a drug to load the HNTs lumen and its delivery rate has been subsequently studied. Curcumin is a yellow lipid-soluble natural pigment extracted from the powdered rhizome of the plant *Curcuma longa*, with a chemical formula [1,7-bis(4-hydroxy-3-methoxyphenyl)-1,6-heptadiene-3,5-dione] [171, 172]. Curcumin is a commonly used food colorant which possesses excellent pharmacological properties such as anti-oxidant [172], anti-inflammatory [173], anti-tumorigenic [174], in addition to numerous desirable biological benefits [175]. Due to the mentioned properties, considerable attention has been paid to curcumin, being one of the most studied natural compounds [176]. However, curcumin has demonstrated to have very low activity in physiological environments owing to its poor solubility in water ($< 1 \mu\text{g/mL}$). Furthermore, it exhibits rapid degradation in alkali conditions (pH 7.4) at physiological temperature [177], which makes curcumin hard to absorb from the gastrointestinal tract after oral administration. Consequently, studies are continuously being developed to achieve appropriate drug delivery systems to enhance in vivo curcumin stability. Some of these efforts have been based upon the use of polymer nanospheres of poly (DL-lactide) [178] and (NIDAM-NVP-(PEG-A)) copolymers [179], also the encapsulation with different bio-microspheres using bovine serum albumin and chitosan [180] or lipid-based nanoparticles [181].

2 Objectives

1. To understand the mechanical effect of inorganic fillers such as hydroxyapatite and halloysite nanotubes into a polyester matrix.

It is aimed to firstly monitor the effects of HA and HNTs on mechanical and thermal properties of PCL in order to determine the additivation threshold and optimize the additivation rate. The results will be subsequently transferred to the following chapters using polymers with different nature to intensively study the biological effect of the fillers, which will also modify the hydrophobicity of the materials.

2. To optimize HNTs' loading with curcumin before their mixture with PCL and HA in the optimal proportion previously established in order to validate the HNTs encapsulation capacity.

The functionalization of HNTs with curcumin has been addressed by using different solvents to prove the capacity of loading and successive delivery of the active agent. Secondly, the modifications on mechanical and thermal properties of the PCL-based hybrids after loading process has been followed. [This experimental part has been partially developed during the research stay in 2015 at the University of Wisconsin Madison in the Wisconsin Institute for Discovery under the supervision of Professor Lih-Sheng (Tom) Turng.]

3. To study the role of HA and HNTs when loaded in polymer matrices of different chemical composition and hydrophilicity, such as PCL- and PHEMA-based polymers.

Structural properties of pairs of polymers with similar chemical natures but different hydrophobicity will be compared. On the one hand, the hydrophobic polyester PCL is modified by its blending with PLA. On the other hand, the hydrophilic acrylate PHEMA is copolymerized with EMA at a ratio of 50/50 wt.%, P(HEMA-co-EMA). These polymers are used as neat resins and combined with HA nanoparticles and HNTs. In particular, the behaviour to be compared is:

- Distribution of the HA and HNT fillers into the polymeric matrices
- Hydroxyapatite nucleation process on the polymer surfaces
- Degradation rate (only in polyesters, for their biodegradable character)

4. To study the influence of the hydrophobic–hydrophilic nature of PCL- and PHEMA-based polymers and their nanocomposites on their *in vitro* biological development.

Cell viability, proliferation, and morphology will be monitored on the two pairs of polymers having different chemical nature. PCL, PCL/PLA and the polyacrylates PHEMA and P(HEMA-co-EMA) are used alone and loaded with HA and HNTs. [This experimental part has been partially developed during the research stay in 2016 at the University of Wisconsin Madison in the Wisconsin].

3 Experimental section

3.1 First chapter – Study of the improvement of PCL thermal and mechanical properties through the addition of HA and HNTs

In a first stage, PCL mechanical and thermal properties were studied by modifying the additivation percentage of HA and HNTs. This preliminary study allowed to understand the synergic effect among the polymeric matrix and the functional groups present on the additives chemical structure. Simultaneously, the additivation threshold was determined, thus optimizing the additivation rate.

3.1.1 Preparation of the PCL-based hybrids

For the purpose of obtaining PCL-base hybrids, seven different types of polycaprolactone (PCL) biomaterials were prepared, containing different mass fractions of hydroxyapatite (HA) and halloysite nanotubes (HNTs), as specified below in Table 7. PCL Capa™ 6500 provided by Solvay Interlox UK, is a high molecular weight thermoplastic linear polyester derived from caprolactone monomer supplied in granular form, approximately 3 mm pellets. With a mean molecular weight of 50 000 Da and a melting point of 58-60°C. Hydroxyapatite nanoparticle ($\text{HCa}_5\text{O}_{13}\text{P}_3$; HA) with <200nm particle size was supplied by Sigma Aldrich, Madrid, Spain. Halloysite nanotubes (HNTs), with molecular formula $\text{Al}_2\text{Si}_2\text{O}_5(\text{OH})_4 \cdot 2 \text{H}_2\text{O}$ (294.19 g/mol), were supplied by Sigma Aldrich, Madrid, Spain. The HA and HNTs mass fractions were chosen based, on the one hand, on the work developed by Biqiong Chen and Kang Sun's [130]. They reported an enhancement of mechanical properties when PCL was reinforced with different amounts of HA, reaching the greatest strength value when the concentration of HA was 20%, and noticing a significant strength decrease when the content of HA increased beyond 20%. And, on the other hand, on the works of Liu *et al.* [143] and Prashantha *et al.* [144], who observed an improvement in flexural properties of the polymer matrix loaded with HNTs, not exceeding 7.5 wt.%. In the latter, the authors correlated the overloading of HNTs with the generation of aggregates acting as weak points and failure initiation sites.

Previous to extrusion mixing process, all the components of each blend formulation specified in Table 7 were dried separately in a vacuum oven (PCL at 45°C for 24 h; HA and HNTs at 200°C for 48 h). 600 g of each manufacturing mixture were next prepared following the percentages specified, manually mixed in a zip bag and mechanically mixed in a twin-screw corotating extruder at 40 rpm, mass dosing of 2.5 kg/h and a mass flow

rate of 30 kg/h. The temperature profile for the four-extruder zone of the barrels is specified in Table 8. After this process, a room temperature cooling during 5 min was needed before the pelletization of the mixture in a jaw mill. The mill used was a jaw crusher BB 300 supplied by Retsch GmbH (Retsch Spain). Samples were injection moulded in a Meteor 270/75 injection machine (Mateu and Solé, Barcelona, Spain). The temperature profile of the extruder was 80°C/80°C/85°C/85°C/90°C, with a mould temperature of 50°C and a cooling time of 6 s. The pressure value of the injection moulding process was 800 pSi and the mould used was a steel mould with mirror finishing with the dimensions recommended by the corresponding standards: strength samples type 1A had dimensions of 170×10×4 mm³ (UNE EN ISO 527), and flexural samples were 90×10×4 mm³ (ISO 178).

Table 7 PCL/HA/HNTs mass percent composition of injected mixtures.

<i>Sample ID</i>	<i>Mass (%)</i>		
	<i>PCL</i>	<i>HA</i>	<i>HNTs</i>
<i>PCL HA 20</i>	80	20	-
<i>PCL HA 20 HNTs 2.5</i>	77.5	20	2.5
<i>PCL HA 20 HNTs 5.0</i>	75	20	5.0
<i>PCL HA 20 HNTs 7.5</i>	72.5	20	7.5
<i>PCL HNTs 2.5</i>	97.5	-	2.5
<i>PCL HNTs 5.0</i>	95	-	5.0
<i>PCL HNTs 7.5</i>	92.5	-	7.5
<i>PCL</i>	100	-	-

In this first stage, eight different types of hybrids were herein extruded, and injection moulded. Pure PCL samples were used as control. From these seven hybrids samples, the optimal was chosen in terms of its mechanical and thermal properties, with the aim of studying the influence of HNTs loaded with curcumin on the final properties of the PCL-based hybrids.

Table 8 Extrusion and injection moulding parameters.

<i>Sample</i>	<i>T1</i> (°C)	<i>T2</i> (°C)	<i>T3</i> (°C)	<i>V</i> (rpm)	<i>P</i> (bar)	<i>volumetric</i> <i>feeding</i> (Kg/h)	<i>Calculated</i> <i>flow</i> (Kg/h)
PCL HA 20	60	70	80	250	50	2.5	30
PCL HA 20 HNTs 2.5	60	70	80	250	50	2.5	30
PCL HA 20 HNTs 5.0	65	75	85	250	45	2.5	T30
PCL HA 20 HNTs 7.5	65	75	85	250	45	2.5	30
PCL HNTs 2.5	65	80	90	250	60	2.5	30
PCL HNTs 5.0	70	80	90	250	65	2.5	30
PCL HNTs 7.5	70	80	90	250	65	2.5	30
PCL	90	85	80	75	60	2.5	30

3.1.2 Thermal characterization

Thermo-analytical techniques are widely used in the characterization of materials. Thermal analysis covers all measurement methods based on the change, with temperature, of a physical or mechanical property of the polymeric material. The conditions of manufacture of a product, as well as its history and thermal treatments, are decisive in the final properties of the material, so thermo-analytical techniques are essential in any control process over the manufacture of a material.

Differential Scanning Calorimetry (DSC)

Differential Scanning Calorimetry allows the study of those processes in which an enthalpic variation occurs, for example, determination of specific heats, melting and boiling temperatures, purity of crystalline compounds, enthalpies and determination of first and second order transitions. Hence, DSC was used to uncover any physical change

in the hybrids and settle subtle temperature variations induced by the addition of inorganic compounds. Measurements were performed in a Mettler-Toledo DSC 821e device (Mettler-Toledo S.A.E., Barcelona, Spain). Each sample consisted in between 5 and 10 mg and was scanned from 30 to 350°C at 10°C·min⁻¹ under atmospheric air.

Measuring crucibles were standard aluminium crucibles, with a net volume of 40 µl, with an aluminium lid and sealing capacity to avoid sample losses. Periodic calibration of the DSC cell was carried out using indium and zinc standards, with well-known melting points and enthalpies. The test conditions used for each of the samples are listed in Table 9 for the single cycle programs.

Table 9 Test conditions used in the Differential Scanning Calorimetry (DSC).

<i>Property</i>	<i>Value</i>
<i>Dynamic Trials</i>	
Material mass	3-6 mg
Atmosphere	air
Temperature ratio	30-300°C
Heating rate	20°C·min ⁻¹
<i>Thermal heating-cooling cycles</i>	
Material mass	3-6 mg
Atmosphere	air
Temperature ratio	10-100°C/100-10°C
Heating rate	20°C·min ⁻¹

Thermogravimetric Analysis (TGA)

Thermogravimetric Analysis is a well proven thermal analysis method for measuring mass changes as a function of temperature. TGA is used in the research and development of various substances and engineering materials in order to obtain knowledge about their thermal stability and composition. In recent decades, TGA has

been used increasingly in quality control and assurance for raw materials and incoming goods, as well as in the failure analysis of finished parts, especially in the polymer-processing industry. Various international standards describe the general principles of thermogravimetry for polymers (ISO 11358).

Thermogravimetric analyses were performed to study plausible physical modifications as a consequence of the temperature and determine the mass loss attributed to polymer degradation, to thereby corroborate the percentage of inorganic additives effectively incorporated to the polymeric matrix. The equipment used was a TGA/SDTA 851 (Mettler-Toledo Inc., Schwerzenbach, Switzerland) with a heating rate from 30 to 350°C at 20°C min⁻¹.

Standard aluminium crucibles with a volume of 70 µl were used to scan the samples.

VICAT tests

Vicat softening temperature is the temperature at which the plastic specimen under study is penetrated to a depth of 1 mm by a flat-ended needle with a 1 mm² circular section loaded with a pre-defined weight (for the Vicat A test, a load of 10 N is used, and for the Vicat B test, the load used is 50 N). VICAT tests were carried out to determine the softening point of the different mixtures, in a Vicat/HDT VHDT 20 device (Metrotec S.A., San Sebastian, Spain). The experiment conditions were chosen from the standards ISO 306 and D1525.

Heat deflection temperature tests (HDT)

Heat deflection temperature tests were undergone to determine the temperature at which the material deforms under a specific load of 200 g, while immersed in a temperature-controlled bath whose temperature increases at a constant rate of 50°C/h. The equipment used was a Vicat/HDT VHDT 20 (Metrotec S.A., San Sebastian, Spain). Tests were carried out with a load of 200 g and a temperature program increase of 50°C/h, following the ISO 75 and ASTM D648 standards.

Dynamic Mechanical Thermal Analyses (DMTA)

Dynamic Mechanical Thermal Analysis allows quantitative determination of the mechanical properties of a sample under an oscillating force and as a function of temperature, time, frequency and strain (DIN EN ISO 6721). The results reveal the linear viscoelastic properties, typically depicted as a graphical plot of E' (storage modulus), E'' (loss modulus), and tanδ (loss factor) versus temperature. The study allows to analyse the viscoelastic behaviour of the materials under stress, to obtain the storage modulus

and thus determine the elasticity variation of each hybrid caused by the incorporation of reinforcing fillers into the polymeric matrix. All composites were scanned in an AR G2 device from TA Instruments (TA Instruments, New Castle, USA). The analyses were carried out in torsion mode with specimens of $40 \times 10 \times 4 \text{ mm}^3$. The heating rate was $2^\circ\text{C} \cdot \text{min}^{-1}$ from 25°C to 80°C at a constant frequency of 1 Hz and a strain of 0.1% as controlled variable. The storage modulus was obtained as:

$$E' = \frac{\sigma_0}{\varepsilon_0} \cos \delta$$

where E' is the storage modulus (MPa), σ and ε are the stress and strain, respectively, and δ is the phase lag between stress and strain.

3.1.3 Mechanical characterization

Aiming to evaluate the dependence of mechanical properties with the addition of the fillers in the polymer matrix, a deep mechanical characterization was carried out to select the blend formulation which better met the structural demand for the intended application. To this end, the material mechanical properties will define how the material responds to an applied load or force.

Hardness Shore D

Hardness Shore tests were carried out to measure the resistance of the material towards indentation, and correlate the empirical hardness relation with the addition of inorganic fillers to the polymeric matrix. The test measures the depth of an indentation in the material produced by a flat tip needle with a given force on a standardized presser foot. This depth is dependent on the material hardness, its viscoelastic properties, the presser foot shape, and the test duration. There are two Shore scales depending on the material nature. The Shore A scale is used for softer materials such as rubbers or elastomers, while the Shore D scale is used for harder materials such as polyolefins, fluoropolymers and vinyls.

Hardness Shore D was measured using a durometer Model 673-D (J. Bot Instruments, Barcelona, Spain) following the UNE-EN ISO 868 standard. Five replicates of each sample were evaluated to obtain an average value.

Impact Charpy tests

The Impact Charpy test determines the amount of energy absorbed by a material during fracture. The apparatus consists of a pendulum of known mass and length that is dropped from a known height to impact a notched material specimen. The energy transferred to the material can be inferred by comparing the difference in the height of the hammer before and after the fracture (energy absorbed by the fracture event).

The test was carried out using a Charpy pendulum (Metrotec S. A., San Sebastian, Spain) with an energy of 1 J, according to ISO 179 standard. Each value was obtained from a minimum of 5 notched samples and calculating the average value, not accepting a deviation above 5%.

Flexural tests

Flexural Tests were performed to establish the material bending behavior under specific forces. The test provides values for the elastic modulus in bending and flexural stress-strain response of the material under a specific applied force.

The Flexural test was performed using an electromechanical universal test machine Elib 30 (Ibertest S.A.E, Madrid, Spain) following the specification established in the ISO 178 standard with an extension rate of 5 mm·min⁻¹.

Tensile tests

Tensile strength is the capacity of a material to withstand loads tending to elongate, and gives the measurement of the maximum stress that the material can withstand while being stretched before breaking. The results show the force per unit area (MPa) required to break the material, in such a manner it is the ultimate tensile strength or tensile strength at break.

These tests were performed using an electromechanical universal test machine Elib 30 (Ibertest S.A.E, Madrid, Spain) following the specification established in the ISO 527 standard, with an extension rate of 10 mm min⁻¹.

3.1.4 Optimization of the HNTs loading with curcumin

After investigating the PCL additivation effect on the mechanical and thermal properties, HNTs were functionalized with curcumin before their mixture with PCL and HA in the optimal proportion previously established. Curcumin with a linear formula (E,E)-1,7-

bis(4-Hydroxy-3-methoxyphenyl)-1,6-heptadiene-3,5-dione, was supplied by Sigma Aldrich, Madrid, Spain.

For that purpose the procedure proposed by Abdullayev and Lvov [141] was followed to introduce curcumin in the nanotubes lumen. Briefly, HNTs powder (10 wt.%) was mixed with a saturated solution of curcumin at room temperature. Water, acetone and ethanol are the most commonly used solvents [139, 182] for curcumin; therefore, in this study the HNTs functionalization efficiency was evaluated for those three solvents. The use of polar solvents enhances the loading effect due to large capillary forces of 200 atm (as estimated by Laplace formula) pushing the solution into the lumen [183]. Vacuum was applied to the solution containing the active agent, to force the entry of the solution into the nanopores and a partial crystallization of the loaded substance took place (Figure 6). This process was repeated 3-4 times in order to increase the loading efficiency. After the loading, the halloysite suspension was centrifuged and rinsed with water in order to remove any loosely attached substance from the external walls and to remove dissolved excess molecules. Finally, the powder was dried at 80°C under vacuum. After functionalization of HNTs with curcumin, hybrids with the best performance previously established were extruded and injection moulded following the extrusion and injection conditions listed in Table 8.

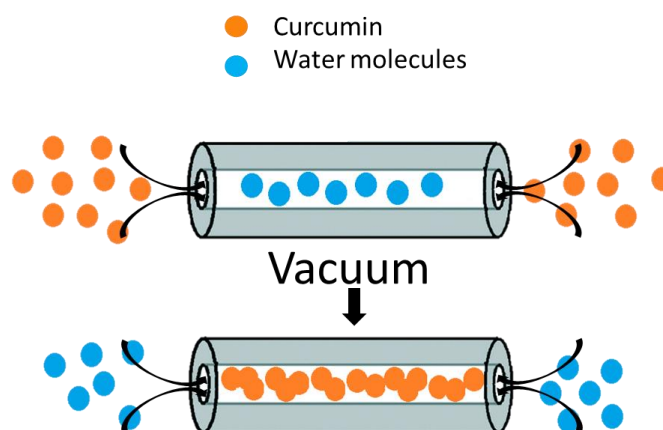


Figure 6 Halloysite nanotubes functionalization process with curcumin proposed by Abdullayev and Lvov [1].

Analysis of the solvent with best performance

TGA measurements, together with SEM images allowed a coarse determination of the amount of curcumin loaded inside HNTs. TGA curves yielded the inorganic mass percentage of different compounds based on degradation temperatures. SEM provided images of the loaded nanotubes where the lumen diameter could be measured.

Scanning Electron Microscopy (SEM) images were obtained to prove the nanotubes dispersion in each matrix as well as to give a qualitative assessment of HNTs loading efficiency. Images were taken in an EOL 1530 FESEM with a 3 kV accelerating voltage using an in-lens detector and a working distance of 1.3 mm. Samples were previously gold coated for 30 s at 45mA in a Denton Vacuum Desk V sputter coater. All image processing was done with the ImageJ software.

Thermogravimetric Analyses (TGA) were performed to study plausible physical modifications as a consequence of the temperature. Specially, TGA was used to calculate the percentage of inorganic compound effectively incorporated into the HNTs lumen and thus, determine which of the three solvents used (water, ethanol or acetone) allowed the incorporation of the greatest amount of curcumin inside the HNTs lumen. The equipment used was a TGA/SDTA 851 (Mettler-Toledo Inc., Schwerzenbach, Switzerland) with a heating rate of 30–350°C at 20°C min⁻¹.

3.1.5 Curcumin delivery rate

This experimental part was carried out in order to prove the HNTs double functionality: on the one hand, the improvement on mechanical properties inferred to the polymeric matrix after the loading procedure; on the other hand, their capacity to carry a drug such as curcumin and its subsequent delivery.

To effectively validate the HNTs ability of delivery, the effect of PCL + HNTs loaded with curcumin was compared with PCL + curcumin. In this sense, curcumin was dispersed in the PCL matrix and its delivery rate was followed. At the same time, in order to quantify the attenuation of delivery capacity when HNTs are entrapped into a polymer matrix, dispersion of HNTs loaded with curcumin in PBS was also studied separately. Sample identification is specified in Table 10. Samples were prepared through solvent casting procedure using dioxane to dissolve PCL and adding the respective fillers (curcumin or HNTs loaded with curcumin). The different dissolutions were placed onto a glass plate of 6 cm of diameter to obtain a final film of 0.2mm thin. After 24h of solvent evaporation in an extraction fume hood, samples were punched into 13 mm diameter circles, immersed individually in 10ml of PBS solution (Sigma) and incubated at 37°C and 5% CO₂. PBS solution was replaced every two days and aliquots of the remanent solution were withdrawn to measure absorbance at 420 nm, 350 nm and 263 nm using an ultraviolet spectrophotometer (Cecil CE9200, Aquarius). Curcumin concentration was calculated from the aliquots making use of a standard calibration curve previously obtained.

Table 10 Sample identification for the curcumin delivery rate evaluation

<i>Sample ID</i>	<i>Composition</i>
HNTs	HNTs loaded with curcumin dispersed in PBS solution
PCL + 7.5% HNTs	PCL + 7.5% HNTs loaded with curcumin
PCL + 0.75% curcumin	PCL + 0.75% curcumin

3.2 Second chapter - Study of the influence of the addition of HA and HNTs on the morphological properties of PCL- and PHEMA-based polymers

Once the influence of the additives on the PCL mechanical properties was evaluated and the thresholds of additives were set in the first part of this work, this investigation moved forward to a second stage. Morphological properties were studied and compared among different pairs of polymers with similar chemical natures but different hydrophobicity. On the one hand, the hydrophobic polyester PCL was modified by its blending with PLA at a ratio of 1:1 wt.%. On the other hand, the hydrophilic acrylate PHEMA was copolymerized with EMA at a ratio of 1:1 wt.%. These polymers were used as neat resins and combined with HA nanoparticles and HNTs.

3.2.1 PCL/PLA-based hybrid samples

PCL/PLA-based hybrid samples were prepared by manually mixing all components, previously dried separately in a vacuum oven (PCL at 50°C, PLA at 60°C, HA at 200°C, and HNTs at 80°C, for 48 hours), in a zip bag with the mass percentage specified in Table 11. A total mass of 600 g of each mixture was prepared. Pure PCL and PCL/PLA 1:1 wt.% samples were used as controls. PLA Ingeo™ biopolymer 6201D is a thermoplastic available in pellet form. With a glass transition temperature of 55-60°C and melting point of 155-170°C, was supplied by NatureWorks LLC (Nature Works LLC, Minnetonka, MN, USA).

The powdery mixtures were next mechanically mixed by extrusion with a twin-screw co-rotating extruder at 40 rpm, with a mass dosing of 2.5 Kg/h and a mass flow rate of 30 Kg/h. The temperature profile for the four extruder barrels was 65°C/75°C/85°C/90°C for

PCL-based hybrids and 170°C/173°C/175°C/180°C for PCL/PLA-based hybrids. Next, 30 min of cooling at room temperature was needed before pelletization of the mixture in a ball mill at room temperature, followed by drying in a vacuum oven at 50°C for 48 h, and then injected moulded in a Meteor 270/75 injection moulding machine (Mateu and Solé, Barcelona, Spain). The temperature profile of the extruder was 80°C/80°C/85°C/85°C/90°C for PCL-based hybrids and 170°C/173°C/175°C/180°C for PCL/PLA-based hybrids, with a mould temperature of 50°C and a cooling time of 6 s. The mould used was a steel mould with mirror finishing with the dimensions recommended by the corresponding standards: strength samples type 1A had dimensions of 170×10×4 mm³ (UNEEN ISO 527), and flexural samples were 90×10×4 mm³ (ISO 178). In parallel, films were obtained through compression moulding, and were consequently laser cut to obtain the 13 mm-diameter samples for subsequent biological experiments.

3.2.2 PHEMA and P(HEMA-co-EMA)-based hybrids

Hydroxyl-2-ethyl methacrylate (96%), (HEMA) with a linear formula $\text{CH}_2=\text{C}(\text{CH}_3)\text{COOCH}_2\text{CH}_2\text{OH}$ and a molecular weight of 130,14 g/mol, was supplied by Sigma-Aldrich (Sigma-Aldrich, Madrid, Spain). Ethyl methacrylate (99%), (EMA) with a linear formula $\text{CH}_2=\text{C}(\text{CH}_3)\text{COOC}_2\text{H}_5$ and a molecular weight of 114,14 g/mol was supplied by Sigma-Aldrich (Sigma-Aldrich, Madrid, Spain).

Hybrid acrylate-based materials were obtained by simultaneous polymerization of the organic (co)monomer mixture with the mass percentage specify in Table 11: neat hydroxyl-2-ethyl methacrylate, HEMA or mixed with EMA at a 1:1 wt.% monomer ratio in the case of the copolymer, were stirred together with 1 wt.% (relative to monomer weight) of benzoin as an ultraviolet initiator of the radical polymerization, and 0.5 wt.% of ethylene glycol dimethacrylate, EGDMA (98%, Sigma–Aldrich), as crosslinking agent. HA and HNTs were previously dried separately in a vacuum oven for 48 h at 200°C and 80°C, respectively, and incorporated into the mixture being stirred for 15 min. Each reactant mixture was injected in glass templates with a standardized strength test template according the UNE-EN ISO 527 standard, polymerized for 24 h in an ultraviolet oven, and thermally post-polymerized for 24 h more in an oven at 90°C. Each film was rinsed for 24 h in boiling ethanol twice and then punched into 13 mm diameter circles for subsequent cell cultures.

Table 11 Weight percentages of the reactants used for sample preparation.

<i>Sample ID</i>	<i>Polymer</i>		<i>Inorganic Loading</i>	
	PCL wt.%	PLA wt.%	HA wt.%	HNTs wt.%
PCL	100	-	-	-
PCL HA 20	100	-	20	-
PCL HA 20 HNTs 7.5	100	-	20	7.5
PCL/PLA	50	50	-	-
PCL/PLA HA 20	50	50	20	-
PCL/PLA HA 20 HNTs 7.5	50	50	20	7.5
	PHEMA wt.%	EMA wt.%	HA wt.%	HNTs wt.%
PHEMA	100	-	-	-
PHEMA HA 20	100	-	20	-
PHEMA HA 20 HNTs 7.5	100	-	20	7.5
PHEMA-co-EMA	50	50	0	-
(PHEMA-co-EMA) HA 20	50	50	20	-
(PHEMA-co-EMA) HA 20 HNTs 7.5	50	50	20	7.5

Mechanical and thermal analyses were performed following the methodology detailed in the previous sections.

3.2.3 Structural properties

Comparison of PCL/PLA based hybrids mechanical properties

To demonstrate improvement of mechanical properties for PCL/PLA blended hybrids, mechanical properties were measured. Young and flexural moduli were obtained as

described in section 3.1.3 *Mechanical characterization*. PCL, PLA and PCL/PLA samples were studied alone and loaded with HA.

Analogously, mechanical properties for PHEMA and P(HEMA-co-EMA)-based hybrids were determined. However, the polymerization process in silicone moulds with probe shape posed several problems and the mechanical results obtained did not give substantial information. For this reason, it was decided not to introduce the obtained results in this work.

Energy-Dispersive X-Ray Spectroscopy (EDS)

The morphology of the samples and distribution of HA and HNTs were studied by Energy-dispersive X-ray spectroscopy in a ZEISS FESEM ULTRATM 55 scanning electron microscope (SEM). To this end, each sample was cut in half to observe both, the surface and transversal section. Two replicates of each sample were placed onto a stub using conductive tape to image the surface dispersion and the transversal side dispersion. The samples were connected to the conductive tape using colloidal graphite and subsequently sputter-coated with carbon under vacuum through a BALL-TEC/SCD 005 sputter coater. The mapping spectra were taken at 15 kV of acceleration voltage and 5 mm of working distance, a secondary electron detector was used. Silicon was used as optimization standard.

3.2.4 Hydroxyapatite nucleation

Hydroxyapatite nucleation was studied on two replicates of each sample. First of all, Simulated Body Fluid (SBF) solution with an ion concentration close to that of human blood plasma, was prepared by the method proposed by Kokubo and coworkers [184, 185]. In order to obtain the SBF, two solutions were prepared. Solution 1 consisted in 1.599 g of NaCl (Scharlau, 99% pure), 0.045 g of KCl (Scharlau, 99% pure), 0.110 g of CaCl₂·6H₂O (Fluka, 99% pure), and 0.061 g of MgCl₂·6H₂O (Fluka) in deionized ultra-pure water (Scharlau) up to 100 ml. Solution 2 was prepared by dissolving 0.032 g of Na₂SO₄·10H₂O (Fluka), 0.071 g of NaHCO₃ (Fluka), and 0.046 g of K₂HPO₄·3H₂O (Aldrich, 99% pure) in water up to 100 ml. Both solutions were buffered at pH 7.4, by adding the necessary amounts of aqueous 1 M tris-hydroxymethyl aminomethane, (CH₂OH)₃CNH₂ (Aldrich), and 1 M hydrochloric acid, HCl (Aldrich, 37% pure). Then, both solutions were mixed to obtain SBF with the following molar ion concentrations: 142 Na⁺, 5.0 K⁺, 1.5 Mg²⁺, 2.5 Ca²⁺, 148.8 Cl⁻, 4.2 HCO₃⁻, 1.0 HPO₄²⁻, 0.5 SO₄²⁻ mM. Two replicates of each sample were immersed in individual vials containing 10 mL of SBF solution with

hydrazine (NaH_2) to prevent bacterial proliferation. The vials were placed in an incubator at 37°C and 5% CO_2 . After 7 and 14 days, one replicate of each sample was removed and prepared to observe their surface through SEM microscopy following the procedure specified above. Pictures were taken at 1000 and 5000 magnifications; EDS pictures were also taken in order to validate the formation of a hydroxyapatite layer and the Ca/P ratio.

3.2.5 Degradation of PCL and PCL/PLA based hybrids

Degradation of PCL and PCL/PLA at ratio 1:1 wt.% loaded with HA and HNTs was followed *in vitro* at 37°C using Phosphate Buffered Saline (PBS 0.01 M (NaCl 0.138 M; KCl - 0.0027 M) with a pH 7.4, at 25°C was supplied by Sigma Aldrich). With the aim of accelerating the process, samples were previously immersed in a 2M NaOH solution for 24 h. Three replicates of each composition were immersed in individual tubes with 10 ml of DPBS (Dulbecco's Phosphate Buffered Saline supplied by Sigma Aldrich) (at pH 7.4) with screw caps and maintained at 37°C in an incubator. Each sample was removed after four, eight and twelve weeks; rinsed thoroughly with deionized water and dried in an oven at 35°C for 12 h. The weight loss and the mechanical integrity of the materials were evaluated.

3.3 Third chapter - Influence of the hydrophobic–hydrophilic nature of PCL- and PHEMA-based polymers and their nanocomposites on their *in vitro* biological development

In this chapter, cell viability, proliferation, and morphology were studied on the two pairs of polymers varying the polymer's chemical surface by blending hydrophilic and hydrophobic polymers, copolymerizing monomers of opposite natures, and/or loading the polymer matrix with nanoparticles such as HA or HNTs. To this end, the polyester PCL, PCL/PLA and the polyacrylates PHEMA and P(HEMA-co-EMA) were used alone and loaded with HA and HNTs. In Table 12, the materials with different hydrophobicity used for this biological study are presented.

Table 12 Materials selected for the biological study.

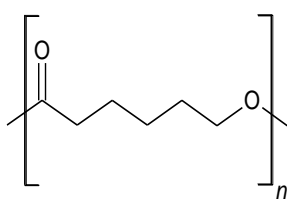
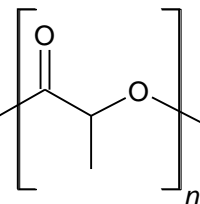
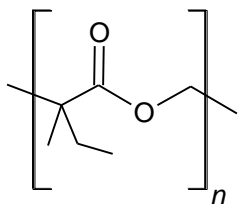
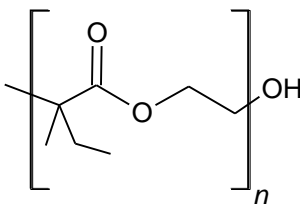
Polycaprolactone PCL	Poly (lactic acid) PLA	Poly (ethylmethacrylat e) PEMA	Poly (2-hydroxyethyl methacrylate) PHEMA
			
Hydrophobic	Moderately hydrophilic	Moderately Hydrophobic	Hydrophilic

Table 13 Weight percentages of the polyester polymers and inorganic fillers used for samples preparation for biological studies.

Sample ID	Polymer		Inorganic		
	PCL wt. %	PLA wt. %	HA wt. %	HNTs wt. %	
PCL	100	0	0	0	Injected & Laser cut Ø 13 mm
PCL HA 20	100	0	20	0	
PCL HA 20 HNTs 7.5	100	0	20	7.5	
PCL/PLA	50	50	0	0	
PCL/PLA HA 20	50	50	20	0	
PCL/PLA HA 20 HNTs 7.5	50	50	20	7.5	

Table 14 Weight percentages of the acrylates polymers and inorganic fillers used for samples preparation for biological studies.

<i>Sample ID</i>	<i>Polymer</i>		<i>Inorganic</i>		
	<i>HEMA wt.%</i>	<i>EMA wt.%</i>	<i>HA wt.%</i>	<i>HNTs wt.%</i>	
PHEMA	100	0	0	0	Polymerized & Punched Ø 13 mm
PHEMA HA 20	100	0	20	0	
PHEMA HA 20 HNTs 7.5	100	0	20	7.5	
PHEMA-co-EMA	50	50	0	0	
(PHEMA-co-EMA) HA 20	50	50	20	0	
(PHEMA-co-EMA) HA 20 HNTs 7.5	50	50	20	7.5	

3.3.1 Contact Angle Measurements

Chemical surface interactions (electrostatic or hydrophobic interactions) are important in the bio-adhesion process. Hydrophobic polymers lead to strong interactions with hydrophobic domains of proteins which would unfold and spread over the polymer surface to reduce the net hydrophobic surface in contact with the solvent medium. Varying the polymer chemical surface by blending hydrophilic/hydrophobic polymers and/or loading the polymer matrix with HA or HNTs would be ways to improve cell adhesion efficiency.

The water contact angles (WCA) of the different nano-composites were measured on the surface of the dry samples in the sessile drop mode. An Easy Drop Standard goniometer model FM140 (110/220 V, 50/60 Hz) supplied by Krüss GmbH (Hamburg, Germany) was used for this purpose. In order to determine the contact angle, the Drop Shape Analysis SW21 (DSA1) software was used and five replicates of each composition were analysed to obtain ten values per sample type, yielding a standard deviation of less than 5%.

3.3.2 Cell Viability and Morphology

Sanitization

Sterilization is a process which avoids contamination of the biomaterials from living microorganisms, including bacteria, yeasts, and viruses. The chosen sterilization technique should maintain structural and biochemical properties of the materials to ensure the intended purpose.

Each sample was rinsed in a 70 vol % ethanol aqueous solution three times for 15 min each (in a laminar flow cabinet from the second rinse on), followed by two more times for 2 h. Then, samples were washed with DPBS (3 rinses of 20 min and 2 more of 1 h) and kept overnight in fresh DPBS. Finally, samples were sterilized with UV light.

Cells conditioning and resuspension

NIH 3T3 fibroblast cells (NIH/3T3 (ATCC® CRL-1658™)) were expanded in the presence of DMEM medium 4.5 g/l glucose (Dulbecco's Modify Eagle Medium-ThermoFisher (Gibco)) supplemented with 10% fetal bovine serum (FBS; ThermoFisher (Gibco)) and 1% penicillin/streptomycin (P/S; ThermoFisher (Gibco)) at 37°C in a 5% CO₂ incubator until confluence.

After reaching confluence (3 days), cells were withdrawn from the culture flask. To proceed, 5 ml of versene solution (0.48 mM) formulated in 0.2 g EDTA (ethyldiaminetetraacetic acid) (Na₄) per liter of phosphate buffered saline (PBS) supplied by ThermoFisher (Gibco), were added for 5 min at 37°C, and then removed. Next, 10 mL of DMEM were added to neutralize the versene, and the resultant solution was centrifuged at 1000 rpm for 5 min.

Cells were resuspended in 1 ml of culture medium, counted and diluted to be seeded (passage 60).

Cell seeding and culture

Cells were seeded on 13 mm diameter samples as 100 µl droplets (0.1 ml), each one containing resuspended cells, so that, the seeding density was 2x10⁴ cells/cm². Samples were incubated for 30 min at 37°C and 5% CO₂ to allow cells to attach on the material surface. Next, 1 ml of DMEM medium was added per well. Culture medium was renewed every day. Samples were withdrawn after 1, 3, 7, and 14 days.

Cell viability assay

Three replicates of each type were withdrawn after each culture time for the analysis. The medium of each well was aspirated, and cultured samples were rinsed with DPBS. Their cytotoxicities were determined by carrying out an MTS (3-(4,5-dimethylthiazol-2-yl)-5-(3-carboxy-methoxyphenyl)-2-(4-sulfophenyl)-2H-tetrazolium; CellTiter 96® Aqueous One Solution cell proliferation assay Promega) assay.

For this purpose, culture medium without phenol red (ThermoFisher Scientific) was mixed with the MTS reactant in a 5:1 ratio, added to the wells, and incubated for 3 h at 37°C in the 5% CO₂ incubator. When incorporated into the cells, the MTS was bio-reduced by metabolically active cells. After the incubation period, 440 µL of each MTS solution were transferred into a new well of a 24-well TCPS plate, and absorbance was read for all three replicates of each sample at 450 nm and 560 nm in a GoldMax Multi Detection System Instinct (Promega Corporation, Madison, WI, USA), taking as a reference the MTS reagent solution incubated likewise in wells empty of cells. Cells cultured directly in polystyrene wells were used as positive controls (non-cytotoxic) for comparison. The MTS reactant solution incubated in wells with acellular materials worked as blank.

Scanning Electron Microscopy (SEM)

Morphology of NIH 3T3 fibroblast cells and their layout on the surfaces were analysed in each cultured sample through Scanning Electron Microscopy (SEM). After 1, 3, 7, and 14 days of incubation, the culture medium was removed, and samples were rinsed with PB. Fixation of samples was carried out with a 4% paraformaldehyde solution in PB (Affymetrix) incubated for 30 h at 37°C, followed by a rinse with PB.

Water of the samples was removed to avoid any deformation of cell morphology when applying vacuum. For this purpose, freeze-drying with liquid nitrogen was done. First, samples were rinsed twice with PBS and then with double deionized water (DDI). Each sample was then quickly frozen in liquid nitrogen and transferred to a freezer-dryer for drying.

Influence of HNTs loaded with curcumin incorporated to the PCL matrix on its biological properties

Aiming to study the viability of the materials loaded with curcumin three replicates of each sample were prepared to compare cell culture and viability. PCL sample was used as control to compare PCL 20 HA 7.5 HNTs and PCL 20 HA 7.5 HNTs + curcumin. To

perform cell culture a 24 well culture plate with a depth of 17mm was used, NIH 3T3 ECACC fibroblasts were used for all biological assays. These cells were cultured in high-glucose DMEM (Invitrogen) supplemented with 10% fetal bovine serum (Gibco). Cells were resuspended, counted, and seeded at a density of 10000 cells/well. Viability was assessed via LIVE/DEAD Viability/Cytotoxicity kits (Invitrogen). The stain used was green fluorescent Calcein-AM to target esterase activity within the cytoplasm of living cells, and red fluorescent ethidium homodimer-1 (EthD-1) to indicate cell death by penetrating damaged cellular membranes.

The cultured samples were washed twice with Hanks' balanced salt solution (HBSS; Thermo Scientific) and then fixed with a 4% paraformaldehyde (Electron microscopy Sciences) in HyClone HyPure molecular biology grade water (from Thermo Scientific) solution for 30 min at room temperature. The rinsed samples were washed by a series of ethanol washes, each for 30 min. Consecutively; higher concentrations were applied with each wash, namely, 50% ethanol, 80, 90, and then 100%. At last, the samples were dried within a vacuum desiccator overnight before gold sputtering for SEM.

3.3.3 Organization of Cell Cytoskeleton

Immunocytochemistry

Simultaneously, analogous cultured samples were rinsed with phosphate buffer (PB 0.1 M, PH= 7,2 supplied by Grainger), fixed with 4% paraformaldehyde (Affymetrix) in PBS (100 ml) for 15 min at room temperature, and rinsed again with PBS twice for 5 min. Permeabilization and blocking were performed using bovine serum albumin (WiCell), 10% goat serum (IgG in solution with a concentration of 45-75 mg protein/ml was supplied by Sigma Aldrich), and 1% Triton X-100 (with a linear formula $t\text{-Oct-C}_6\text{H}_4\text{-(OCH}_2\text{CH}_2)_x\text{OH}$, $x= 9\text{-}10$ was supplied by Sigma Aldrich) in PBS, at 500 μl per sample, for 1 h at room temperature.

Samples were next stained using Vinculin (Anti-Vinculin antibody produced in mouse (monoclonal VIN-11-5, ascites fluid) with a protein concentration by Biuret of 15-55 mg/ml and a molecular mass of 130kDa was supplied by Sigma Aldrich) as the primary antibody at a 1:300 proportion with a blocking solution at 4°C in the dark. Vinculin was used to stain vinculin, which is a cytoskeletal protein involved in the linkage of integrin adhesion molecules to the actin cytoskeleton. Hence, using vinculin, the focal adhesion associated with cell-cell and cell-matrix junctions could be detected. After 15 h (or overnight), samples were rinsed with PBS and incubated with goat anti-mouse Cy5

secondary antibody (ThermoFisher) at a 1:1000 proportion with a blocking solution, for 1 h, at room temperature in the dark. Finally, PBS was used to rinse the samples. Next, samples were incubated for 1 h in phalloidin (1:250) (Sigma Aldrich) to stain actin filaments, and DAPI (4,6-diamidino-2-phenylindole with a linear molecular structure $C_{16}H_{17}Cl_2N_5$ and a molecular weight of 350,25 g/mol was supplied by ThermoFisher), at a ratio of 1:2000 in PBS, was used to stain the nuclei. Finally, PBS was used to rinse the samples. They were examined under a Nikon ECLIPSE 80i fluorescence microscope (Nikon Instruments, Inc., Amsterdam, The Netherlands).

4 Results and discussion

4.1 First chapter – Study of the improvement of PCL thermal and mechanical properties through the addition of HA and HNTs

4.1.1 Thermal characterization

Polymers are very sensitive to temperature changes and many factors contribute to affect their thermal behaviour. Thermal properties of polymers are equally as important as the mechanical properties. Thermal analysis involves several techniques to assess the material behaviour vs. temperature changes. The aim of these analyses is to set a relationship between the material physical properties and temperature. To study the thermal stability, thermal transitions and the possibility of their modification in the composites, different techniques were used.

Differential Scanning Calorimetry (DSC)

In a first stage, DSC was performed in order to determine the possible changes in thermal properties of the different obtained composites.

Heat flux of DSC plots was normalized in order to make the different curves comparable. Samples with a mass between 6.0 g and 9.5 g were used for the analysis. Melting temperature (T_m (°C)) is an endothermic process, which absorbs heat and was calculated by taking the highest value of the endothermic peak. Enthalpy (J/g) was calculated by integrating the area under the endothermic peak corresponding to the melting transition. Decomposition temperature T_d (°C) was obtained by taking the temperature when the polymer starts to decompose. From the results presented in Table 15 it is observed that with the addition of fillers in the PCL matrix, the melting temperature remains almost stable, with a maximum difference of 2°C. This slight difference does not affect the injection moulding processability with the consequent energy saving [186]. However, the addition of HNTs rises the onset of degradation with the greater value when the two fillers are added, reaching values of 274°C (results are in consistency with TGA curves observed in Figure 8). It provides a great thermal stability range, shifting the start of the main mass loss 20°C compared with PCL samples (250°C). This temperature shift could be explained by a change of simple chain scission degradation process common in raw PCL [187] to a complex two-step nucleation driven degradation mechanism, which implies the starting of the degradation process at discrete points (where the clay is

added) from where it extends to the rest of the polymer [188]. Thus, the thermal decomposition process is delayed due to the slow formation of those discrete points.

Table 15 Differential Scanning Calorimetry results for PCL-based hybrids. Samples with a mass between 6.0 g and 9.5 g were used for the analysis. Enthalpy (ΔH (J/g)) is given as the integral area of the melting transition, melting (T_m) and decomposition temperature (T_d) is expressed in $^{\circ}\text{C}$.

<i>Sample</i>	<i>Mass (mg)</i>	<i>ΔH (J/g)</i>	<i>T_m ($^{\circ}\text{C}$)</i>	<i>T_d ($^{\circ}\text{C}$)</i>
PCL HA 20	8.8	-108.96	64.69	268.11
PCL HA 20 HNTs 2,5	7.0	-58.71	62.80	268.89
PCLA HA 20 HNTs 5,0	9.2	-50.11	62.40	274.69
PCL HA 20 HNTs 7,5	9.3	-60.30	63.08	271.86
PCL HNTs 2,5	7.1	-56.88	63.17	238.78
PCL HNTs 5,0	9.0	-79.32	61.12	262.60
PCL HNTs 7,5	6.6	-51.26	61.74	261.61
PCL	6.9	-72.46	63.76	250.26

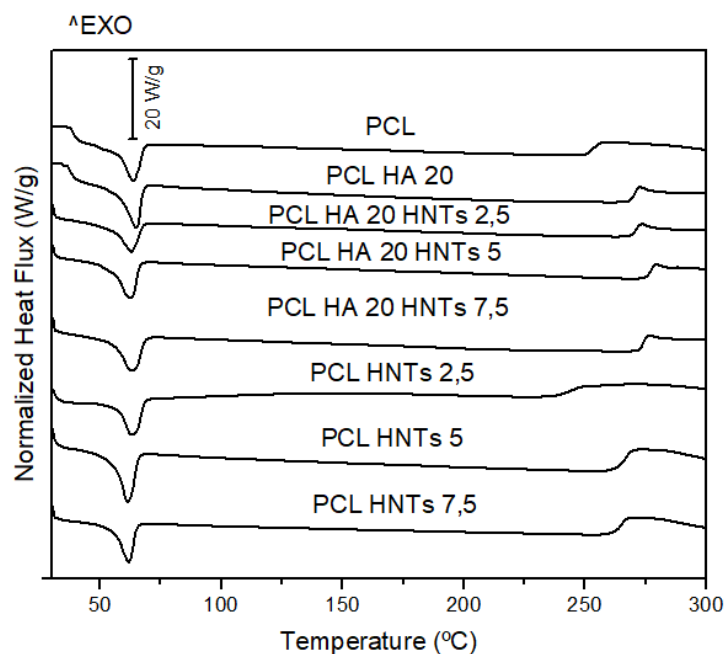


Figure 7 Comparison of Differential Scanning Calorimetry curves for PCL-based hybrids showing the normalized heat flux vs. temperature for PCL-based hybrids.

Thermogravimetric Analysis (TGA)

Samples with a mass between 6.0 g and 9.5 g were used for the analysis. The measured mass for samples was normalized in order to make the different curves comparable. Two experimental parameters were simultaneously determined for the polymer mixtures: mass loss (%) and mass residual ratio (%), these two parameters sum together to equal 100 %. Mass loss (%) and mass residual ratio (%) were studied in a range of temperature of 200 °C ($T_{\text{initial}}=300\text{ °C} - T_{\text{final}}= 500\text{ °C}$). Results are expressed in Table 16. TGA analyses exhibited, as expected, a residual mass of 30% corresponding to the total inorganic load of HA and HNTs. The representative curves of samples loaded with HA show high thermal stability supplied by calcium apatite present in the HA molecules. Only a 4% of weight loss of HA is attributed to the absorbed water and CO₂ registered from 600 to 1000°C [189]. In light of these results, the incorporation of HA and HNTs as fillers in PCL matrix has not drawbacks in common manufacturing processes. If the viscosity of the mixture increases in any case, only some adjustments in pressure or time cycle would be necessary.

Table 16 Thermogravimetric Analysis results for PCL-based hybrids. Samples with a mass between 6.0 g and 9.5 g were used for the analysis. Mass loss (%) and mass residual ratio (%) were studied in a range of temperature of 200 °C

Sample	$T_{\text{initial}} - T_{\text{final}}$ (°C)	Mass loss (%)	Mass Residual Ratio (%)
PCL HA 20	300-500	-77.63	22.4
PCL HA 20 HNTs 2,5	300-500	-76.62	23.4
PCLA HA 20 HNTs 5,0	300-500	-74.22	25.8
PCL HA 20 HNTs 7,5	300-500	-70.74	29.3
PCL HNTs 2,5	300-500	-88.58	11.4
PCL HNTs 5,0	300-500	-89.64	10.4
PCL HNTs 7,5	300-500	-87.41	12.6
PCL	300-500	-91.75	8.2

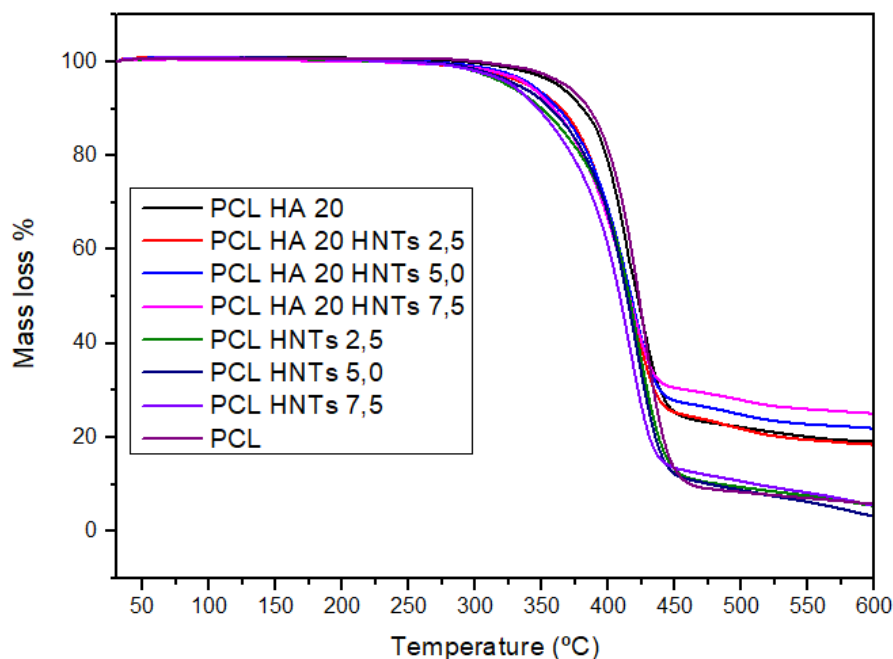


Figure 8 Comparison of TGA curves showing the mass loss (%) vs. temperature for PCL-based hybrids.

VICAT tests and heat deflection temperature tests (HDT)

To complete the thermal analysis, VICAT and HDT tests were performed in order to determine heat resistance characteristics of the material and to precisely define the thermal behavior in order to establish the polymer processability parameters. In injection moulding process, the removal of the piece from the mold has to be near or below the HDT temperature, this means that part deformation will be held within acceptable limits after removal.

For VICAT analysis two replicates per sample were tested, results shown in Table 17 gives the temperatures obtained from the two analysis T1 (°C) and T2 (°C), For HDT analysis, only one replicate per sample was tested, results shown in Table 17 gives the T1 (°C) of each sample. VICAT and HDT data shown in Table 17 revealed that the temperature change between samples was not higher than 2°C. For example, value of VICAT temperature of PCL is 54.3°C, while that of samples with the highest loading, PCL HA 20 HNTs 7.5 is 54.9°C. The increase in temperature with the addition of HNTs can be ascribed to the hydrogen bond interactions between the hydroxyl group present in HNTs surface and the carboxyl groups of ester linkage in PCL molecular chain [143]. These results do not provide substantial information other than that required to perform an optimum mixing of the material as it was specified in the temperature profile for the four extruder zone of the barrels.

Table 17 VICAT tests results and heat deflection temperatures (HDT) for PCL-based hybrids. VICAT analysis show results for two replicates of each sample, while HDT analysis show only one replicate for each sample.

Sample	VICAT				HDT
	T1 (°C)	T2 (°C)	\bar{x}	s	T1 (°C)
PCL HA 20	56.8	56.6	56.7	0.14	35.8
PCL HA 20 HNTs 2,5	55.6	55.6	55.6	0.00	37.6
PCLA HA 20 HNTs 5,0	55.0	55.2	55.1	0.14	37.4
PCL HA 20 HNTs 7,5	54.8	55.0	54.9	0.14	38.6
PCL HNTs 2,5	55.4	55.6	55.5	0.14	32.0
PCL HNTs 5,0	54.6	54.6	54.6	0.00	38.8
PCL HNTs 7,5	54.2	54.6	54.4	0.28	34.6
PCL	54.8	53.8	54.3	0.71	37.8

Dynamic Mechanical Thermal Analyses (DMTA)

Aiming to complete the thermal properties, Dynamic Mechanical Thermal Analyses were carried out. Considering the glass transition of PCL (-60 °C), one of the most reported thermal transitions, previous studies have demonstrated that the glass transition is not affected by the addition of different amounts of filler in polymeric matrix as PCL or polyethylene [190, 191]. For this reason, the temperature range studied in DMA analysis was set from 25 °C to 80 °C. Figure 9 plots the evolution of the storage modulus as a function of the temperature.

The obtained results for DMA indicate a decrease in the storage modulus around 50 °C - 55 °C as a consequence of the softening, due to the melting of PCL matrix leading to an increase in chain mobility. It can be seen an increment of around 109% in the storage modulus with the addition of HA. Furthermore, the addition of HNTs results in an increment of mechanical properties. Nevertheless, besides the increment of mechanical properties obtained when adding HNTs, the main purpose was to use them as delivery systems [153]. According to Lun *et al.* and Schmitt *et al.*, the composite with 7.5% of

HNTs guarantees enough tubular structures to be used as storage of specific drugs [192, 193].

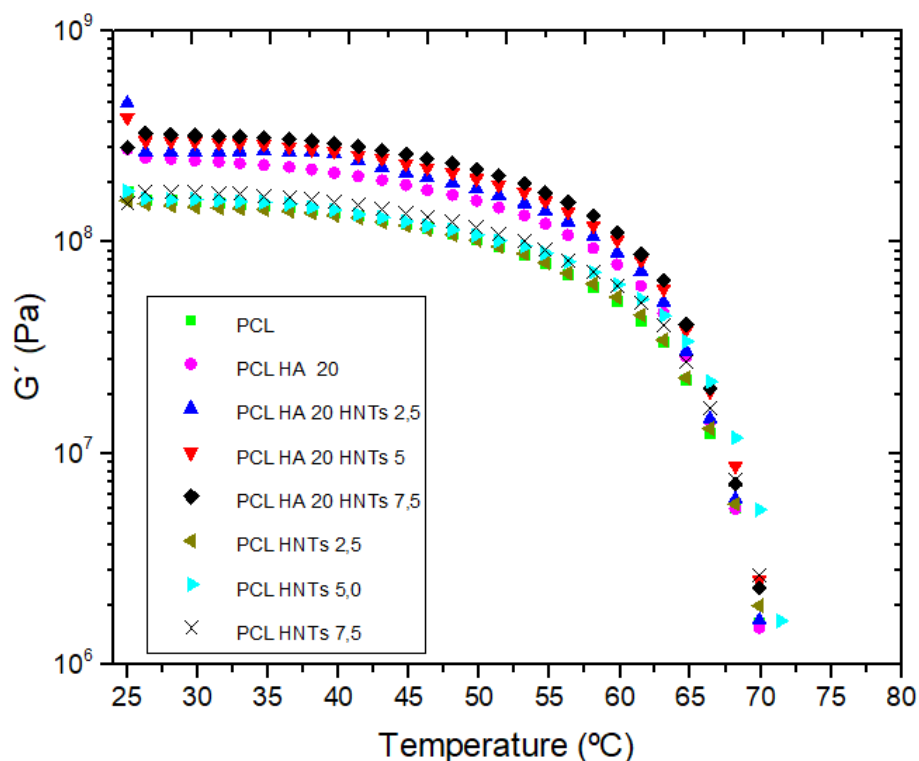


Figure 9 Dynamical Mechanical Thermal Analysis curves (storage modulus) for PCL-based hybrids.

4.1.2 Mechanical characterization

Shore D Hardness

Shore D Hardness was measured as a first approximation to determinate the mechanical properties. Results are shown in Table 18, five replicates of each sample were evaluated and the final average value (\bar{x}) and the standard deviation (s) was obtained. If Shore D Hardness value of neat PCL is compared with samples with 20% of HA and 7.5% of HNTs, an increase of 10.3% was obtained (p -value=0.4). Analysing the data, the introduction of HA and HNTs filler increases Shore D Hardness of the composites, so it seems evident that a synergic effect between the addition of HA and HNTs has been produced, increasing 5% the Shore D Hardness value. Therefore, it is possible that the filler acts filling the empty spaces between the polymer chains as different authors have demonstrated [194-196].

Table 18 Shore D Hardness results for PCL-based hybrids. Values represented for 5 replicates of each sample indicating the average value (\bar{x}) and standard deviations (s).

Sample	1	2	3	4	5	\bar{x}	s
PCL HA 20	49	50	49	50	50	49.6	0.55
PCL HA 20 HNTs 2.5	50	50	51	51	51	50.6	0.55
PCL HA 20 HNTs 5.0	50	50	51	51	50	50.4	0.55
PCL HA 20 HNTs 7.5	52	52	52	53	52	52.2	0.45
PCL HNTs 2.5	48	48	48	47	47	47.6	0.55
PCL HNTs 5.0	47	47	46	47	48	47	0.71
PCL HNTs 7.5	46	46	47	47	47	46.6	0.55
PCL	48	48	47	48	48	47.8	0.45

Charpy Impact tests

Charpy Impact results presented in Table 19 show different behaviour as function of filler type. For example, when both fillers are added to the polymer matrix, HA provides a decrease in toughness with the increase of the amount of HNTs. However, with HNTs alone, the capacity to absorb impacts increases considerably with the increase of HNTs amount in the polymer. The capacity to absorb impacts goes up to 50% when 7.5% of HNTs is added. These results suggest that strong interactions between PCL and HNTs are achieved, allowing more efficient load transfer [147]. Notwithstanding, one of the main drawbacks of loading polymers is the decrease of absorbed energy by the polymer during the impact or deformation [190].

Table 19 Impact Charpy analysis results for PCL-based hybrids. Values represented for 5 replicates of each sample indicating the average value (\bar{x}) and standard deviations (s).

Sample	1	2	3	4	5	\bar{x}	s
PCL HA 20	0.56	0.52	0.54	0.56	0.56	0.55	0.02
PCL HA 20 HNTs 2.5	0.43	0.43	0.46	0.45	0.44	0.44	0.01
PCL HA 20 HNTs 5.0	0.38	0.39	0.38	0.33	0.39	0.37	0.03
PCL HA 20 HNTs 7.5	0.3	0.33	0.34	0.32	0.32	0.32	0.01
PCL HNTs 2.5	0.47	0.53	0.49	0.48	0.51	0.50	0.02
PCL HNTs 5.0	1.18	1.17	1.06	1.14	1.09	1.13	0.05
PCL HNTs 7.5	0.78	0.85	0.8	0.8	0.81	0.81	0.03
PCL	0.53	0.53	0.53	0.52	0.5	0.52	0.01

Analysing the Charpy impact test, a failure surface morphology study was needed for two reasons: first of all, to give a logical explanation to the impact test results. Secondly, to observe the proper distribution of the HA and HNTs fillers in the PCL matrix. The study of the different images obtained by SEM showed two types of morphologies (Table 20). As a representative sample of composite with low toughness, the images of PCL HA 20 HNTs 7.5 sample (3.2 KJ/m²) showed a homogeneous surface, without excessive cracks, feature that is typically present in brittle materials [197]. These samples are characterized for the lack of failure surface. Moreover, in these samples is possible to observe a homogenous distribution of particles of HA and HNTs, entailing a correct compatibility between the fillers and the PCL matrix. This fact can be confirmed by the absence of large gaps between both components [198]. On the other hand, samples with high toughness, for example PCL HTNs 7.5 (8.1 KJ/m²), have a high roughness surface. In these samples the heterogeneity is higher than in samples with low toughness. The surface is characterized by a non-uniform appearance, with parallel lines of PCL consequence of the advanced rate of the cracks during the fracture. This kind of morphology can be detected in ductile samples. In the same way, samples with low toughness showed distribution of dispersed particles, which could facilitate the correct delivery of drugs present in the lumen of the HNTs.

Table 20 Impact Charpy SEM failure surface morphology for PCL-based hybrids

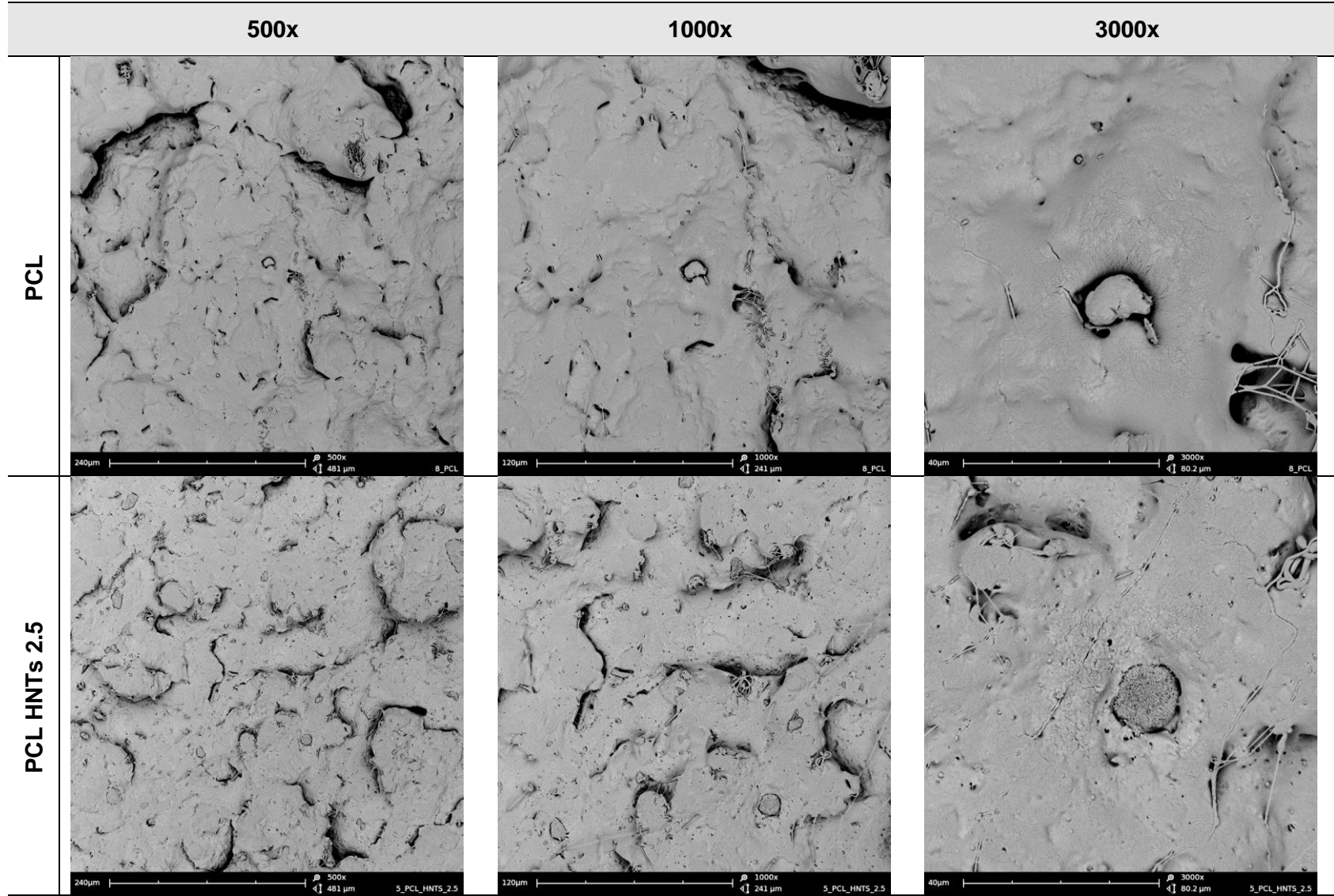


Table 19 Impact Charpy SEM failure surface morphology for PCL-based hybrids

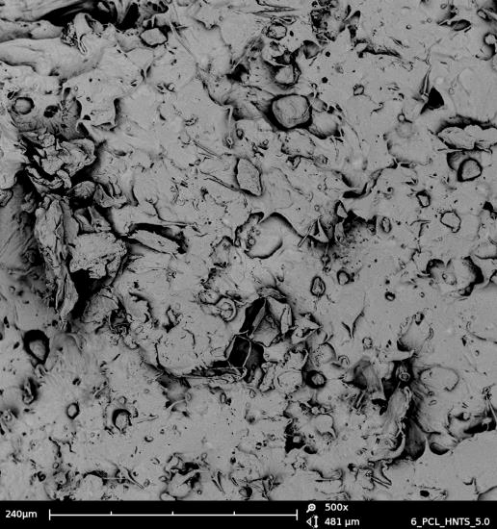
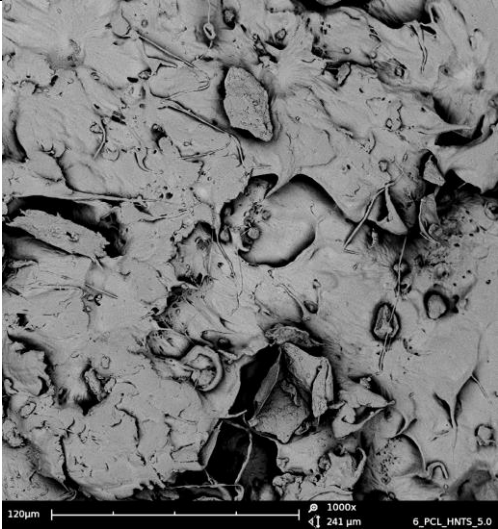
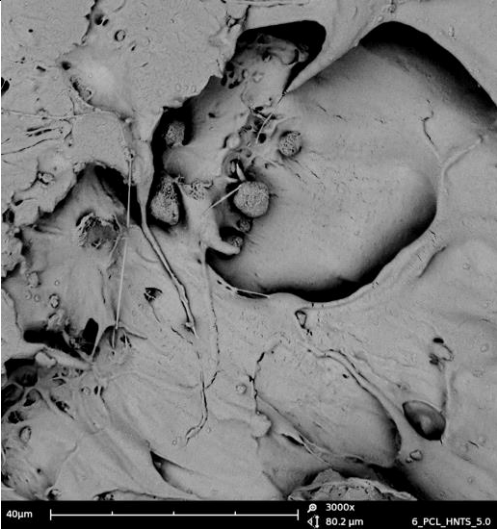
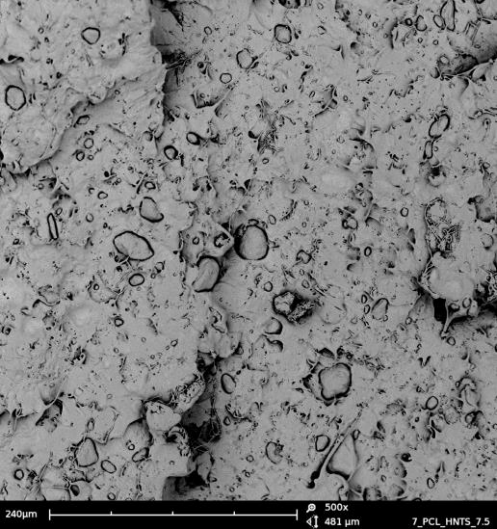
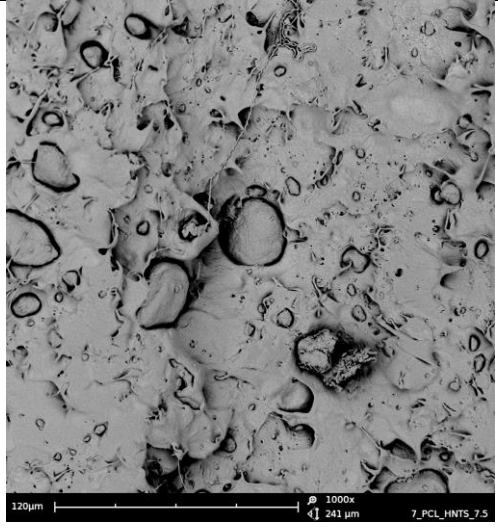
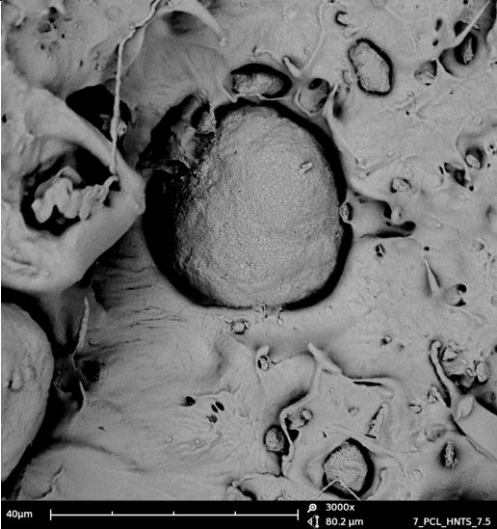
	500x	1000x	3000x
PCL HNTs 5.0			
PCL HNTs 7.5			

Table 19 Impact Charpy SEM failure surface morphology for PCL-based hybrids

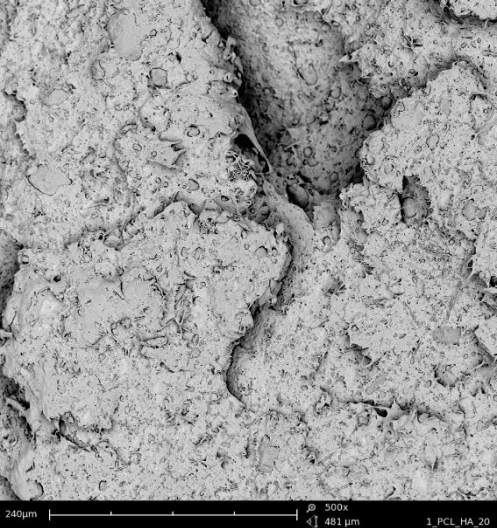
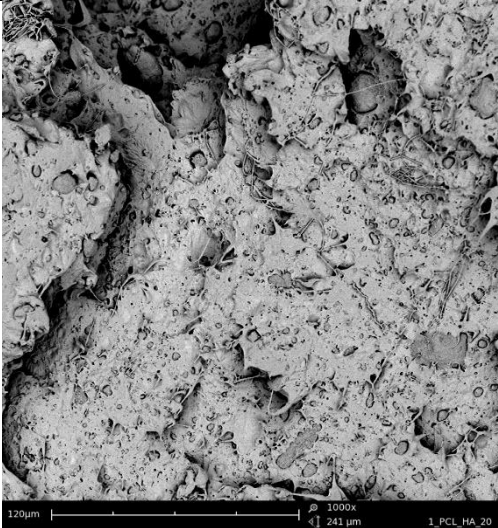
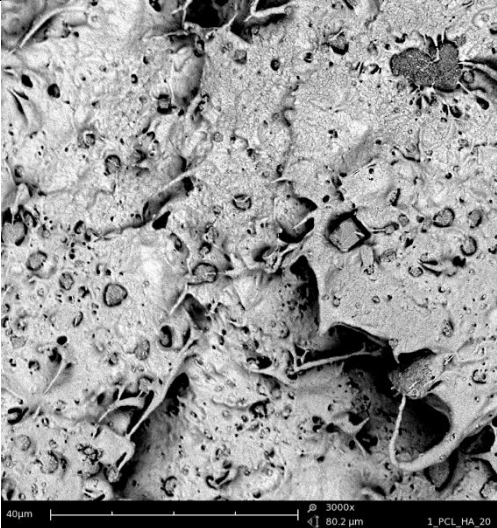
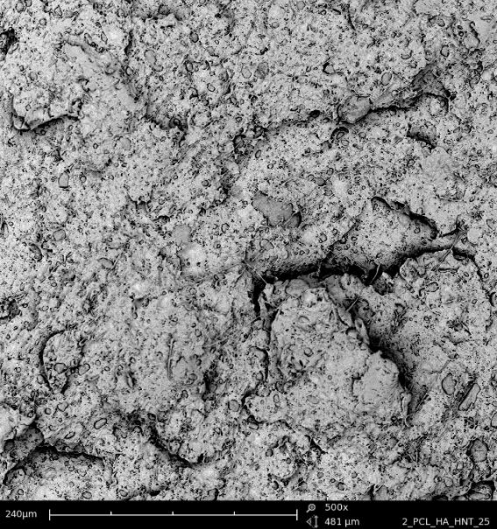
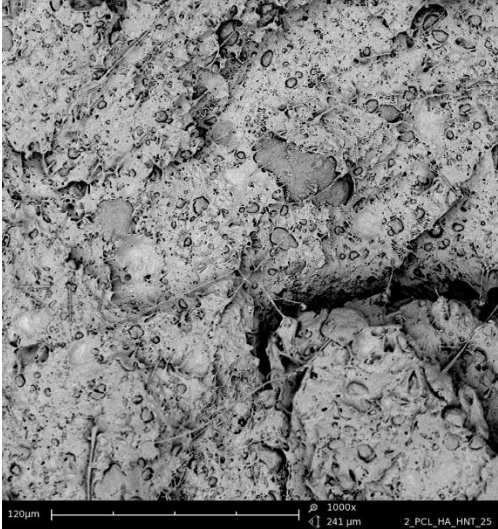

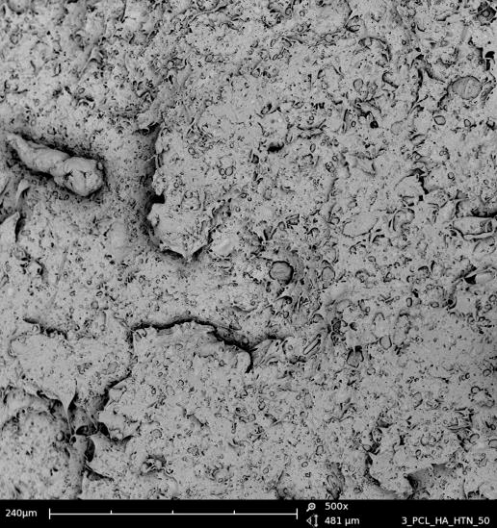
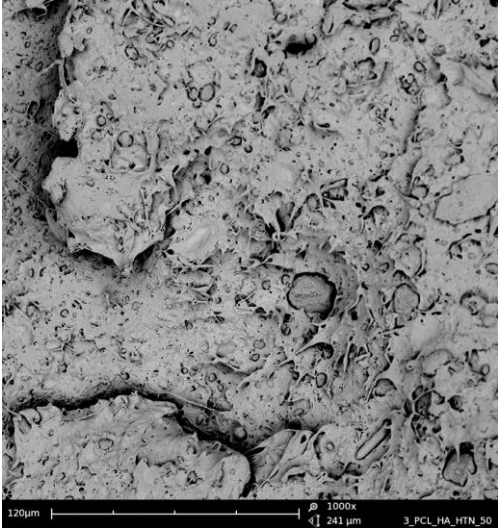
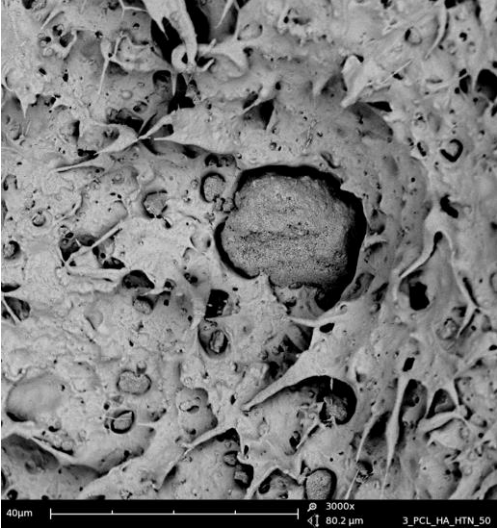
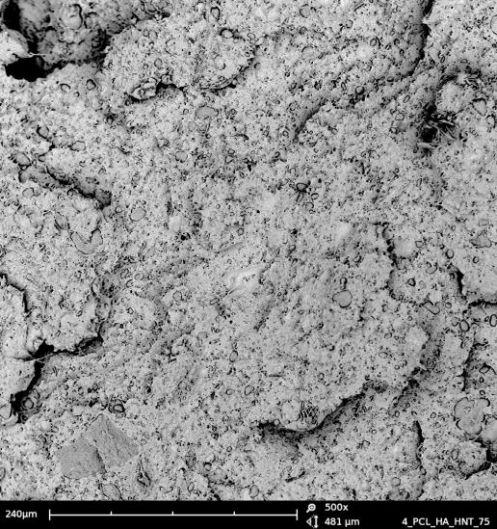
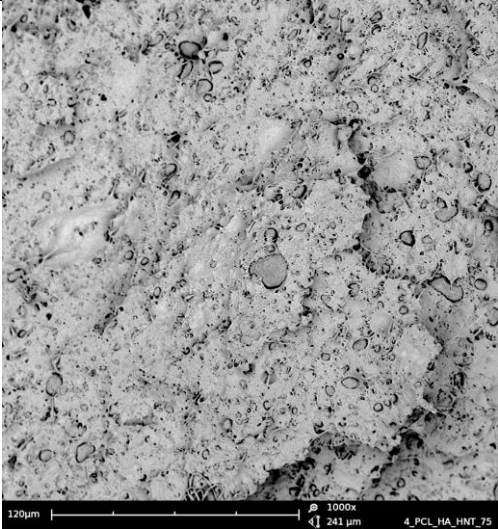

	500x	1000x	3000x
PCL HA 20			
PCL HA 20 HNTs 2.5			

Table 19 Impact Charpy SEM failure surface morphology for PCL-based hybrids

	500x	1000x	3000x
PCL HA 20 HNTs 5.0			
PCL HA 20 HNTs 7.5			

Flexural tests

Mechanical properties were completed with the determination of the flexural behaviour of the different composites. As it can be seen in Table 21, flexural modulus improves as the HNTs percentage increased, reaching values of up to 112.3% in samples with 20% of HA and 7.5% of HNTs, with a flexural modulus of 886.8 MPa (standard deviation =42.1). On the other hand, a different behaviour was registered with the lack of HA, samples containing only PCL and HNTs had practically identical flexural properties that raw PCL samples. This behaviour agrees with hardness results. Nevertheless, a decrease of flexural properties exceeding 7.5 wt.% of HNTs was tested by Liu *et al.* [143] and Prashantha *et al.* [144], correlating the overloading of HNTs with the generation of agglomerates acting as weak points and failure initiation sites.

However, the values of flexural moduli obtained are lower compared to the majority of human bones, as reported in [199]. Nevertheless, the values obtained can be compared with those of human trabecular bone, which is typically between 7000 and 25.000 MPa, although these values depend on different variables such as type of bone, age, location, and health factors [200-203].

Table 21 Flexural analysis results for PCL-based hybrids. Five replicates of each sample were studied, the mean value (\bar{x}) and standard deviation s are indicated.

		Load (N)	Flexural modulus (MPa)	Flexural strength (MPa)	Load (N)	Flexural modulus (MPa)	Flexural strength (MPa)
Sample		PCL			PCL HA 20		
mean value	\bar{x}	40.82	417.66	23.30	48.60	626.74	29.33
Standard deviation	s	1.71	28.69	1.39	1.93	32.36	1.15
Sample		PCL HNTs 2.5			PCL HA 20 HNTs 2.5		
mean value	\bar{x}	40.98	439.20	24.76	52.18	770.91	31.50
Standard deviation	s	0.95	27.46	0.57	1.47	50.18	0.90
Sample		PCL HNTs 5.0			PCL HA 20 HNTs 5.0		
mean value	\bar{x}	39.74	443.80	23.97	53.80	863.81	32.50
Standard deviation	s	1.05	27.22	0.64	1.95	32.20	1.19
Sample		PCL HNTs 7.5			PCL HA 20 HNTs 7.5		
mean value	\bar{x}	41.86	483.59	25.30	53.80	886.81	33.60
Standard deviation	s	1.47	53.75	0.89	1.58	47.08	2.75

Tensile tests

Tensile strength was measured to evaluate the capacity of the material to withstand loads tending to elongate. Results presented in Table 22 show similar values for all samples with values around 20 MPa. Elastic moduli show the best mechanical performances when the two fillers are added simultaneously, reaching values up to 230.22 ± 4.12 MPa with 20% of HA and 5.0% of HNTs.

Table 22 Tensile analysis results for PCL-based hybrids. Five replicates of each sample were studied, the mean value (\bar{x}) and standard deviation s are indicated.

		Tensile strength (MPa)	Young modulus (MPa)	Tensile strength (MPa)	Young modulus (MPa)
<i>Sample</i>		PCL		PCL HA 20	
mean value	\bar{x}	23.76	153.80	19.234	157.73
Standard deviation	s	0.29	15.0	2.03	13.2
<i>Sample</i>		PCL HNTs 2.5		PCL HA 20 HNTs 2.5	
mean value	\bar{x}	17.764	143.69	20.17	227.86
Standard deviation	s	2.014	3.81	1.57	23.0
<i>Sample</i>		PCL HNTs 5.0		PCL HA 20 HNTs 5.0	
mean value	\bar{x}	17.67	141.80	19.8	230.22
Standard deviation	s	3.01	6.04	0.73	4.11
<i>Sample</i>		PCL HNTs 7.5		PCL HA 20 HNTs 7.5	
mean value	\bar{x}	18.17	145.96	18.93	163.22
Standard deviation	s	2.50	12.2	0.34	9.21

4.1.3 General observations: Improvement of PCL mechanical properties with HA and HNTs

In the following, the different results obtained for thermal and mechanical analysis for PCL-based hybrids had been merged and compared in Figure 10. Analyzing the data (Figure 10), it is evident that a synergic effect between HA and HNTs in the polymeric matrix occurs. Comparing the results within different samples and PCL raw material, a noticeable improvement of mechanical properties was achieved with the simultaneous addition of the two fillers. If Shore D Hardness value of neat PCL is compared with samples with 20% of HA and 7.5% of HNTs, an increase of 10.3% was obtained (standard deviation=0.4). Flexural modulus improved as the HNTs percentage increased, reaching values of up to 112.3% in samples with 20% of HA and 7.5% of

HNTs, with a flexural modulus of 886.8 MPa (standard deviation=42.1). Young's Modulus was observed to increase to 109.3% with the addition of the two fillers reaching its greatest value of 449.6 MPa (standard deviation= 17.12) when 7.5% of HNTs was added. Dynamic Mechanical Analysis (DMA) at human body temperature, 37°C, indicates that the addition of HA and HNTs as fillers entails an enhancement of the storage modulus being again the hybrid loaded with 7.5% HNTs the material that shows the highest value. On the other side, samples with only HNTs as filler show a decrease in Shore D Hardness average values, with similar flexural and strength results compared to those of raw PCL samples. Hence, the addition of only HNTs does not provide a substantial improvement, but loading PCL with both fillers leads to an enhancement of mechanical properties with 20% HA and 7.5% HNTs.

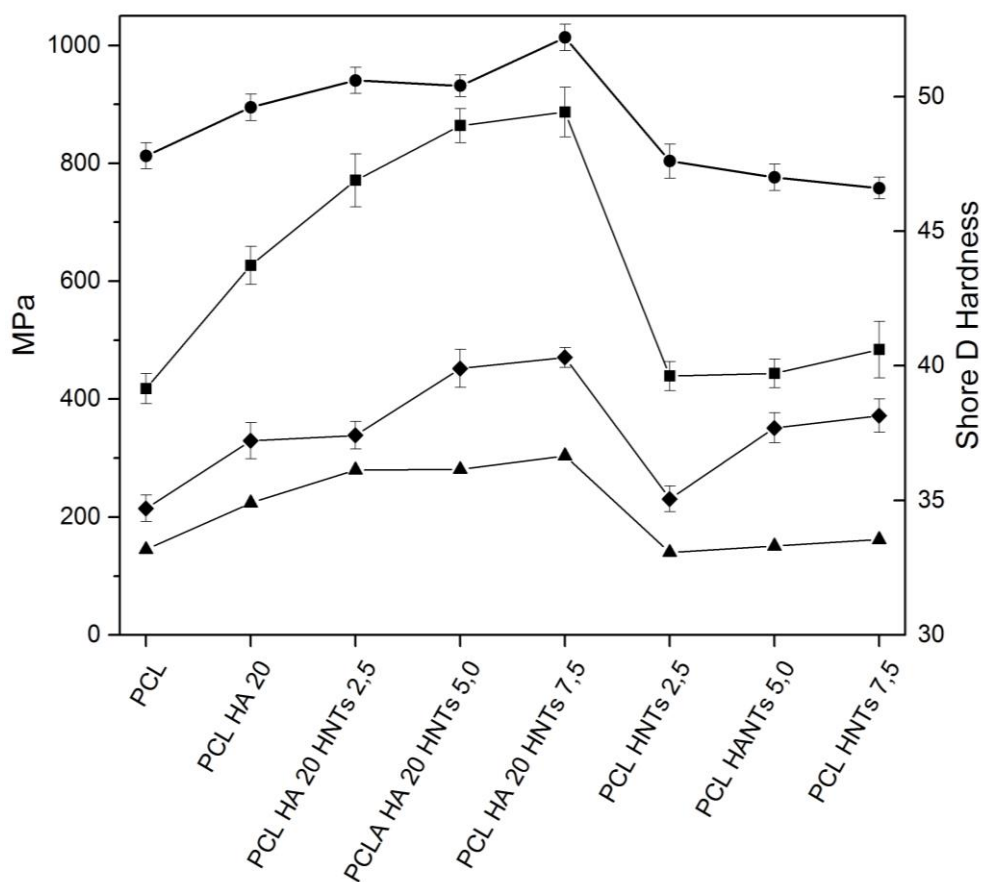


Figure 10 Comparison of mechanical properties of the different nanohybrids and PCL as control. —▲— DMA (MPa), —◆— Young's modulus (MPa), —■— Flexural modulus (MPa), —●— Shore D Hardness (secondary axis).

These results suggest that strong interactions between PCL, HA and HNTs occur, allowing a more efficient load transfer [147]. These must be hydrogen bondings between the hydroxyl groups present in the surface of HNTs and the carboxyls present in the ester

linkages of the PCL molecular chains [143]. Additionally, it cannot be ruled out that the fillers act to fill the empty spaces between the polymer chains as different authors have suggested [194-196].

Regarding the impact test, it highlights the difference in results as a function of the added filler. In general terms, a reduction of absorbed energy by the polymer is detected, resulting from the introduction of HA and HNTs simultaneously. A PCL unfilled has a toughness of 13.1 kJ/m², while as for example, in sample with 20% of HA and 7.5% of HNTs the toughness is reduced to 8.0 kJ/m². Thus, as expected, the addition of fillers provokes a lower toughness of samples. However, an interesting aspect is detectable: in samples with HNTs but not HA, the absorbed energy was greater. For example, samples with 5 or 7.5% of HNTs have a toughness around 25 kJ/m². Therefore, addition of only HNTs induces an increase in the toughness of the samples, possibly due to the tubular shape of HNTs, structure able to absorb energy during impacts.

In this section the first objective proposed in this thesis has been fulfilled by establishing the addition threshold and optimizing the addition rate. The materials with the best behaviour were those with 5 and 7.5 wt.% of HNTs, keeping constant the 20 wt.% of HA. Although both materials showed similar thermal and mechanical properties, a 7.5 wt.% of HNTs was established as the optimum percentage, because it allows a greater loading with the selected drug. Therefore, the second objective proposed in this thesis could be accomplished in the following section 4.1.4 through HNTs loading optimization with curcumin.

4.1.4 Optimization of the HNTs loading with curcumin

Thermogravimetric Analysis (TGA)

TGA curves presented in Figure 11 were obtained with a maximum temperature of 600°C to determine which of the three solvents used (water, ethanol or acetone) allowed the incorporation of the greatest amount of curcumin inside the HNTs lumen. Two significant mass loss stages are discerned in Figure 11 for all solvents within the same range of temperature and a similar residual mass. The first step, between 210°C-277°C with a mass loss of around 3.5%, is attributed to the thermal decomposition of curcumin, which is known to occur in two overlapped stages [204, 205]: the first one (215°C-354°C) represents the degradation of acetone acetaldehyde while the second (215°C-469°C) corresponds to the decomposition of phenyl oxyacetic acid molecules [205]. It is noteworthy to point out that a loading efficiency of merely 10 wt.% of nanotubes can be

achieved according to literature [206]. The second degradation stage identified for the three solvents, within the temperature range of 413°C-490°C and a mass loss of 12.5%, is due to a combination of thermal decomposition of curcumin and the dehydroxylation of HNTs [207]. Dehydroxylation has been postulated to be analogous to thermal dehydroxylation and degradation of halloisite due to the similarity between the structure and chemistry between halloisite and kaloinite [208], where most of the OH groups are removed. Although results are quite similar independently of the solvent, HNTs functionalized with acetone exhibit a slightly higher mass loss percentage taking into account both steps, hence a greater amount of curcumin is introduced in the HNTs lumen by using acetone as solvent.

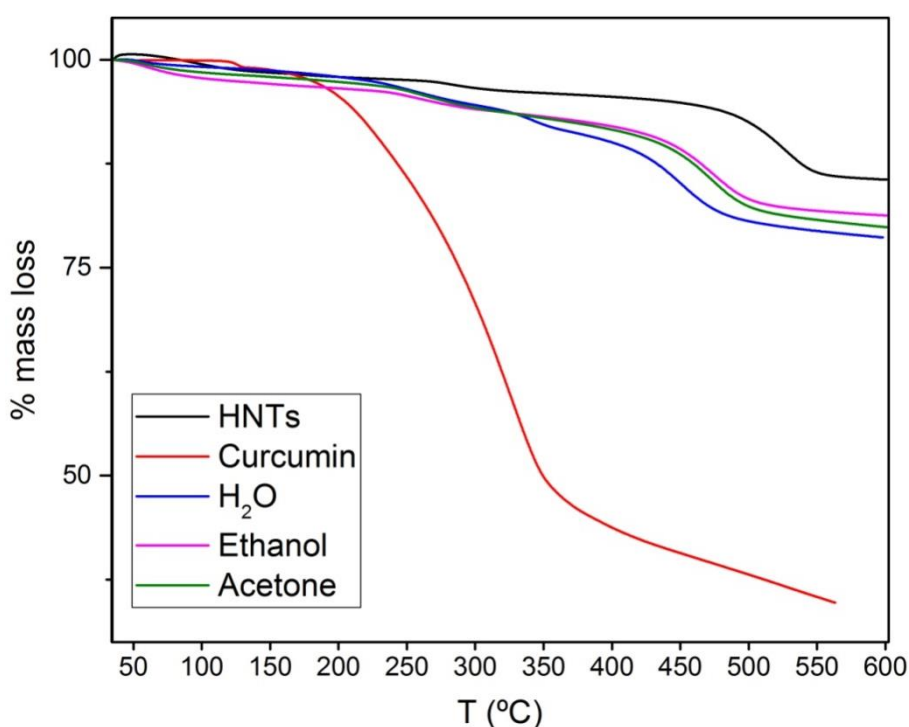


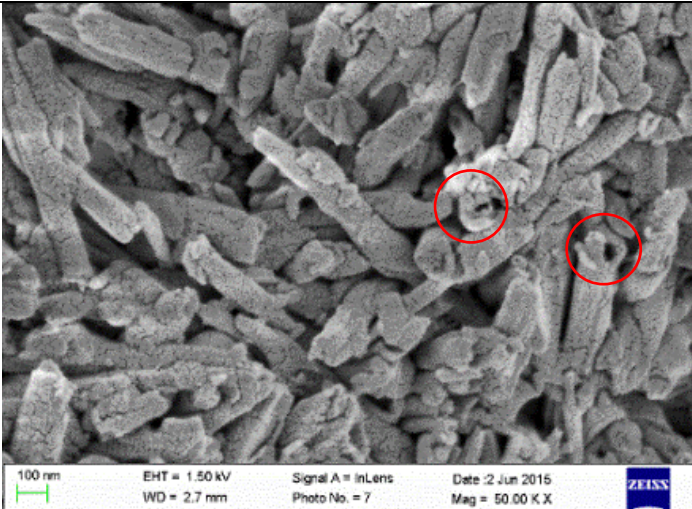
Figure 11 Normalized mass loss vs. temperature of halloysite nanotubes functionalized with curcumin using three different solvents (ethanol, acetone or water). The thermograms for HNTs and curcumin are given for comparison.

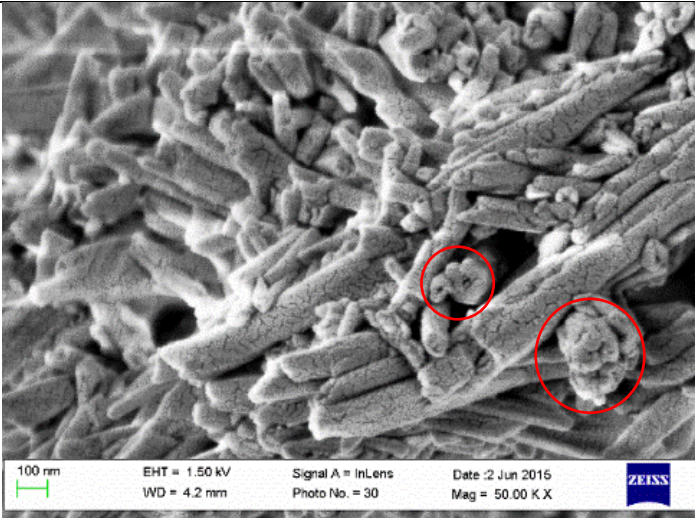
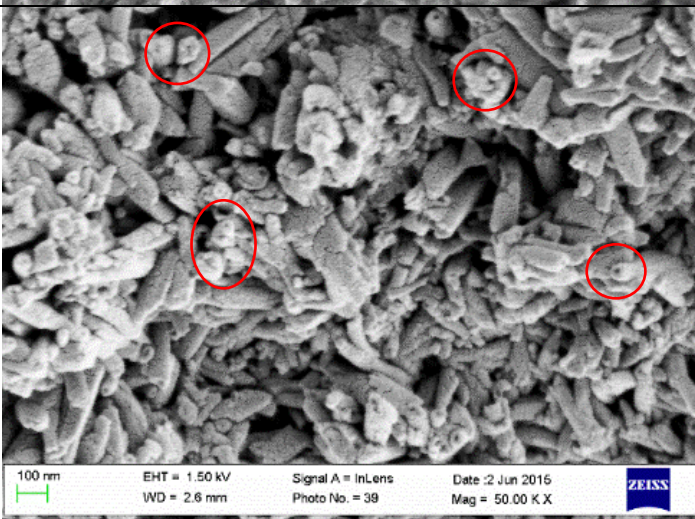
Scanning Electron Microscopy (SEM)

SEM images shown in Table 23, were obtained with the aim of visually assessing the functionalization efficiency corresponding to each solvent. Traces of active agent attached to the outer surface of HNTs cannot be excluded, even though it is difficult to distinguish them. Nonetheless, the same loading procedure was followed by Riela *et al.* [209] using ethanol as solvent and reported a successful encapsulation. Similar results using poly(amidoamine) dendrimers as container were also reported by Wang *et al.*

[210]. If attention is paid to the inner diameter of the nanotubes in the SEM images, narrower diameters can be observed for HNTs when acetone was used as a solvent, suggesting that curcumin molecules are attached to the inner surface of the nanotubes. These results agree with the solubility of curcumin in each solvent (solubility values in Table 23 were provided by the supplier Sigma Aldrich) and the TGA results, concluding that using acetone as solvent, yields the highest amount of curcumin inside the HNTs lumen. The functionalization efficiency can thus be linked to the solubility of curcumin in each solvent. With curcumin being nearly insoluble in water (<0.1 mg/ml), its concentration in the solution would be small, hence only a small amount of curcumin would be introduced into HNTs lumen using water as solvent. Conversely, with a solubility of >50 mg/mL in acetone, the amount of curcumin inside the nanotubes is expected to be greater for the same dissolution volume compared with those in water or ethanol (the solubility of curcumin in ethanol is 10 mg/mL).

Table 23. Comparison of the curcumin loading efficiency in HNTs using SEM images to evaluate the diameter of the loaded nanotubes with curcumin using water, ethanol or acetone as a solvent.

Water	
Solubility < 0.1 mg/ml 3.95% mass loss 1st step 12.47% mass loss 2nd step	<p>100 nm EHT = 1.50 kV Signal A = InLens Date :2 Jun 2015 WD = 2.7 mm Photo No. = 7 Mag = 50.00 K X ZEISS</p>

<i>Ethanol</i>	
<p style="text-align: center;">Solubility 10 mg/ml</p> <p style="text-align: center;">3.10% mass loss 1st step</p> <p style="text-align: center;">12.35% mass loss 2nd step</p>	
<i>Acetone</i>	
<p style="text-align: center;">Solubility >50 mg/ml</p> <p style="text-align: center;">4.46% mass loss 1st step</p> <p style="text-align: center;">13% mass loss 2nd step</p>	

Influence of HNTs loaded with curcumin incorporated to the PCL matrix on its mechanical and thermal properties

Incorporation of HNTs, previously loaded with curcumin, to PCL matrix provokes a reduction on mechanical properties as compared with those of PCL HA20 HNTs7.5 samples (Table 24). The improvement of flexural modulus with the addition of HA and HNTs to the PCL matrix was 112.33%. However, when HNTs were functionalized with curcumin, the flexural modulus decreased 30.55%. Nevertheless, the results obtained for PCL HA20 HNTs7.5 + curcumin are 47.47% higher than those of neat PCL. A significant reduction of tensile strength was also observed with the addition of curcumin being 50% less than that of PCL HA20 HNTs7.5 samples.

Table 24. Mechanical properties of PCL, PCL HA20 HNTs7.5 and PCL HA20 HNTs7.5+curcumin samples. Values represented for 5 replicates of each sample indicating the average value (\bar{x}) and standard deviations (s).

	PCL	PCL HA20 HNTs7.5	PCL HA20 HNTs7.5 + curcumin
Flexural modulus (MPa)			
average value (\bar{x})	449.45	886.8	615.91
Standard deviation (s)	20	37.53	3.36
Tensile strength (MPa)			
average value (\bar{x})	214.82	449.62	224.85
Standard deviation (s)	18.45	17.12	4.73

Thermal analysis of HNTs loaded with curcumin and incorporated to PCL revealed an increment of 5°C in the melting temperature when comparing with neat PCL and PCL loaded with HA and HNTs (Table 25). This effect can be explained by a complex two-step nucleation-driven degradation mechanism induced by the introduction of fillers [188], which appears to provide a greater thermal stability range without affecting the injection moulding processability.

Table 25. Thermal properties of PCL, PCL HA20 HNTs7.5 and PCL HA20 HNTs7.5+curcumin samples, where $T_{m,onset}$ is the temperature at the melting onset, $T_{m,peak}$ is the temperature at the peak maximum, and Δh_m is the heat adsorbed per mass unit.

Sample	$T_{m,onset}$ (°C)	$T_{m,peak}$ (°C)	Δh_m (J/g)
PCL	54.15	58.27	54.81
PCL HA20 HNTs7.5	53.32	60.03	40.78
PCL HA20 HNTs7.5 + curcumin	53.43	60.92	43.1

SEM images were taken to qualitatively analyse the morphology of the materials (Figure 12). Clusters with size around 6 μm were observed in PCL HA20 HNTs7.5 + curcumin samples, which could explain the loss of mechanical properties (Table 24). Indeed, HNTs aggregates are known to usually act as crack initiation sites leading to sudden failure of

the material [144, 211]. Aggregate formation seems to be accentuated during the drying process after functionalization of HNTs with the consequent reduction of water molecules, resulting in less interactions between them and HNTs [212]. Aggregates of hollow nanotubes are induced by edge to edge and face to edge interactions between HNTs resulting in zig-zag structures [213]. In further works, the aggregates formation could plausibly be avoided by the dispersion of the powder in polar solvents such as acetone, followed by mechanical stirring [214], alternatively or simultaneously to the modification of the HNTs surface [215], and additionally with successive extrusion steps previous to injection moulding [211].

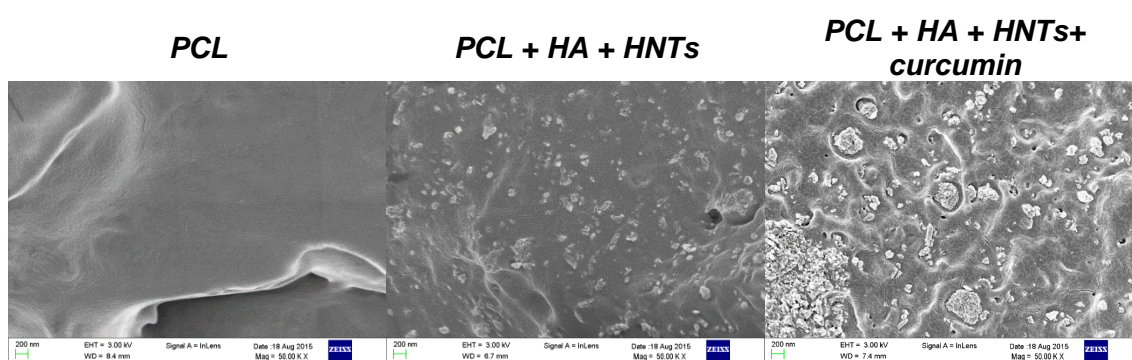


Figure 12. SEM images of PCL, PLA HA20 HNTs7.5 and PCL HA20 HNTs7.5 + curcumin samples, the last two showing HNTs aggregates.

4.1.5 Curcumin delivery rate

In order to evaluate the delivery rate of curcumin, firstly a calibration curve was prepared. For this purpose, three curcumin dissolutions with increasing concentrations were prepared in PBS (0.0025 mg/10mL, 0.005 mg/10mL and 0.01 mg/10mL) and the absorbance was measured at 263nm, 350nm and 420nm.

Evaluated samples are specified in Table 10 (HNTs, PCL+7.5%HNTs and PCL + 0.75% curcumin). Two replicates per sample were placed in different vials containing 10mL of PBS. Aliquots were taken every two days and their absorbance was measured. Results are presented in Figure 13 showing accumulation of curcumin concentration (mg/10mL) vs time (days).

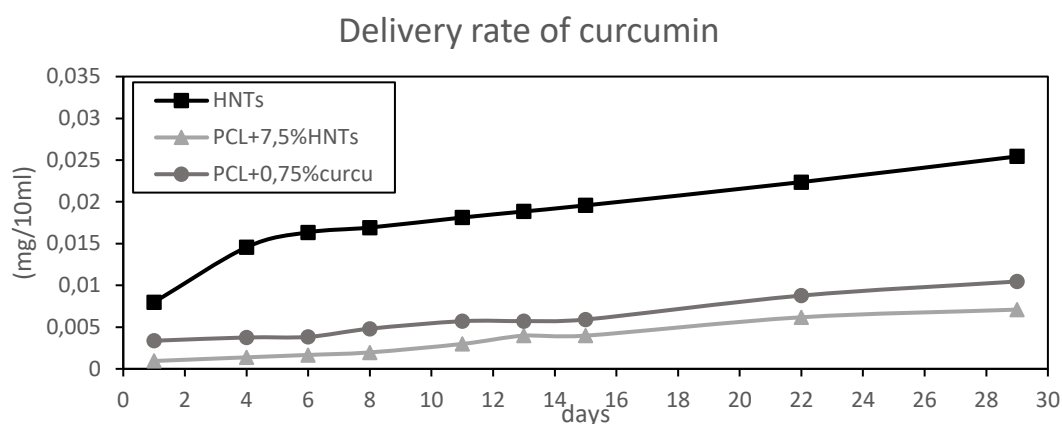


Figure 13 Curcumin delivery rate measurements presented as cumulative concentration vs time for HNTs loaded with curcumin and dispersed in PBS, PCL aditivated with HNTs loaded with curcumin, and PCL aditivated with curcumin.

A sharp increase of curcumin release can be seen during the first four days of the experiment, especially in the dispersed HNTs samples, probably because of remanent curcumin onto the nanotubes surface which was not properly removed after the loading procedure. A general tendency of decrease of the curcumin amount released is seen over time. After one week of release, at day 22 and 29, the concentration increases for all the samples due to the greater time of delivery with regard to the previous measures. Results are coherent with a typical kinetics of delivery [179, 180]. In view of the results, at initial stages the concentration of curcumin delivered is higher in the HNTs loaded with curcumin dispersed in PBS, because of the remanent curcumin attached to the HNTs outer surface. However, when curcumin is introduced into the nanotubes and entrapped in the polymer, the release rate decreases. Notwithstanding, at longer periods of time, the three curves meet, revealing that the delivery kinetics is comparable for the three studied samples.

4.1.6 General Observations: Loading HNTs with curcumin and delivery rate

HNTs loading with curcumin using saturated solutions of acetone, ethanol and water, was studied through a qualitative analysis of curcumin solubility, Thermal Analysis and Scanning Electron Microscopy. Although the techniques used gave indirect results for loading efficiency, the observations suggest that the greatest efficiency was obtained when acetone was used as a solvent. First of all, curcumin solubility was greater in acetone compared with ethanol or water. Thus, an equal volume of solvent introduced in the HNTs lumen will entail higher concentration of curcumin. Secondly, TGA results for HNTs functionalised with acetone gave higher mass loss percentage in the first and

second step associated to the thermal decomposition of curcumin, implying a greater amount of curcumin introduced in the HNTs lumen. Finally, SEM images showed narrower diameters for HNTs when acetone was used as a solvent, suggesting that curcumin molecules are attached to the inner surface of the nanotubes.

Subsequently, HNTs functionalized with curcumin in acetone saturated solution were mixed and injected with PCL and HA to be mechanically and thermally tested. The results showed that functionalization of HNTs with curcumin gave a reduction of the mechanical properties compared with the hybrids studied in the previous section without functionalization of HNTs. The properties loss is due to the agglomerates formation during the drying process. The curcumin delivery rate was also studied observing a decreased activity when curcumin is introduced into the nanotubes and entrapped in the polymer. However, at longer periods of time, the three curves (curcumin from HNTs, from neat PCL and from HNTs-loaded PCL) run in parallel, revealing that the delivery kinetics is comparable for the three studied samples.

4.2 Second chapter - Study of the influence of the addition of HA and HNTs on the morphological properties of PCL- and PHEMA-based polymers

4.2.1 Structural properties

Comparison of PCL/PLA based hybrids mechanical properties

Mechanical properties for PCL/PLA based hybrids were studied in order to verify the improvement on Young and Flexural moduli when PCL is mixed with PLA and loaded with HA (Figure 14 and Table 26). Accordingly, PCL, PLA and PCL/PLA raw polymers and additivated with 20wt% HA were melt injected following the specifications on section 3.2.1 *PCL/PLA-based hybrid samples*. Five replicates of each sample were studied. Young modulus gave an increase of 281.72 % when comparing PCL/PLA with PCL raw polymer. When HA was added to the PCL/PLA polymer matrix, an increase of 271.42 % was observed compared with PCL aditivated with HA. Similar results were obtained for Flexural modulus with an increase of 332.17 % for PCL/PLA samples and an 364.02 % when loading with HA. In view of these results, mechanical properties of PCL are effectively improved when mixing with 50wt% of PLA and 20wt% of HA.

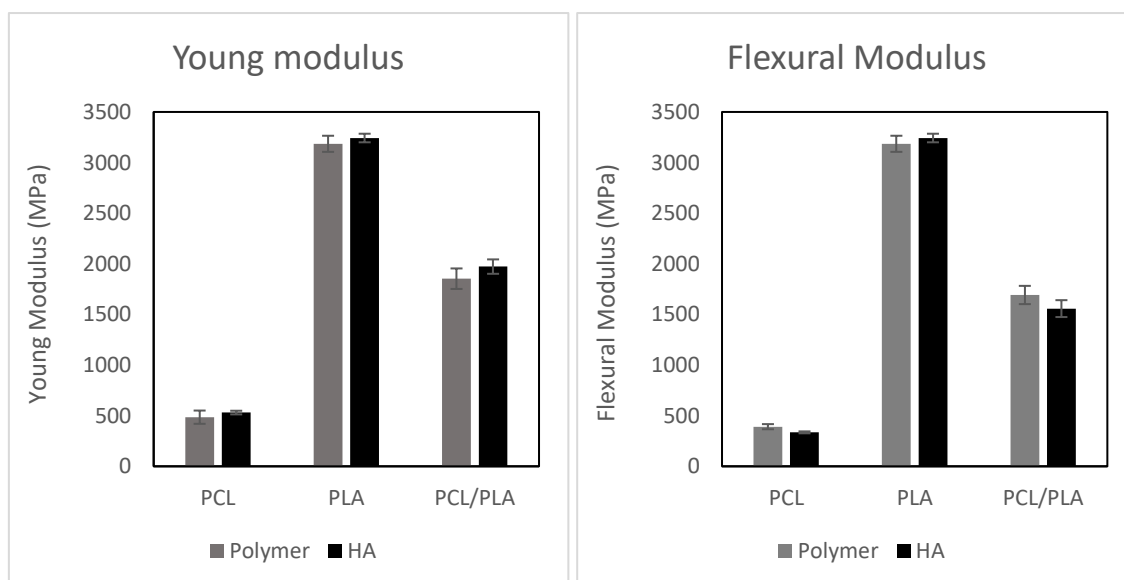


Figure 14 Representation of Mechanical properties for PCL/PLA based hybrids. On the left Young modulus and standard deviation of PCL/PLA based hybrids. On the right, Flexural modulus and standard deviation of PCL/PLA based hybrids.

Table 26 Mechanical properties for PCL/PLA based hybrids. Young and Flexural moduli mean value for 5 replicates of each sample and the standard deviation.

	<i>Young Modulus (MPa)</i>			<i>Flexural modulus (MPa)</i>		
	<i>PCL</i>	<i>PLA</i>	<i>PCL/PLA</i>	<i>PCL</i>	<i>PLA</i>	<i>PCL/PLA</i>
Polymer (\bar{x})	485.48	3185.50	1853.17	391.61	3185.50	1692.43
s	65.54	79.63	101.32	25.41	79.63	90.01
Polymer + HA (\bar{x})	531.13	3242.80	1972.76	335.73	3242.80	1557.86
s	18.14	42.48	71.03	9.43	42.48	83.45

Energy-Dispersive X-Ray Spectroscopy (EDS)

SEM images were first taken to qualitatively analyze the morphology of the materials. Results showed homogeneous flat surfaces in all samples, independently of their composition (data not shown). Surface and transversal section EDS mapping images were obtained to assess the distribution of the loadings throughout the samples: calcium (Ca) and phosphorus (P) standing for HA and aluminum (Al) and silicon (Si) for HNTs, while oxygen (O) and carbon (C) show the polymer matrix. Figure 15 shows the corresponding mappings for the transversal sections of samples loaded with HA and HNTs. The surfaces showed in all cases a homogeneous distribution of HA and HNTs. Transversal section images show that HA is homogeneously distributed throughout the samples in all cases (for this reason, images of samples loaded only with HA are not shown). However, HNTs are distributed in the samples in a dissimilar way, depending on their chemical composition: on PCL samples they are well dispersed, but form small sporadic aggregates when PCL is combined with PLA, and these aggregates are more prevalent and increase in size in the P(HEMA-co-EMA) copolymer and the PHEMA homopolymer, not being significant differences between them. This effect could be explained due the hydrophobic character of the nanotubes, given by its relatively low content of hydroxyl groups on their surfaces, resulting in a good dispersion in non-polar polymers [216] and creating agglomerations in hydrophilic polymers due to the lower interfacial adhesion.

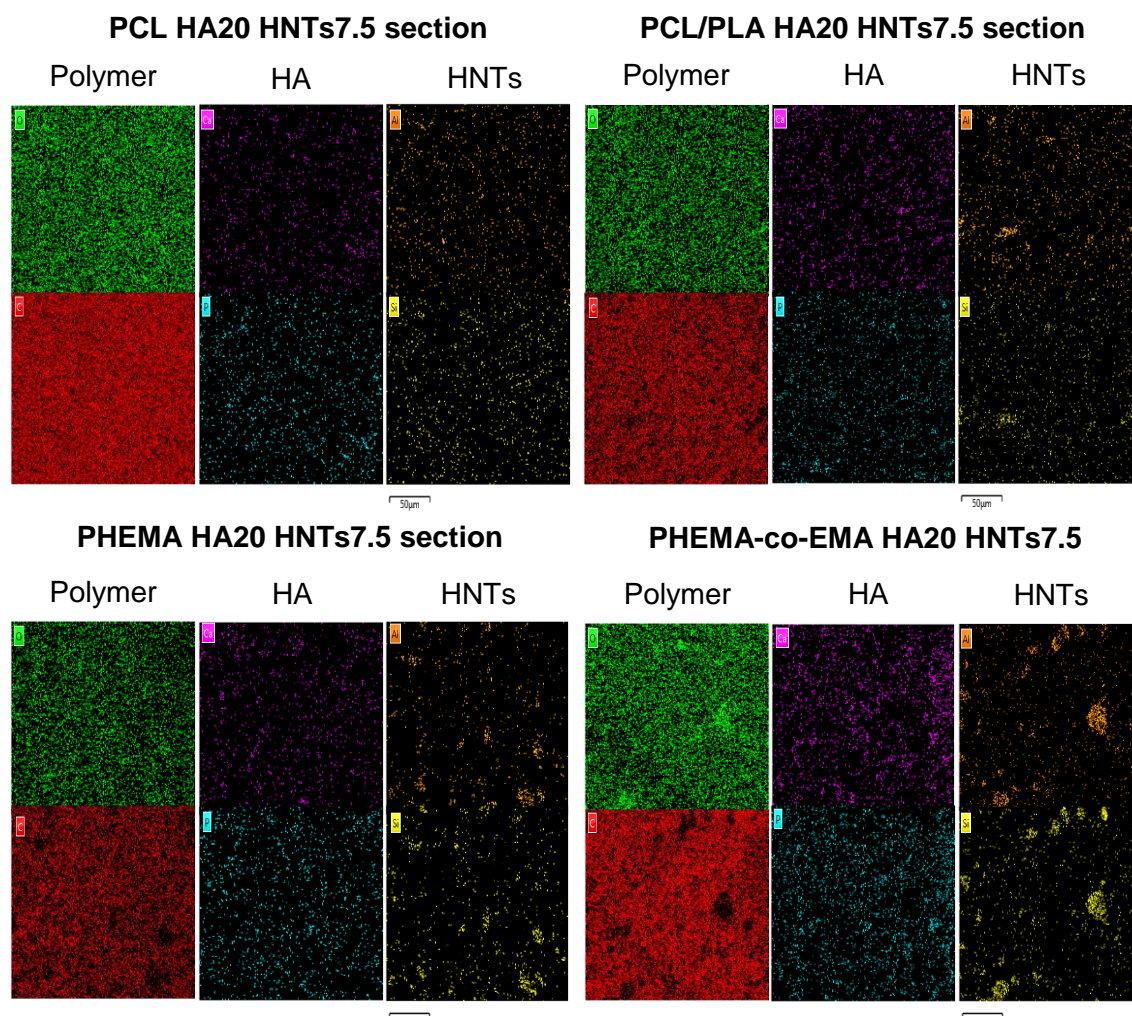


Figure 15 Energy-dispersive X-ray spectroscopy (EDS) for copolymers samples loaded with HA and HNTs (PCL HA20 HNTs7.5, PCL/PLA HA20 HNTs7.5, PHEMA HA20 HNTs7.5, PHEMA-co-EMA HA20 HNTs7.5)

4.2.2 Hydroxyapatite nucleation

Aiming to analyse the formation of a hydroxyapatite layer on the surface of the different materials, microscopic images were taken, and 5000 magnifications images are presented in Table 27. EDS spectra were also obtained in order to validate the formation of a layer of hydroxyapatite and the Ca/P ratio.

From the results presented in Table 27, after 7 days in SBF, the PCL based hybrids did not efficiently induce any apatite growth, while the polymethacrylate-based hybrids did. The precipitates on the PCL, PCL/PLA and PHEMA without needle-like conformation correspond to the salts dissolved in the SBF medium, generally NaCl (EDS spectra not shown). In PHEMA surface some HA crystals have nucleated and precipitated salts from the SBF are also observed simultaneously. P(HEMA-co-EMA) surface exhibits plenty of precipitates forming big and defined cauliflowers with needle-shaped crystals intricately

intertwined forming the typical porous cauliflower HA structures [119]. Once apatite has nucleated in a certain location, it grows outwards in a radial pattern [217], leading to cauliflower or hemispherical structures that merge to form a continuous layer.

Samples with HA fillers provide nucleating sites, also silanol groups (Si-OH) present in the HNTs would provide favourable sites for apatite nucleation, although this mechanism is not totally clear yet it is speculated that electrostatic interactions drive to the formation of calcium silicates [120]. Comparing neat polymers (especially PCL and PCL/PLA blend) with materials aditivated with HA and HNTs, nucleation efficiency increases with the addition of the fillers. It is thought that both polar carboxy and hydroxy groups induced apatite nucleation [119].

Greater bioactivity is seen for P(HEMA-co-EMA) with respect to PHEMA due to the less hydrophilic character of P(HEMA-co-EMA), in which the number of polar groups available on the surface for nucleation per unit volume is greater. Consequently, the absorption efficiency of Ca^{2+} ions from the SBF solution by the P(HEMA-co-EMA) surface is higher, increasing the Ca^{2+} ion concentration at the surface and thus, the formation of nucleation sites for the Ca-P [218]. Grape-like aggregates of cauliflowers observed, especially in P(HEMA-co-EMA), are generated by the secondary nucleation sites provided by the apatite molecules of the first layer, giving place to spherical formations which grow perpendicularly to the surface leading to the formation of clusters or grape-like structures [219].

From the EDS results, the Ca/P atomic ratio has been calculated in each case for comparison with that of the stoichiometric HA ($\text{Ca}_{10}(\text{PO}_4)_6(\text{OH})_2$), Ca/P $\frac{1}{4}$ 1.67 [220]. In most of the calculations presented in Table 27, Ca/P atomic ratio remains between the accepted values of 1.3-2.0; thus, there are calcium phosphate deposits with cauliflowers morphology that resembles physiological apatite structures.

Table 27 SEM and EDS images taken for hydroxyapatite nucleation analysis. 5000 magnification pictures are shown, and formation of hydroxyapatite cauliflower-like structures can be observed in the surface of some materials. The Ca/P ratio was calculated in order to verify the hydroxyapatite layer formation.

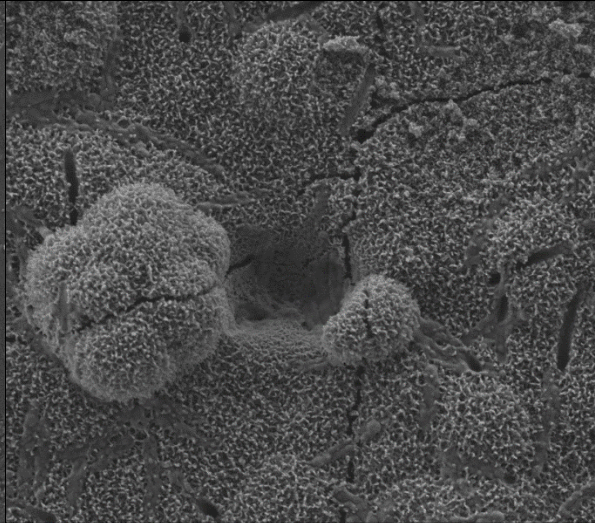
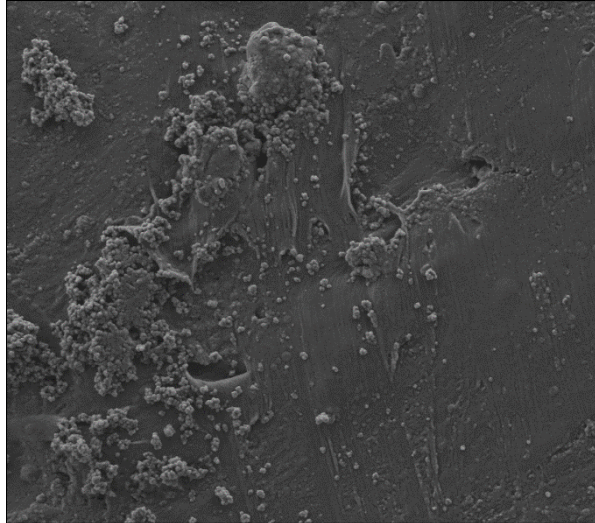
7 days					
PCL		PCL HA20		PCL HA20 HNTs7.5	
<small>Mag = 5.00 K X ULTRA 55.44.22</small> <small>WD = 7.4 mm EHT = 2.00 kV Noise Reduction = Pixel Avg.</small>		<small>Mag = 5.00 K X ULTRA 55.44.22</small> <small>WD = 6.6 mm EHT = 2.00 kV Noise Reduction = Pixel Avg.</small>		<small>Mag = 5.00 K X ULTRA 55.44.22</small> <small>WD = 5.4 mm EHT = 2.00 kV Noise Reduction = Pixel Avg.</small>	
Ca/P=1.87		Ca/P=1.7		Ca/P=1.65	

14 days

PCL

PCL HA20

PCL HA20 HNTs7.5



Mag = 5.00 K X
ULTRA 55-44-22

1 μm

WD = 5.2 mm

EHT = 2.00 kV

Noise Reduction = Pixel Avg.

Signal A = SE2
ESB Grid = 800 V

Ti Mag = 5.00 K X
ULTRA 55-44-22

1 μm

WD = 5.4 mm

EHT = 2.00 kV

Noise Reduction = Pixel Avg.

Signal A = SE2
ESB Grid = 800 V

Time Mag = 5.00 K X
ULTRA 55-44-22

1 μm

WD = 4.1 mm

EHT = 2.00 kV

Noise Reduction = Pixel Avg.

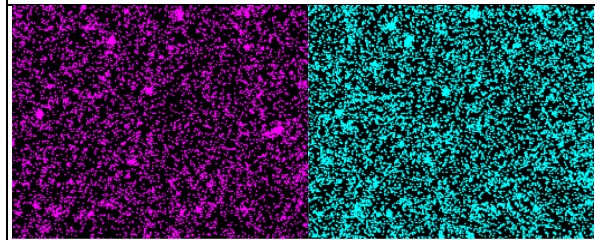
Signal A = SE2
ESB Grid = 800 V

Time

Ca/P=1.55

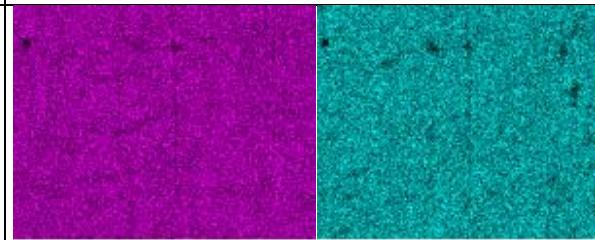
Ca/P=1.45

Ca/P=1.55



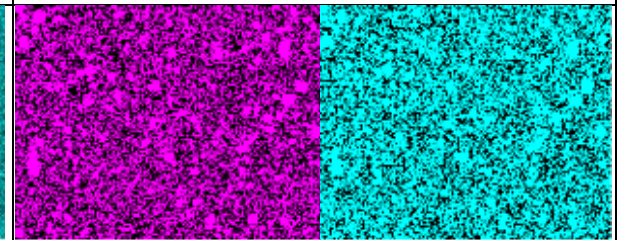
50 μm

50 μm



50 μm

50 μm



50 μm

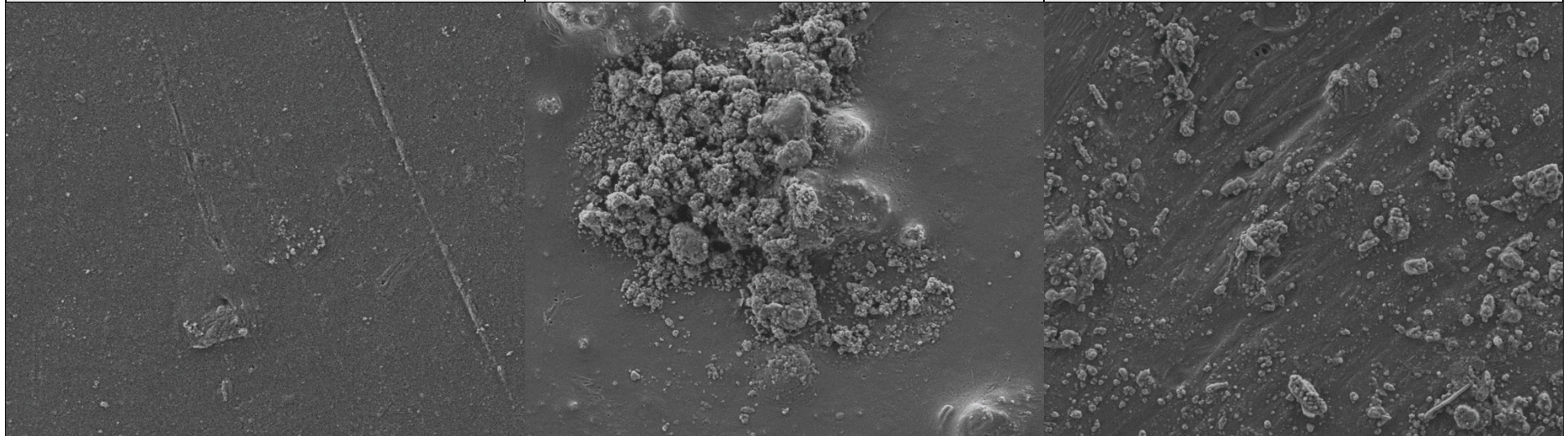
50 μm

7 days

PCL/PLA

PCL/PLA HA20

PCL/PLA HA20 HNTs7.5

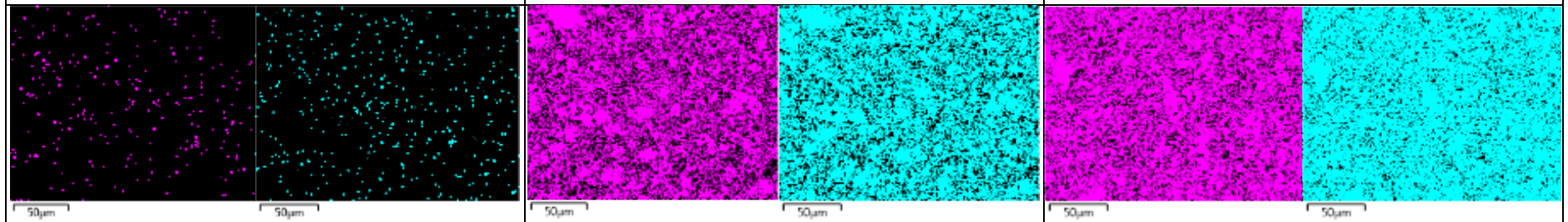


Mag = 5.00 K X 1 μm WD = 5.7 mm EHT = 2.00 kV Signal A = SE2 Time :11: Mag = 5.00 K X 1 μm WD = 5.6 mm EHT = 2.00 kV Signal A = SE2 Time :11: Mag = 5.00 K X 1 μm WD = 5.4 mm EHT = 2.00 kV Signal A = SE2 Time :11:
ULTRA 55.44.22 Noise Reduction = Pixel Avg. ESB Grid = 800 V ULTRA 55.44.22 Noise Reduction = Pixel Avg. ESB Grid = 800 V ULTRA 55.44.22 Noise Reduction = Pixel Avg. ESB Grid = 800 V

Ca/P=1.2

Ca/P=1.63

Ca/P=1.60

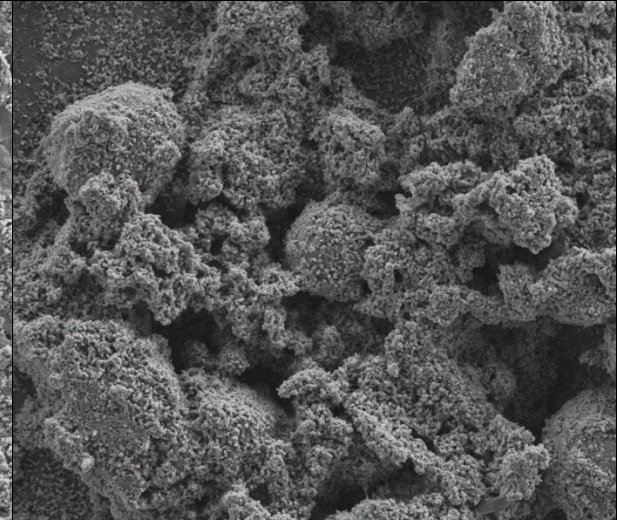
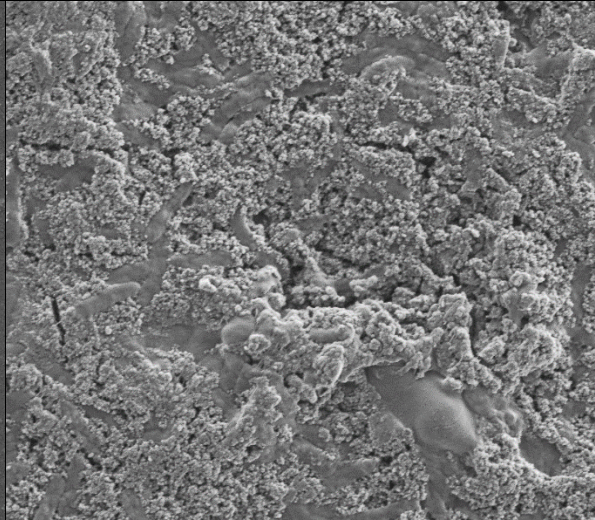
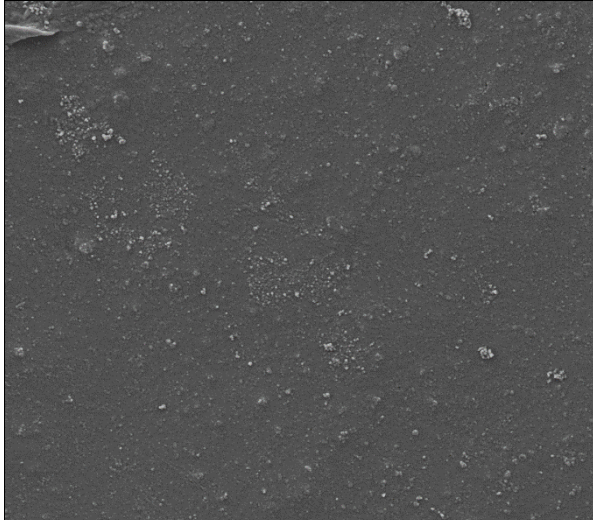


14 days

PCL/PLA

PCL/PLA HA20

PCL/PLA HA20 HNTs7.5



Mag = 5.00 K X
ULTRA 55.44.22

1 μm

WD = 5.7 mm

EHT = 2.00 kV

Signal A = SE2

ESB Grid = 800 V

Ti Mag = 5.00 K X
ULTRA 55.44.22

1 μm

WD = 7.4 mm

EHT = 2.00 kV

Signal A = SE2

ESB Grid = 800 V

Time Mag = 5.00 K X
ULTRA 55.44.22

1 μm

WD = 6.9 mm

EHT = 2.00 kV

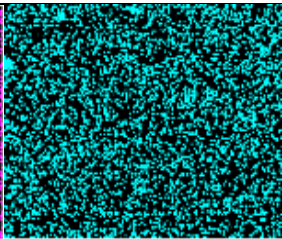
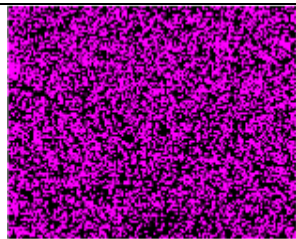
Signal A = SE2

ESB Grid = 800 V

Ca/P=1.2

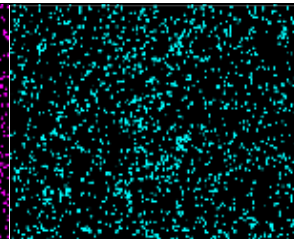
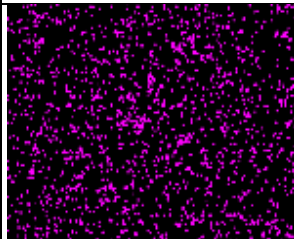
Ca/P=1.61

Ca/P=1.65



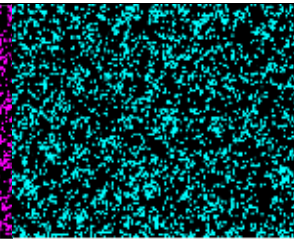
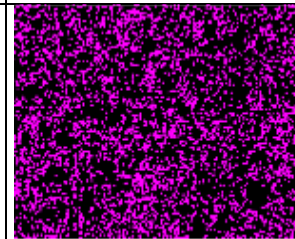
50 μm

50 μm



50 μm

50 μm



50 μm

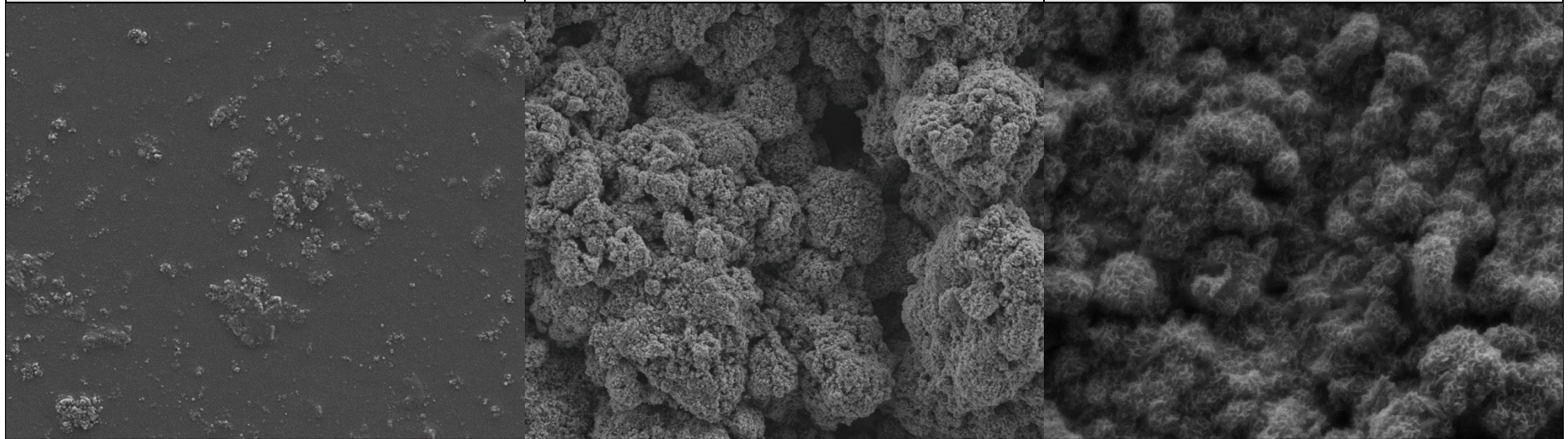
50 μm

7 days

PHEMA

PHEMA HA20

PHEMA HA20 HNTs7.5

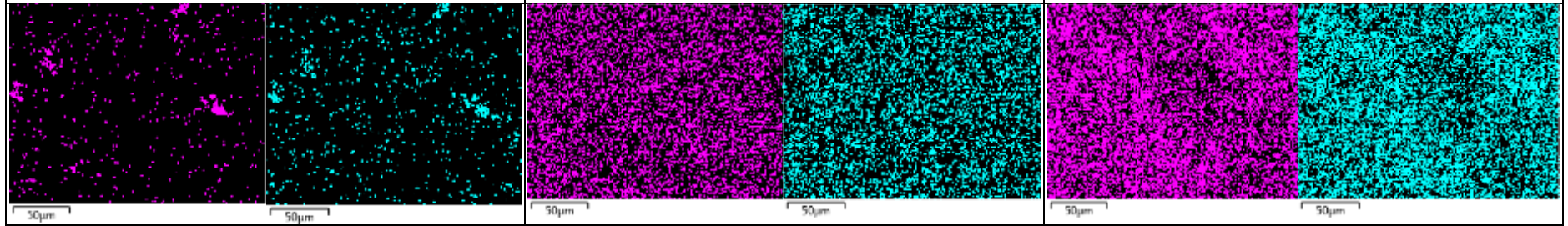


Mag = 5.00 K X 1 μm WD = 6.2 mm EHT = 2.00 kV Signal A = SE2 Noise Reduction = Pixel Avg. Time :15: Mag = 5.00 K X 1 μm WD = 6.9 mm EHT = 2.00 kV Signal A = SE2 Noise Reduction = Pixel Avg. Time :15: Mag = 5.00 K X 1 μm WD = 7.0 mm EHT = 2.00 kV Signal A = SE2 Noise Reduction = Pixel Avg. Time :14:

Ca/P=1.86

Ca/P=1.9

Ca/P=1.51

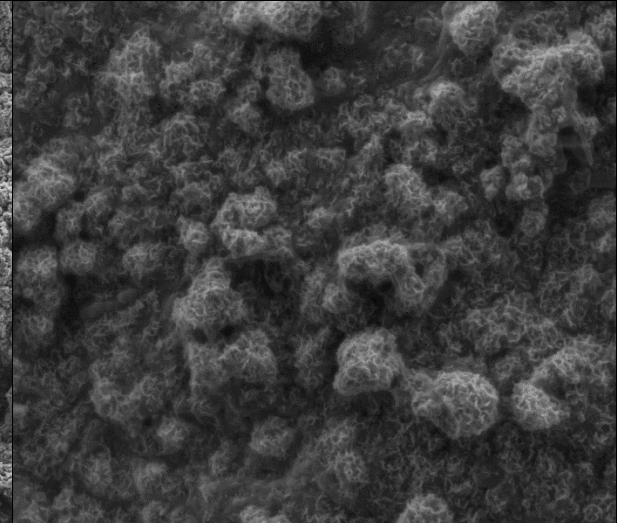
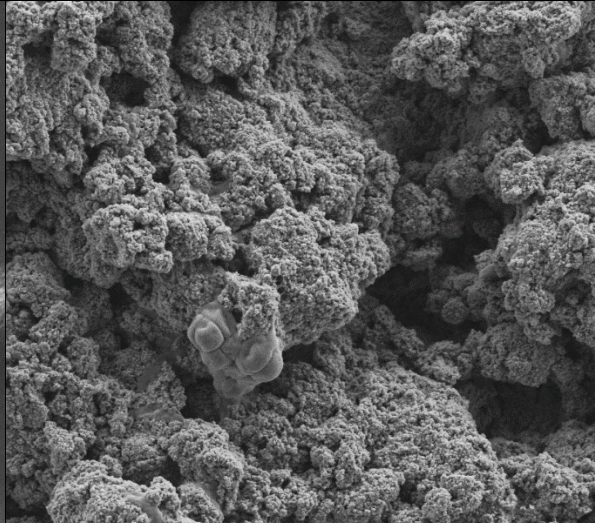
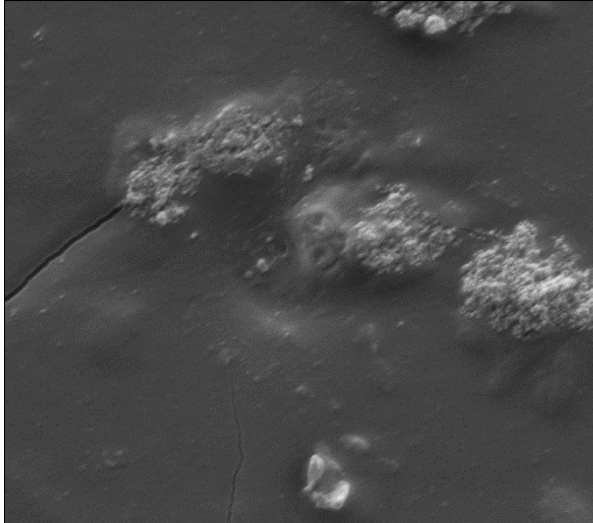


14 days

PHEMA

PHEMA HA20

PHEMA HA20 HNTs7.5



Mag = 5.00 K X
ULTRA 55-44-22
1 μm
WD = 6.2 mm
EHT = 2.00 kV
Noise Reduction = Pixel Avg.
Signal A = SE2
ESB Grid = 800 V

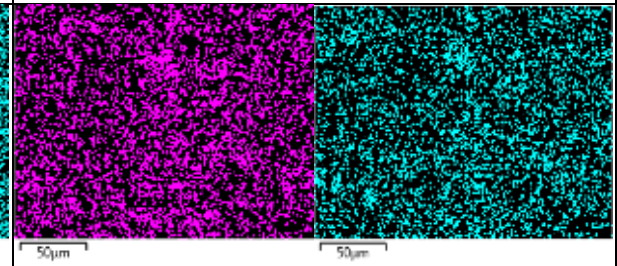
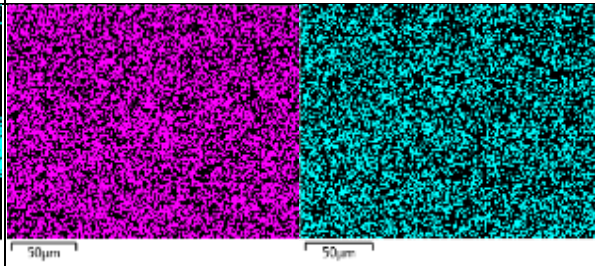
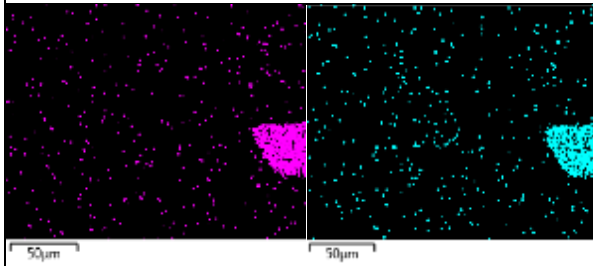
Mag = 5.00 K X
ULTRA 55-44-22
1 μm
WD = 6.7 mm
EHT = 2.00 kV
Noise Reduction = Pixel Avg.
Signal A = SE2
ESB Grid = 800 V

Mag = 5.00 K X
ULTRA 55-44-22
1 μm
WD = 6.9 mm
EHT = 2.00 kV
Noise Reduction = Pixel Avg.
Signal A = SE2
ESB Grid = 800 V

Ca/P=0

Ca/P=1.75

Ca/P=1.6

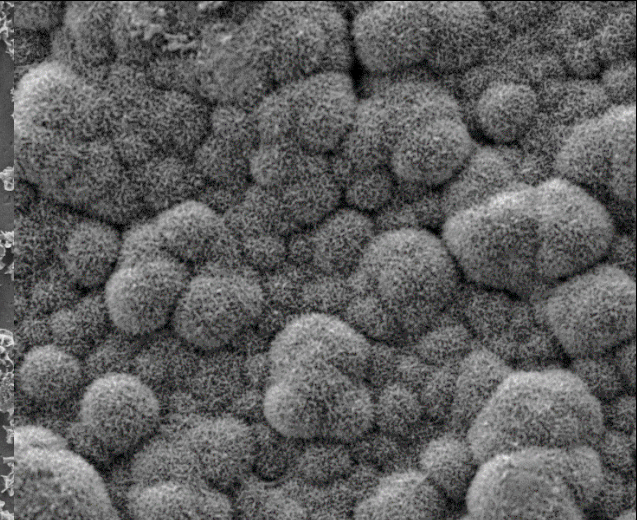
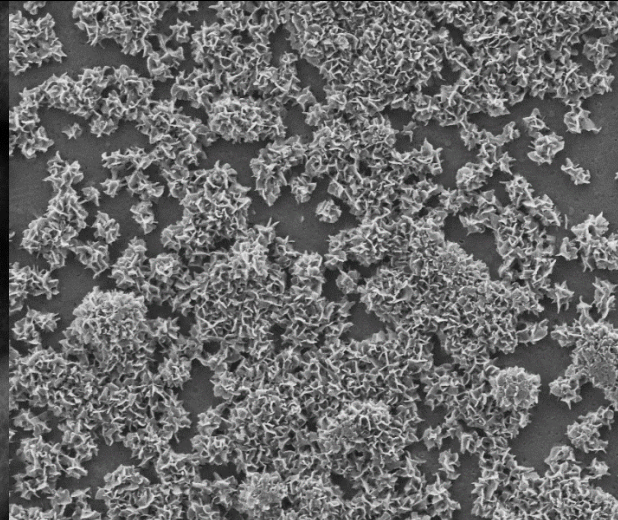
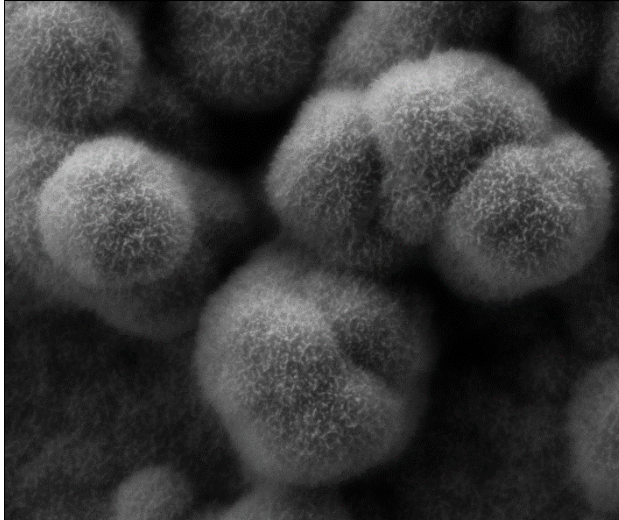


7 days

P(HEMA-co-EMA)

P(HEMA-co-EMA) HA20

P(HEMA-co-EMA) HA20 HNTs7.5



Mag = 5.00 K X 1 μm WD = 7.4 mm EHT = 2.00 kV Signal A = SE2 Time :14: Mag = 5.00 K X
ULTRA 55.44.22 Noise Reduction = Pixel Avg. ESB Grid = 600 V ULTRA 55.44.22

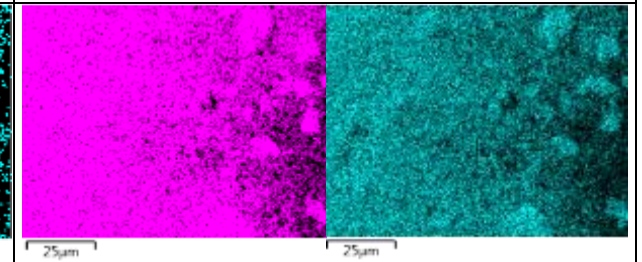
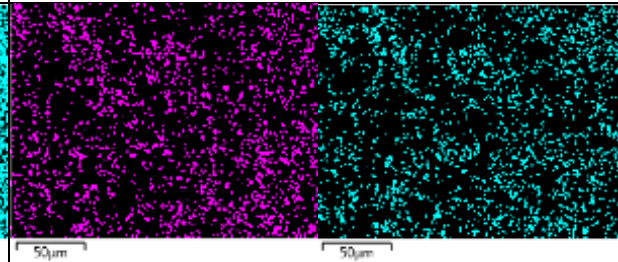
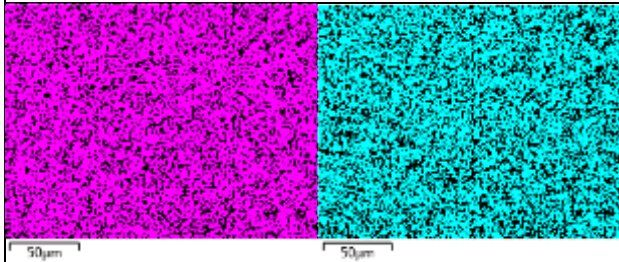
1 μm WD = 6.9 mm EHT = 2.00 kV Signal A = SE2 Time :15: Mag = 2.05 K X
ULTRA 55.44.22 Noise Reduction = Pixel Avg. ESB Grid = 800 V ULTRA 55.44.22

2 μm WD = 5.9 mm EHT = 2.00 kV Signal A = SE2 Time :13:
ULTRA 55.44.22 Noise Reduction = Pixel Avg. ESB Grid = 800 V

Ca/P=1.60

Ca/P=1.65

Ca/P= 1.53

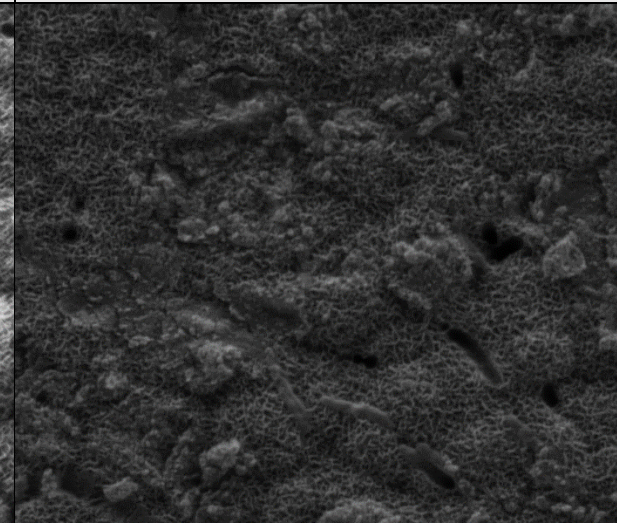
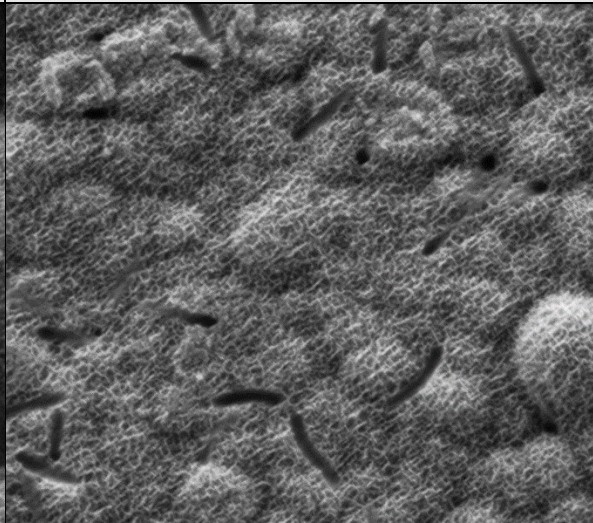
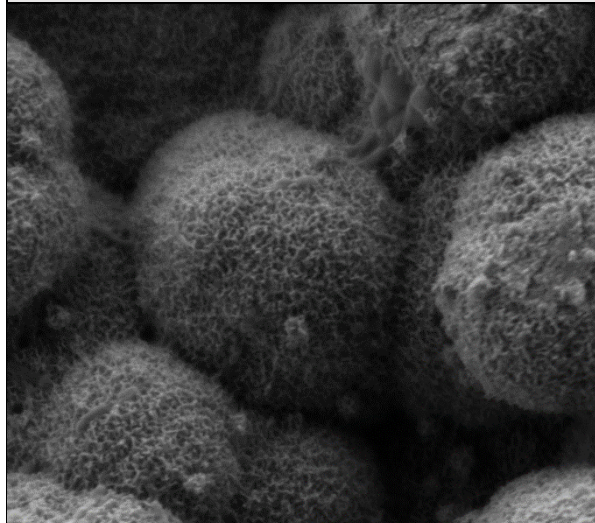


14 days

P(HEMA-co-EMA)

P(HEMA-co-EMA) HA20

P(HEMA-co-EMA) HA20 HNTs7.5



Mag = 5.00 K X
ULTRA 55.44.22
1 μm
WD = 6.5 mm
EHT = 2.00 kV
Noise Reduction = Pixel Avg.
Signal A = SE2
ESB Grid = 800 V

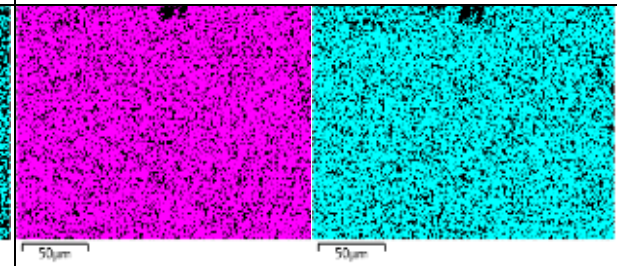
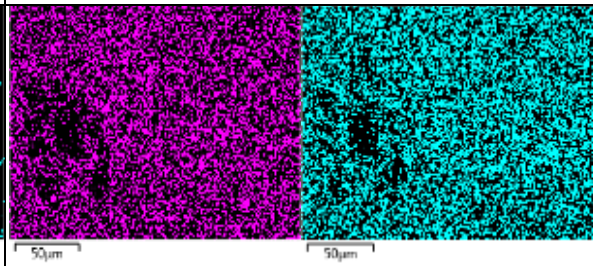
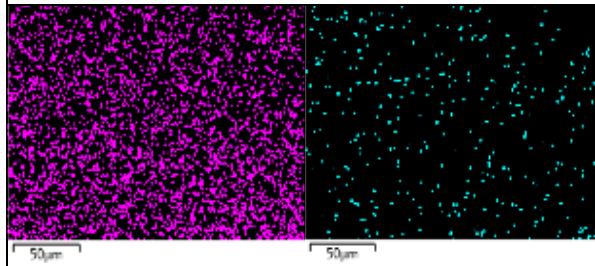
Ti Mag = 5.00 K X
ULTRA 55.44.22
1 μm
WD = 6.0 mm
EHT = 2.00 kV
Noise Reduction = Pixel Avg.
Signal A = SE2
ESB Grid = 800 V

Time Mag = 5.00 K X
ULTRA 55.44.22
1 μm
WD = 5.9 mm
EHT = 2.00 kV
Noise Reduction = Pixel Avg.
Signal A = SE2
ESB Grid = 800 V

Ca/P=1.60

Ca/P=1.47

Ca/P=1.58



4.2.3 Degradation of PCL and PCL/PLA based hybrids

Mass loss of each sample was determined by measuring the mass loss at each time point (4, 8 and 12 weeks) using an electronic balance with a resolution of 0.1 mg:

$$\% \text{ Mass loss} = \frac{M_i - M_f}{M_i} \times 100$$

where M_i is the initial mass and M_f is the final mass. The stress-strain curves were obtained to evaluate the loss of mechanical properties, specifically the Young modulus, after degradation.

Table 28 Degradation results for PCL- and PCL/PLA-based materials. % mass loss, Young modulus (MPa) and % of Young modulus upkeep over a period of 4, 8 and 12 weeks.

Sample		%Mass loss	Young Modulus (MPa)	% Young Modulus upkeep
PCL	Week 4	0,37% ± 0.03	273,66 ± 9.15	100%
	Week 8	0,39% ± 0.03	208,82 ± 12.16	76%
	Week 12	0,44% ± 0.02	168,40 ± 11.65	62%
PCL HA	Week 4	0,11% ± 0.03	270,22 ± 25,12	100%
	Week 8	0,17% ± 0.02	261,99 ± 9,25	97%
	Week 12	0,21% ± 0.02	261,27 ± 19,34	97%
PCL HA HNTs	Week 4	0,10% ± 0.06	246,93 ± 33,40	100%
	Week 8	0,16% ± 0.01	190,77 ± 17,64	77%
	Week 12	0,18% ± 0.01	174,51 ± 8,43	71%
PCL/PLA	Week 4	0,95% ± 0.11	813,61 ± 32,76	100%
	Week 8	1,14% ± 0.01	657,80 ± 3,50	81%
	Week 12	1,35% ± 0.09	891,19 ± 11,79	110%

PCL/PLA HA	Week 4	11,42% ± 1.83	461,14 ± 54,56	100%
	Week 8	12,08% ± 2.84	382,07 ± 35,12	83%
	Week 12	11,98% ± 0.79	437,81 ± 45,44	95%
PCL/PLA HA HNTs	Week 4	39,37% ± 2.55	328,29 ± 0,42	100%
	Week 8	39,53% ± 1.37	366,60 ± 36,42	112%
	Week 12	47,32% ± 3.04	384,66 ± 52,29	117%

From the results presented in Figure 16, it was seen that materials based on PCL did not show significant morphological changes after 12 weeks of degradation in PBS at 37°C, fact that coincided with the overall slow degree of mass loss. Although mass loss proceeds gradually for all samples based on PCL, a rapid mass loss spike for neat PCL over 12 degradation weeks was observed compared with the samples with inorganic fillers. The lower % mass loss observed in samples with HA could be explained by the fact that HA contains hydroxyl groups that may neutralize the medium by reacting with the degradation acid by-products, reducing the effect of acid catalysis on the hydrolysis of PCL [221]. From the observation of Lam *et al.* [86] the degradation of PCL seems to proceed through surface degradation and there are not evidences of internal autocatalysis. Surface degradation gives place to mass loss of the polymer surface over time without affecting the molecular weight of the internal bulk of the polymer. An unchanged molecular weight implies an efficient transmission of mechanical forces when the material is loaded.

From the analysis of the mechanical properties of materials based on PCL (Figure 16), it can be said that Young Modulus decreases gradually with % mass loss. PCL samples show a sharp decrease of Young modulus, but samples with HA maintain their Young modulus due to the reinforcing effect provided by the filler. However, samples with HA and HNTs show a progressive decrease of mechanical properties over time because the addition threshold can be exceeded with the degradation of the polymer and agglomerates could act as weak points and failure initiation sites.

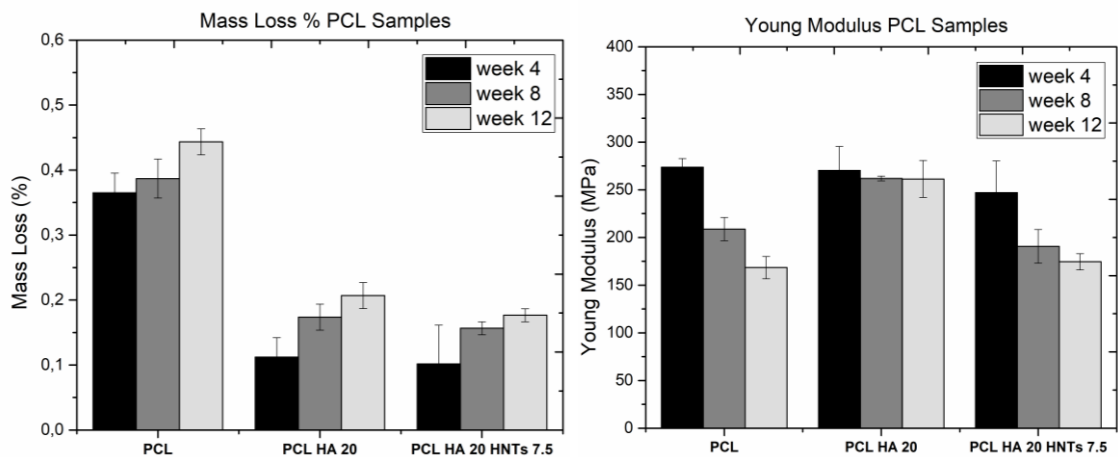


Figure 16 Left: Results of degradation % mass loss over 4, 8 and 12 weeks for PCL based materials. Right: Results of degradation Young Modulus over 4, 8 and 12 weeks for PCL based materials

As opposed to the observation of materials based on PCL (Figure 16), blends of PCL/PLA showed acute morphological changes after degradation in PBS at 37°C, with a maximum rate of mass loss of 41% after 12 weeks for samples with the two fillers (Figure 17). PCL hydrophobicity owing to its chemical structure of five carbons per chain unit, are responsible for the slow hydrolysis rate. Blending PCL with PLA provides hydrophilic units and decreases the overall crystallinity of PCL, improving the water molecules accessibility to ester linkages, thus increasing the rate of hydrolysis [222]. Addition of fillers confers a more hydrophobic character, and nano-roughness of the surface facilitates the interaction with water molecules and thus the hydrolytic cleavage. Due to the fluctuation on results caused by the short number of PCL/PLA blends tested for Young modulus (Table 28), conclusions will be expressed as general observations. Results for mechanical properties are in consistency with the mass loss. For PCL/PLA blends, the faster degradation rate related to the more hydrophilic character and the presence of more amorphous phase, leads to a faster drop of mechanical properties.

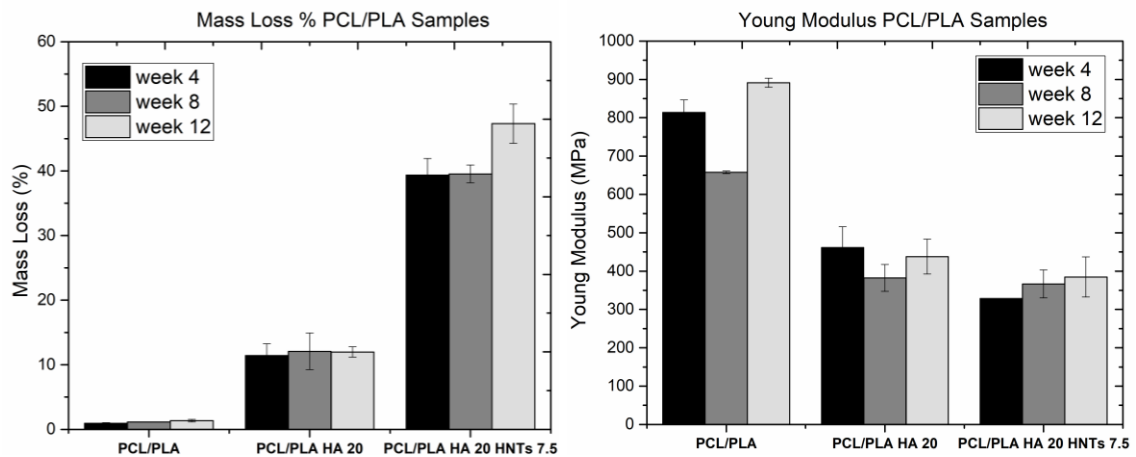


Figure 17 Left: Results of degradation % mass loss over 4, 8 and 12 weeks for PCL/PLA based materials. Right: Results of Young Modulus following 4, 8 and 12 weeks of degradation for PCL/PLA based materials.

4.2.4 General observations: Influence of the addition of HA and HNTs on the morphological properties of PCL- and PHEMA-based polymers

In the first chapter the aditivated threshold for PCL was established as 20% of HA, according to the literature, and 7.5% of HNTs was chosen rather than 5%, to have a higher percentage of HNTs loaded with a selected drug. After this preliminary study on the effect of inorganic fillers into a polyester matrix, the results were transferred to the followings chapters, were polymers with different nature were studied. Thus, the third objective of this thesis was addressed. In this sense, the structural properties of two pairs of polymers with similar chemical natures but different hydrophobicity were compared. First, PCL was blended with PLA with the aim of enhancing PCL mechanical properties while a moderately hydrophilic character was conferred driving to an acceleration of the degradation rate. Secondly, PHEMA was chosen to compare how the highly hydrophilic character affects the morphological and biological properties of the selected fillers. Accordingly, distribution of the HA and HNTS fillers into the polymeric matrices was studied through EDS mapping, yielding a homogeneous distribution of HA on all polymers but showing big aggregates of HNTs when the hydrophilic character increases. This effect could be explained due the hydrophobic character of the nanotubes, given by its relatively low content of hydroxyl groups on their surfaces, resulting in a good dispersion in non-polar polymers and creating agglomerations in hydrophilic polymers due to the lower interfacial adhesion. Hydroxyapatite nucleation of polymers surfaces was also studied, showing a not efficient induction of apatite growth on hydrophobic materials, but great hydroxyapatite cauliflower-shape crystals formation on moderately

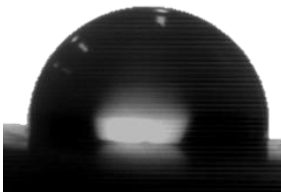
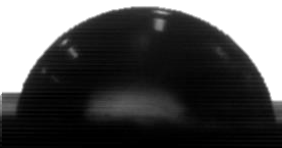
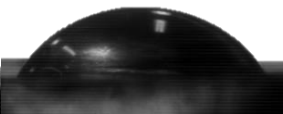

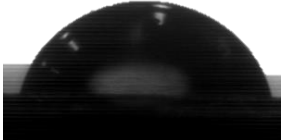
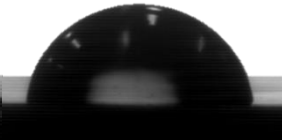

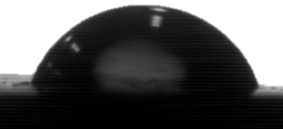
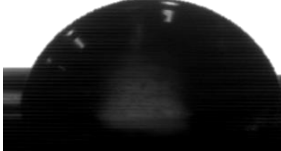
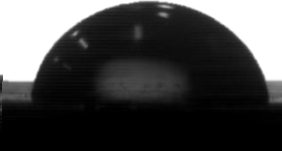
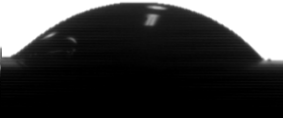
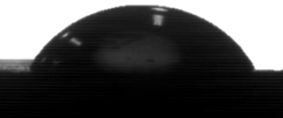
hydrophilic surfaces, which increases the number of nucleation sites for the Ca-P per surface unit. Finally, the degradation rate of PCL, PCL/PLA based hybrids was evaluated, concluding that blending PCL with PLA and the addition of fillers provides hydrophilic units and decreases the overall crystallinity of PCL, improving the water molecules accessibility to ester linkages, thus increasing the rate of hydrolysis and the hydrolytic cleavage. Mechanical properties are in consistency with the mass loss, the faster degradation rate leads to a faster drop of mechanical properties. In view of the results obtained in this chapter, an overall conclusion can be discerned: polymers with moderately hydrophilic character induce a higher rate of hydroxyapatite nucleation and a faster degradation rate. However, HNTs tends to form big aggregates when the hydrophilic character increases, driving to crack initiation sites and failure of the material.

4.3 Third chapter - Influence of the hydrophobic–hydrophilic nature of PCL- and PHEMA-based polymers and their nanocomposites on their *in vitro* biological development

4.3.1 Contact Angle Measurements

Surface wettability of cellular materials was previously determined by water contact angle measurements. In Table 29, images of the water droplets are shown. The results are divided into three rows with regard to composition: the first row contains the raw polymers PCL, PCL/PLA, PHEMA, and P(HEMA-co-EMA); the second row contains those loaded with 20% HA; and the third row includes the polymers loaded with 20% HA and 7.5% HNTs. PCL is at the hydrophobic end, with a contact angle of 105°. Meanwhile, PHEMA is at the hydrophilic end, with a contact angle of 59.7°. The addition of HA and HNTs clearly improved surface wettability on PCL (mean contact angle value decreased around 22%). This effect was hardly observed in the PCL/PLA mixture taking into account the standard deviation. The addition of HA and HNTs in PHEMA increased its surface wettability (mean contact angle value decreased around 18%), but that of P(HEMA-co-EMA) remained constant. In summary, it appears that the addition of HA and HNT increased the wettability of neat samples (PCL and PHEMA), but not mixed samples (PCL/PLA and P(HEMA-co-EMA)).

Table 29 Contact angle results of raw polymers (PCL, PCL/PLA, PHEMA, P(HEMA-co-EMA)) compared with those loaded with HA, and HA and HNTs. \bar{x} and s stand for average contact angle and standard deviation, respectively.

<i>Polymer</i>			
PCL	PCL/PLA	PHEMA	P(HEMA-co-EMA)
			
$\bar{x} = 105^\circ$ $s = 3.6$	$\bar{x} = 83.7^\circ$ $s = 4.6$	$\bar{x} = 59.7^\circ$ $s = 4.5$	$\bar{x} = 73.7^\circ$ $s = 4.5$
Polymer + 20% HA			
			
$\bar{x} = 80.9^\circ$ $s = 2.2$	$\bar{x} = 85.9^\circ$ $s = 4.9$	$\bar{x} = 54.8^\circ$ $s = 3.8$	$\bar{x} = 78.4^\circ$ $s = 4.64$
Polymer + 20% HA + 7.5% HNTs			
			
$\bar{x} = 76.8^\circ$ $s = 2.6$	$\bar{x} = 86.1^\circ$ $s = 2.3$	$\bar{x} = 48.1^\circ$ $s = 4.6$	$\bar{x} = 75.7^\circ$ $s = 5.2$

4.3.2 Cell Viability and Morphology

Cell Viability Assay

MTS results were taken for triplicate for each sample obtaining standard deviation values lower than 0.05. The results were represented numerically in table form (Table 30) and graphically, for a better understanding, dividing the data in two sections: short periods of time (1 and 3 days) (Figure 18, A) and long periods of time (7 and 14 days) (Figure 18, B) with the aim of visually assess cell viability results.

Three different groups of materials were compared. First, the raw polymers were compared (PCL, PCL/PLA, PHEMA, and P(HEMA-co-EMA)), and in the second and third rows, HA or HA and HNTs were incorporated. In all of them, a similar trend was seen. At day 1 and 3 of cell culture, the materials showing the highest absorbance values (highest amount of cells, highlighted in green) for all of the three groups were PCL/PLA, PCL/PLA HA20, and PCL/PLA HA20 HNTs7.5, being these materials moderately hydrophobic. However, at longer cell culture periods, day 7 and 14, the materials with the highest values of absorbance were P(HEMA-co-EMA), P(HEMA-co-EMA) HA20, and P(HEMA-co-EMA) HA20 HNTs7.5, which are moderately hydrophilic. In view of the results, the addition of HA and HNTs improved the materials' cell viability.

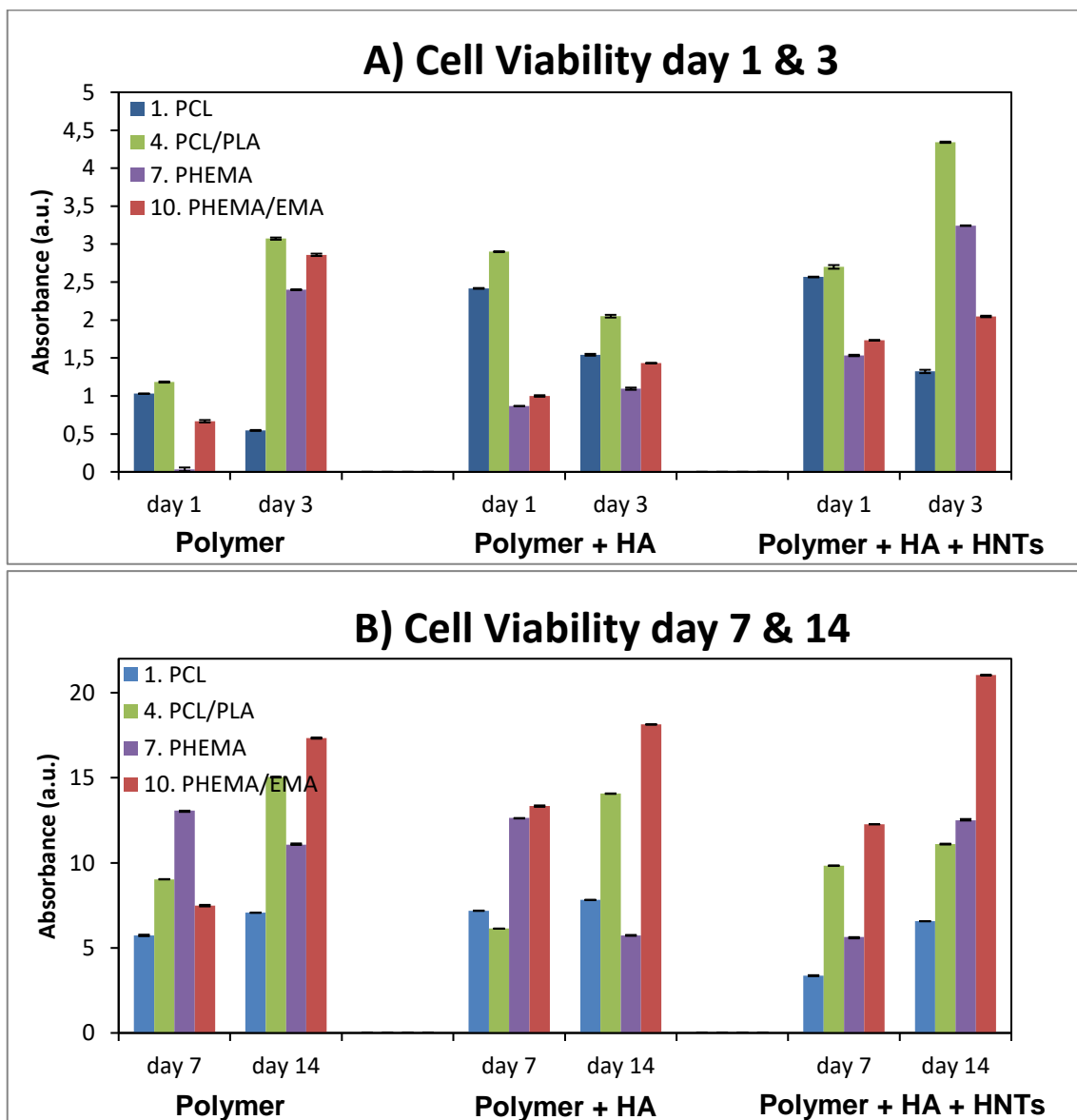


Figure 18 MTS Cell viability results comparing first the raw polymers, secondly the addition of HA, and third the addition of HA and HNTs. A) Cell viability at initial stage and B) Cell viability at long periods of cell culture.

Table 30 MTS Cell viability results divided into three different groups of materials according to their inorganic loading: in the first group, raw polymers PCL, PCL/PLA, PHEMA, and P(HEMA-co-EMA) are compared; in the second and third groups, HA or HA and HNTs are incorporated and compared.

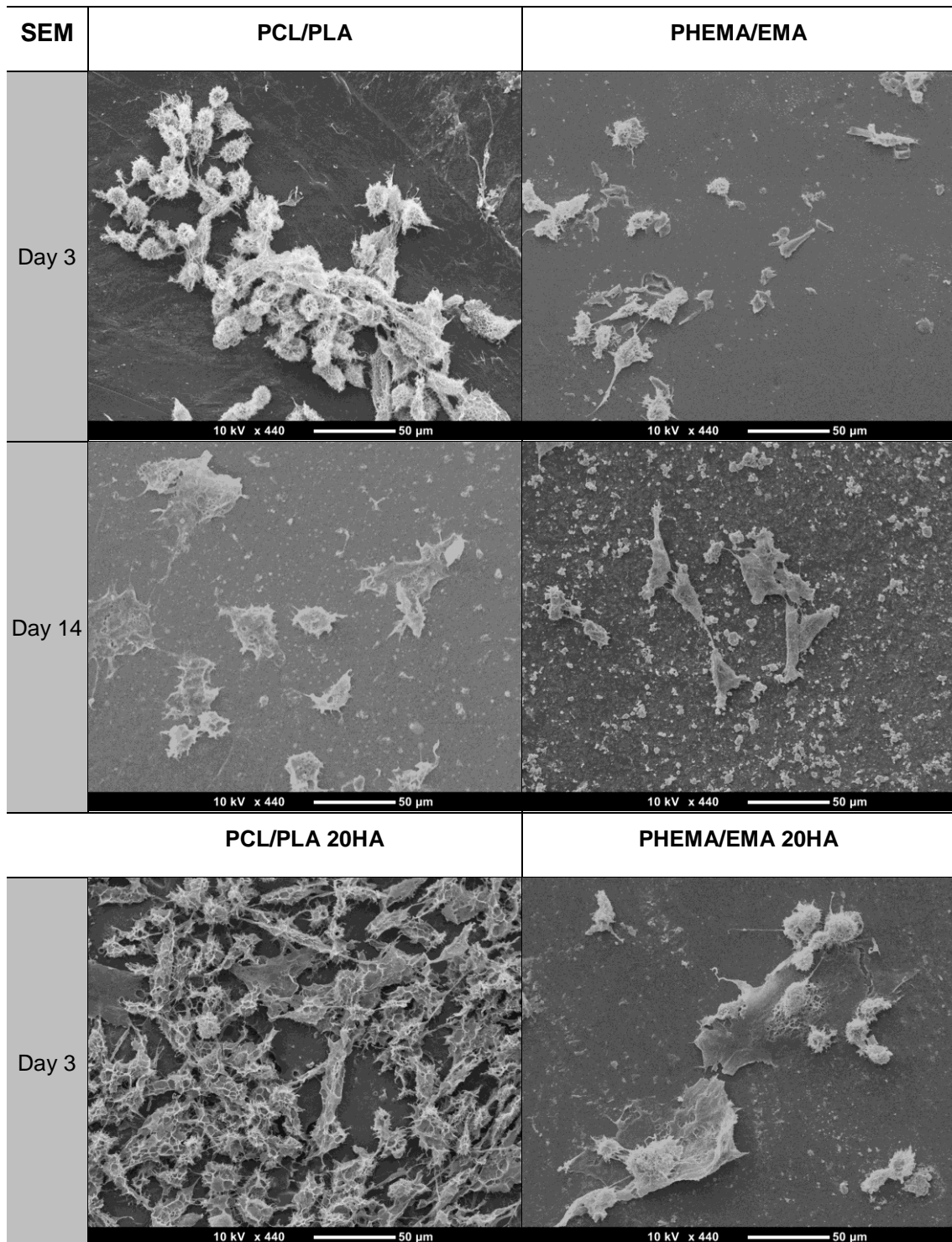
MTS	Group 1: Raw Polymers				Group 2: HA Incorporation				Group 3: HA and HNTs Incorporation			
	PCL	PCL/PLA	PHEMA	PHEMA-co-EMA	PCL 20HA	PCL/PLA 20HA	PHEMA 20HA	PHEMA-co-EMA 20HA	PCL 20HA 7.5HNTs	PCL/PLA 20HA 7.5HNTs	PHEMA 20HA 7.5HNTs	PHEMA-co-EMA 20HA 7.5HNTs
day 1	1.03	1.18	0.03	0.67	2.42	2.90	0.87	1.00	2.57	2.7	1.53	1.73
day 3	0.55	3.07	2.40	2.86	1.55	2.05	1.2	1.43	1.32	4.34	3.24	2.05
day 7	5.73	9.03	13.07	7.48	7.18	6.13	12.63	13.33	3.37	9.83	5.63	12.27
day 14	7.07	15.03	11.07	17.33	7.82	14.07	5.73	18.13	6.57	11.10	12.5	21.03

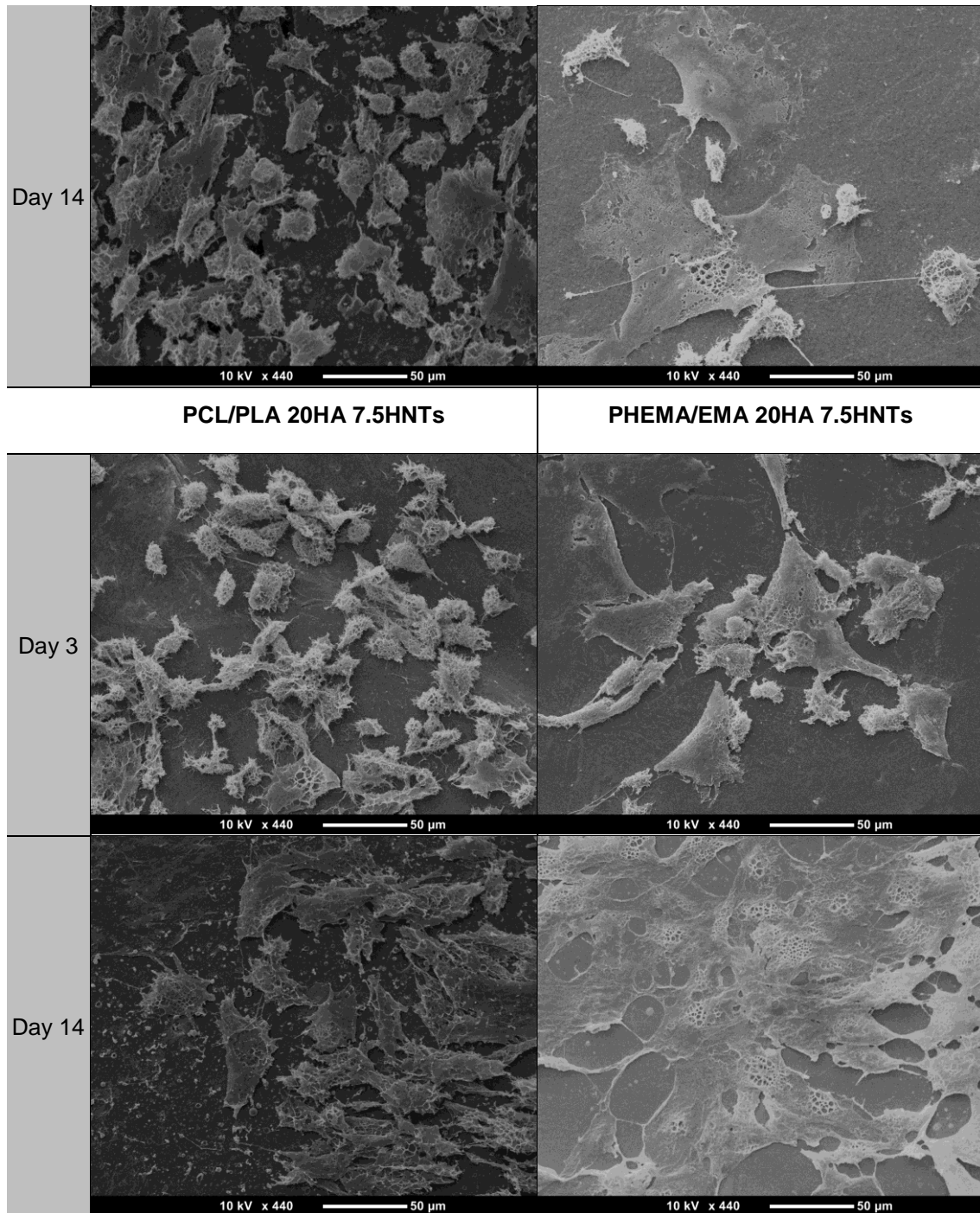
Thus, in order to simplify our experimental data, in the following sections, we will only show and discuss this group of six materials, differentiating between moderately hydrophobic materials (PCL/PLA, PCL/PLA HA20, and PCL/PLA HA20 HNTs7.5) and moderately hydrophilic ones (P(HEMA-co-EMA), P(HEMA-co-EMA) HA20, and P(HEMA-co-EMA) HA20 HNTs7.5).

Scanning Electron Microscopy (SEM)

In the SEM images of morphology (Table 31), at the initial stages, it can be observed how cells on moderately hydrophobic surfaces (PCL/PLA) have better interactions with neighbouring extracellular matrices than with the biomaterial surface via the proteins adhered to it. Accordingly, a cell monolayer is formed with few bonding sites with the biomaterial surface, and a round cell shape prevails. Conversely, on moderately hydrophilic surfaces (P(HEMA-co-EMA)), although the cells are more isolated, the extracellular matrix of each individual cell seems to be spread out on the material with several bonding sites, thus yielding better cell attachments on the biomaterial and, consequently, a flat cell shape. SEM observation are coherent with MTS results.

Table 31 SEM images (400 X) of the polymers showing the highest absorbance values in MTS assays: PCL/PLA, P(HEMA-co-EMA), raw and loaded with HA or HA and HNTs, after 3 and 14 days of culture.





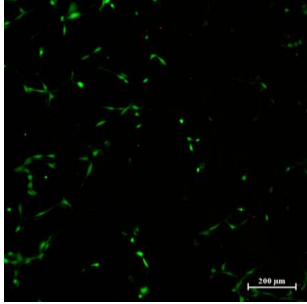
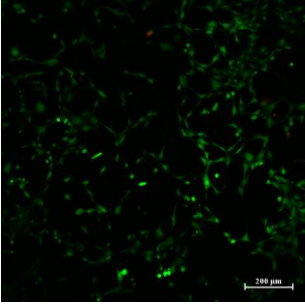
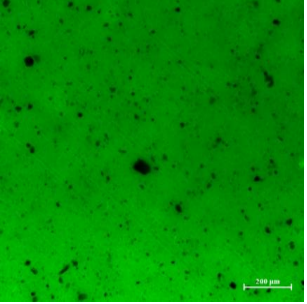
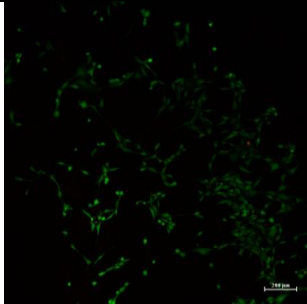
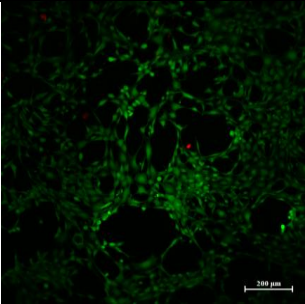
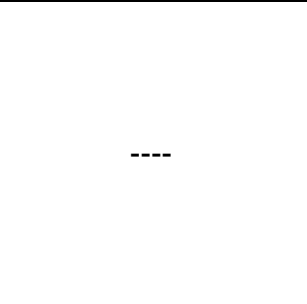
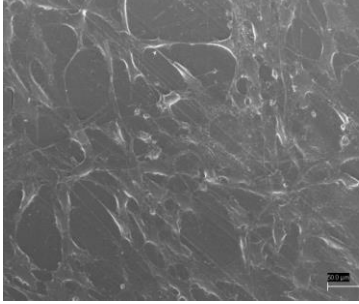
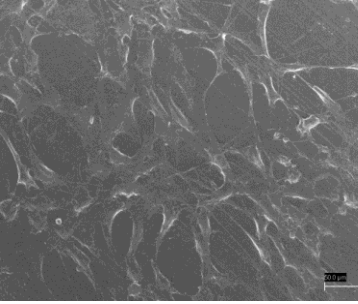
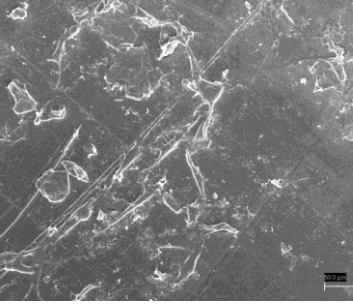
4.3.3 Organization of Cell Cytoskeleton

Influence of HNTs loaded with curcumin incorporated to the PCL matrix on its biological properties

Cell viability of the samples loaded with curcumin was studied (Table 32). However, it has to be taken into account that the anti-oxidant and anti-inflammatory effect of curcumin will eventually inhibit the proliferation of several cells. Indeed, Merrell *et al.* [223] observed significant decrease of viability in samples loaded with curcumin.

However, more than 70% of the cells were viable on the samples, indicating their low cytotoxicity.

Table 32 Influence of HNTs loaded with curcumin incorporated to the PCL matrix. Cell viability of samples aditivated with curcumin.

PCL	PCL 20 HA 7.5 HNTs	PCL 20 HA 7.5 HNTs + curcumin
3 days		
		
7 days		
		
SEM images		
		

Fluorescence characterization results show better cell viability on samples filled with HA and HNTs than on neat PCL. However, curcumin provokes fluorescence in the nanocomposite, hence cells cannot be distinguished under the fluorescence microscopy.

In SEM images, adhered cells can be observed on both of the PCL and PCL 20 HA 7.5 HNTs specimens, showing an extended morphology. On the contrary, interactions

between cells and curcumin loaded samples are not observed probably because curcumin inhibits cell adhesion, in agreement with Merrell *et al.* [223].

Immunocytochemistry

Immunocytochemistry images for the raw (PCL/PLA and P(HEMA-co-EMA)) and loaded materials, after 3 days of culture, are shown in Figure 19 and Figure 20. Results after 14 days are not shown because the huge cells agglomerates did not shed information on cell attachment to the material surface. These results are in accordance with the MTS and SEM images. For raw P(HEMA-co-EMA) materials (Figure 19), the images show isolated cells with good cell attachment on the surface and spreading of the cytoskeleton with a flat surface. Using goat anti-mouse Cy5 secondary antibody (white) as stain, we were able to observe vinculin protein (involved in focal adhesions with integrin), which was distributed throughout the cells and boosted interactions with the surface. However, on PCL/PLA surfaces, cells aggregated in clusters, showing a rounded shape. Similar results are observed in Figure 20, where moderately hydrophilic surfaces (P(HEMA-co-EMA) HA20 and P(HEMA-co-EMA) HA20 HNTs7.5)) show higher cytoskeleton spreading than moderately hydrophobic ones (PCL/PLA HA20, PCL/PLA HA20 HNTs7.5).

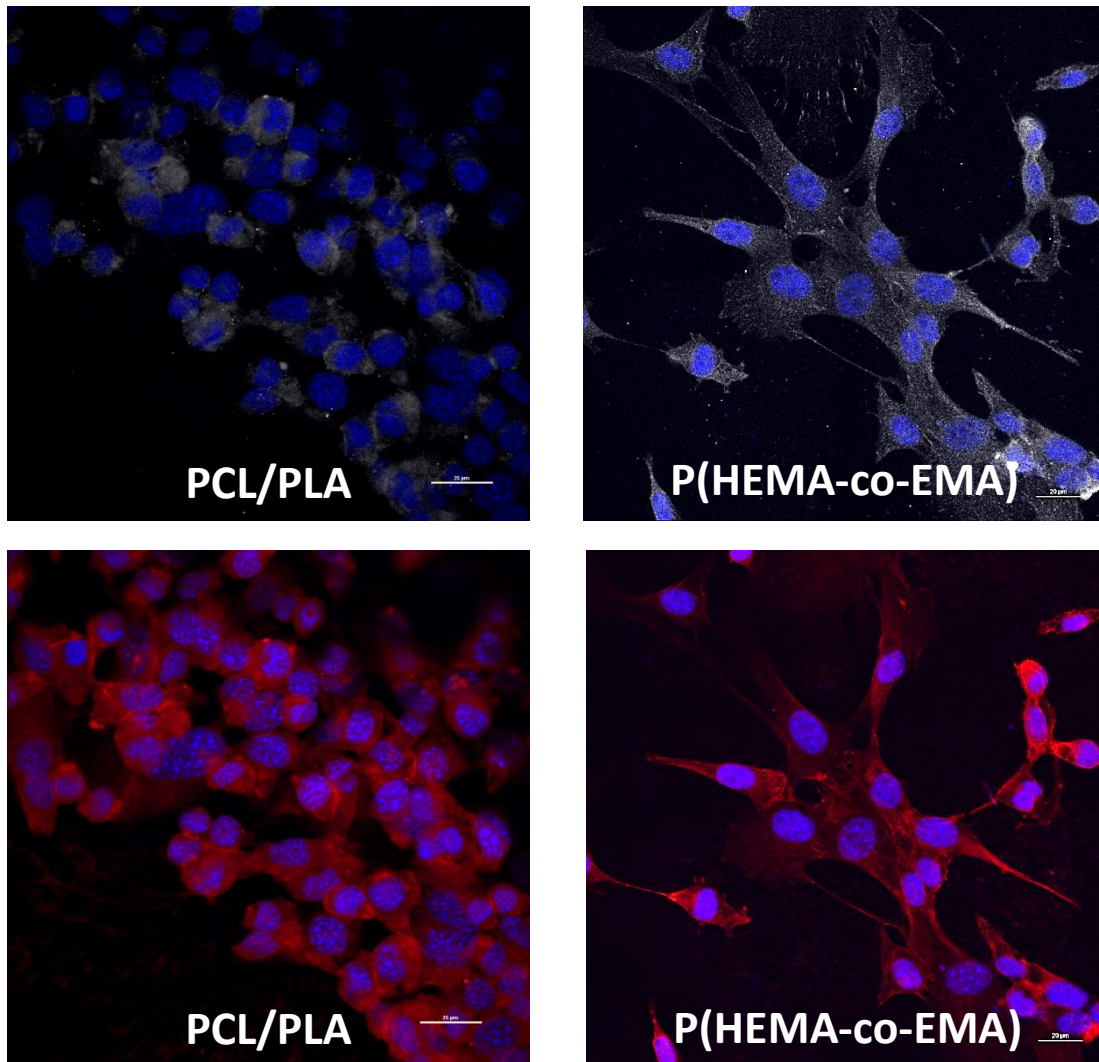


Figure 19 Immunocytochemistry images for raw PCL/PLA and P(HEMA-co-EMA) samples (scale bar 25 µm). Comparison of cell attachment and spreading depending on the surface hydrophobicity after 3 days of culture. Vinculin staining for focal adhesions is shown in white in the top row for the two materials, together with DAPI staining of the nuclei. Phalloidin staining of the actin cytoskeleton is shown in the bottom row in red. (DAPI staining in blue, vinculin in white in the top row, and phalloidin in red in the bottom row.)

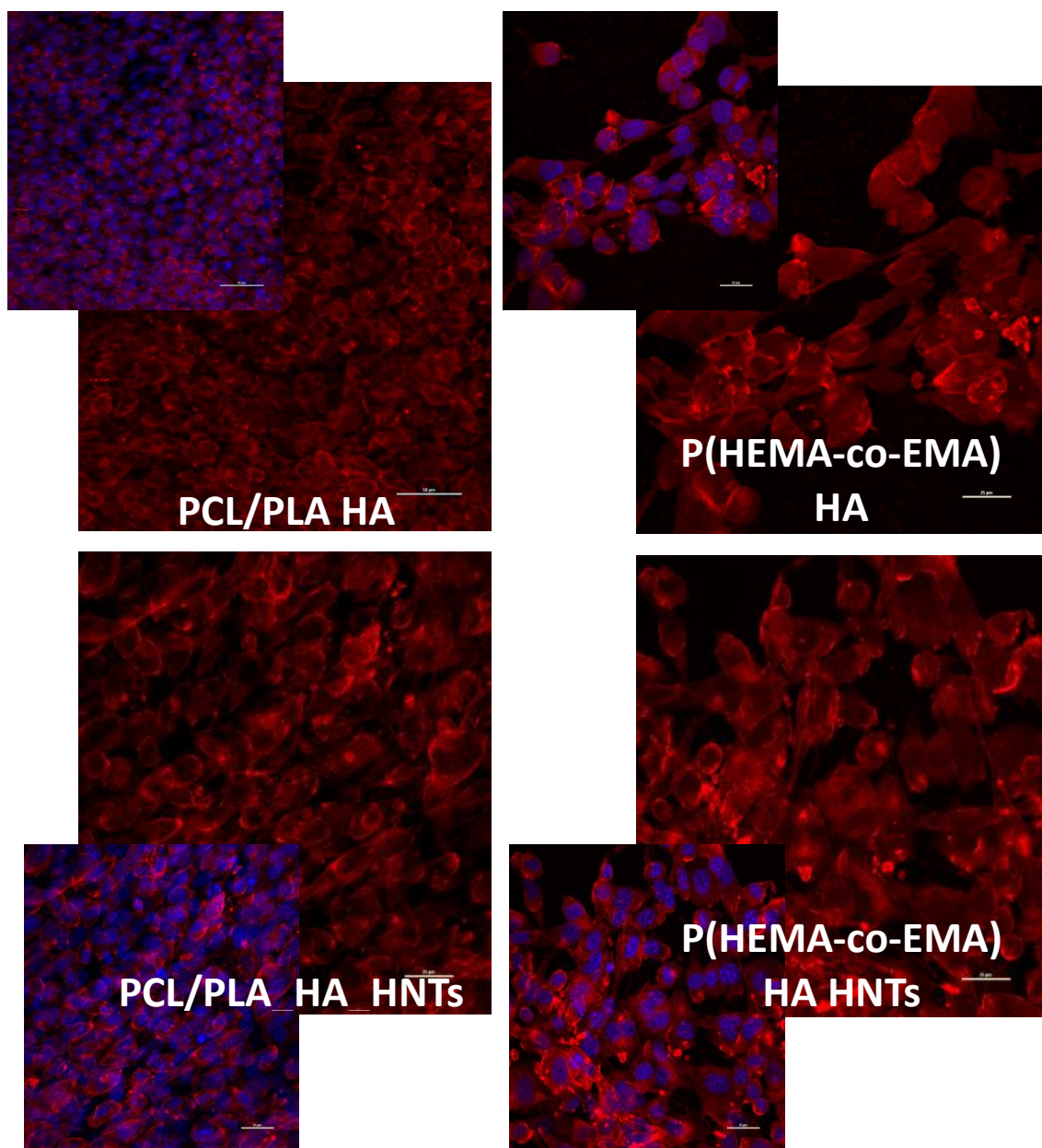


Figure 20 Immunocytochemistry images (scale bar 25 μm) comparing moderately hydrophobic (PCL/PLA) and hydrophilic P(HEMA-co-EMA) surfaces loaded with HA and HNTs at day 3 of culture (DAPI staining in blue and phalloidin in red).

4.3.4 General observations for cell interaction influenced by the hydrophobic–hydrophilic nature

Polymer surface wettability is known to affect cell attachment for water contact angles in the range of 40° – 70° [224]. Polymers with contact angles lying more or less in this range, with different chemical natures, were thus selected for this analysis, and their hydrophilicity was slightly modified by blending or copolymerizing with others of the same

family. HA and HNTs are interesting inorganic additives and were added herein to analyse their effect in terms of wettability and biological development.

In order to explain our results, how proteins interact with polymer surfaces needs to be understood. The two most abundant proteins in plasma are albumin and fibronectin. Albumin (M_w of 69,000) is the first protein to be adsorbed on the biomaterial surface and inhibits cell adhesion [225, 226]. On the other hand, fibronectin (M_w of 440,000) increases fibroblast attachment and spreading [227] and plays a very important role in the interaction with the surface of an artificial device [228, 229]. Fibronectin interacts with integrin [230], acting as a “bridge” between fibronectin and the cytoskeleton [231, 232], anchoring these cells to the biomaterial or extracellular matrix. This interaction is primarily responsible for the ability of cells to adhere to the surface of a biomaterial. According to the Vroman effect, smaller and more abundant proteins present in the medium dominate the biomaterial surface after short durations of exposure due to their higher collision rates. Various exchange processes occur thereafter and proteins with higher affinities replace them and take over the surface. Finally, after a very long time, only the proteins with the highest affinities remain present on the surface [233]. Therefore, albumin and fibronectin mutually compete for adsorption on any exposed surface.

In order to confirm this assumption, Albumin and Fibronectin competitive adsorption was followed on polyesters. This study was performed in the framework of a project progressing concurrently to this Thesis, which explains why PLA (moderately hydrophobic) and PHB (hydrophobic) -instead of PCL- surfaces were considered. Competitive adsorption of Fibronectin obtained from human serum and Albumin obtained from bovine serum albumin (BSA) was determined by immunofluorescence for short periods of time (1 day). Three solutions (of Fibronectin and Albumin separately for individual adsorption, and a third solution of a mixture of both) were used in this study, at concentrations of 20 $\mu\text{g}/\text{mL}$ in DPBS at pH of 7.4. 1.4 mL of the solution was prepared in each case. Subsequently, 100 μL of each solution was dropped onto the surface materials and incubated for 30 min at 37°C. After washing twice with PBS for 5 min, the specimens were incubated with a primary antibody BCA and Fibronectin for 1 h. The specimens were rinsed twice with DPBS for 5 min. Then, the mixed solution of Alexa 488 and 633 was incubated in a dark place for 1 h. The samples were then observed under confocal laser scanning microscopy. For quantitative evaluation of protein adsorption, the images obtained were analysed with the ImageJ software from 5 random zones and

by quantifying the relative area of adsorbed proteins. Results were gathered in the Table 33.

Table 33 Albumin and Fibronectin competitive absorption on PLA (moderately hydrophobic) and PHB (hydrophobic), measuring five replicates of each sample and obtaining the mean value and standard deviation.

Protein	PLA	PLA + HA	PHB	PHB + HA
Albumin	92.29% ± 1.35	96.8% ± 0.7	15.4% ± 7.56	73.4% ± 11.62
Fibronectin	7.71% ± 1.35	3.2% ± 0.7	84.6% ± 7.56	26.64% ± 11.62

Considering that PLA is a moderately hydrophobic material and PHB is a hydrophobic material and knowing that addition of HA provides a more hydrophilic character, from the results showed in Table 33 can be said that Albumin tends to bind to more hydrophilic surfaces. However, for hydrophobic surfaces, Fibronectin binds in a higher percentage.

Herein it was observed that, at the initial stages, cells preferably proliferate and colonize moderately hydrophobic surfaces (PCL/PLA). Thus, cells appear with a round shape, where interactions occur primarily between them or with the extracellular matrix, thus resulting in a monolayer of cells with few bonding sites with the polymer surface. Over longer culture periods, though, cell proliferation occurs on more hydrophilic materials (P(HEMA-co-EMA)), on which cells exhibit a flatter shape, thus establishing contact with the polymer over its surface. Regarding loading with inorganic nanoparticles (HA and HNTs), cell viability and proliferation improved compared to the raw materials. This improvement can be attributed to the generation of new reactive sites with Ca^{2+} and PO_4^{3-} groups present in HA available for binding with negative carboxylate and positive amino groups in proteins, respectively [125-128, 234-236]. Furthermore, the formation of hydrogen bonds between HNTs and proteins [170] led by silanol groups (Si-OH) [169] located at the surfaces of HNTs [106] can also take place.

Our results show greater cell proliferation on moderately hydrophobic materials at the initial stages whereas over longer culture periods, cell proliferation occurs on more hydrophilic materials. Similar results were found by Zhou *et al.* [168] who used polyvinyl alcohol (PVA; which is a highly hydrophilic hydrogel) and surprisingly observed a higher cell proliferation (using NIH 3T3 fibroblasts) in the polystyrene control (hydrophobic) at

day 1 of culture. However, after 4 or 7 days of culture, neat PVA showed higher cell viability. They stated that highly polar OH groups on neat PVA film might account for the delayed attachment of bone cells. We assume that such cell spreading reduction observed on hydrophobic surfaces at long culture times might occur as a consequence of two effects: protein absorption competition and the steric hindrance effect (solvation), which are analysed separately below.

Competitive Absorption

The reduction in cell spreading at long culture times observed in our study may be the result of the binding level of non-adhesive proteins such that albumin, which competes with adhesive proteins such fibronectin (plot representation can be observed in Figure 21) [237]. Albumin tends to bind to hydrophobic surfaces by various hydrophobic interactions; Ying *et al.* [238] reported such interactions between hydrophobic surfaces and flexible albumin molecules. Albumin does not adsorb on hydrophilic surfaces likely because of electrostatic repulsion forces between the negatively charged surfaces and the albumin molecules. Conversely, fibronectin binding is greater on hydrophilic surfaces due to hydrogen bonding [239]. In view of these considerations, it seems unlikely that the proteins compete for the same sites even though they may compete for space. Nuttelman *et al.* [240] stated that cell adhesion proteins initially bind in a stronger way to surfaces with greater hydrophobicity; however, there is an associated loss of activity because on a highly hydrophobic surface, fibronectin may unwind into an inactive filamentous structure, and this denatured form of fibronectin hinders cell adhesion [241, 242].

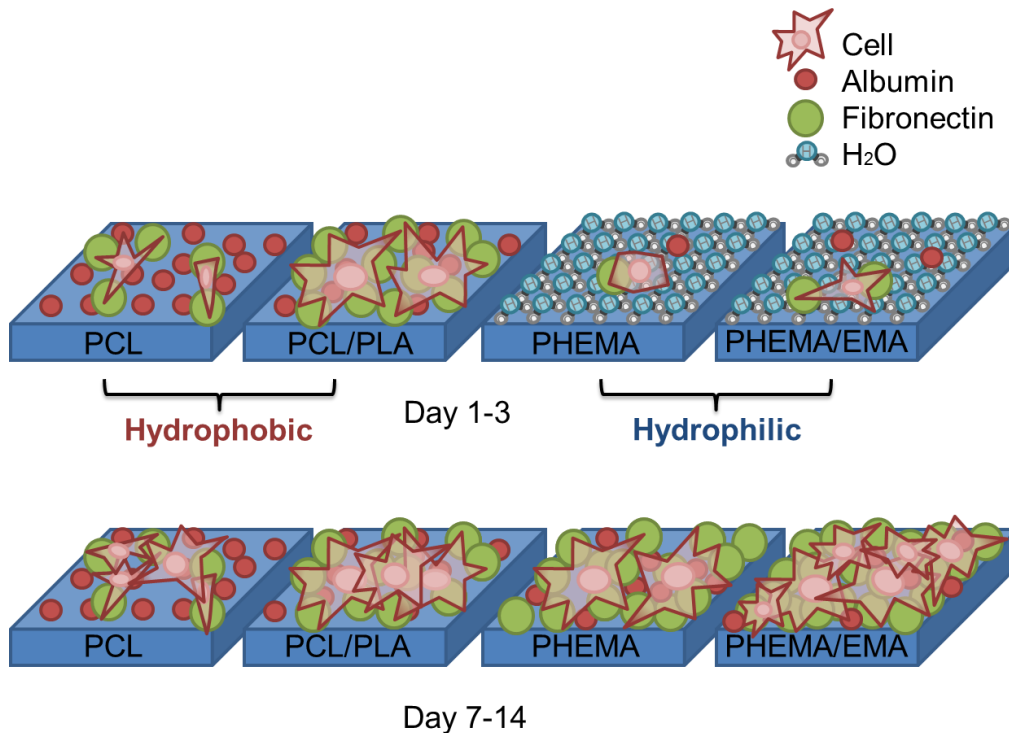


Figure 21 Competitive protein absorption between fibronectin and albumin at the initial stages and over longer culture periods.

Water Steric Hindrance (Solvation)

It was herein observed that cell proliferation increased on hydrophilic surfaces after seven days, a fact that can be explained because, during the initial stages, hydrophilic surfaces are highly solvated; hence, cells (and proteins) cannot closely approach such a substrate and, therefore, might not stick. Hydrophilic surfaces induce a strong organization of two to three layers of water molecules, repelling the shear plane to about 1 nm from the surface [243], repulsing protein adsorption by steric hindrance effects (Figure 22 (A)). As a result, the adsorption is retarded, leaving the adsorbed proteins more time to rearrange their structure before the neighbouring sites are occupied by newly arriving proteins, thus allowing more time for them to “spread” out over the surface if the rate of the newly arriving molecules is low. As a consequence, the final extent of structural rearrangements (and hence the adsorbed amount) will depend on the relative rates of arrival and structural changes. For hydrophobic surfaces, on the other hand, the stagnant layer may be restricted to the ions [243] (Figure 22 (B)), where water tends to hydrogen bond to neighbouring water molecules, resulting in a highly ordered water structure. Disruption of this structure (dehydration) by adsorption of a protein to the surface increases the entropy of the system because proteins would unfold and spread over the surface to reduce the net hydrophobic surface in contact with the medium [244],

which is thermodynamically favoured. Dehydration of a hydrophobic surface is driven by entropy gain and, therefore, promotes adsorption to occur spontaneously. As a result, adsorption to hydrophobic substrates is generally irreversible, whereas adsorption to hydrophilic substrates is reversible.

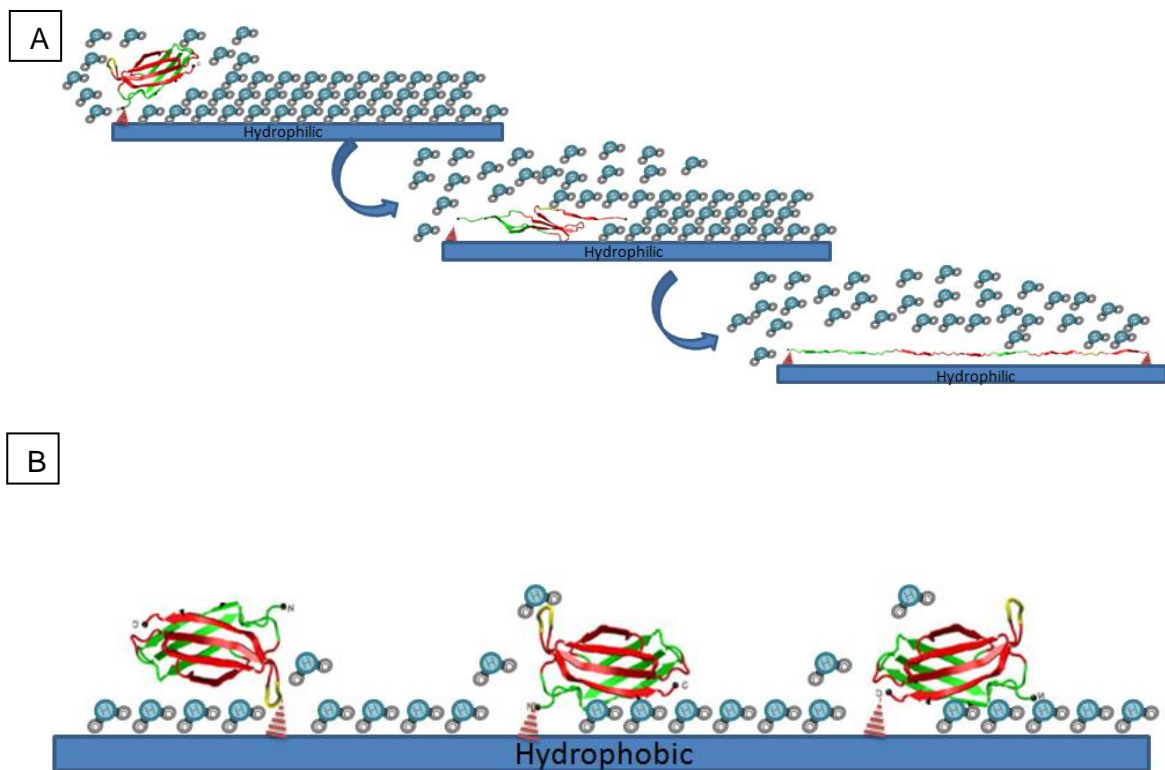


Figure 22 Solvation effect. (A) Solvation on hydrophilic surfaces induces a 1 nm layer of water, delaying protein approach, and hence, absorption. (B) On hydrophobic surfaces, the layer of water is restricted to ions.

In this chapter, the fourth objective of the thesis was approached and the *in vitro* biological development of the different pair of polymers was studied regarding its hydrophobicity character. First, the surface wettability was measured through water contact angle establishing that PCL is at the hydrophobic end, while PHEMA is at the hydrophilic end. The addition of HA and HNTs clearly improved surface wettability of neat samples, but not mixed samples (PCL/PLA and P(HEMA-co-EMA)). Cell adhesion, morphology and proliferation was studied through MTS assay, Scanning Electron Microscopy and Immunocytochemistry assay. All the results obtained for the three studies were coherent among them: On moderately hydrophobic polyesters cells tended to proliferate and showed a round shape at the initial stages resulting in a monolayer of cells with few bonding sites between the polymer surface. On the contrary, on hydrophilic

acrylates cell proliferation was found at longer periods, with cells exhibiting a flatter shape and establishing contacts with the polymer surface. In view of these results, a proposed explanation is introduced:

- Hydrophobic surfaces: Albumin (inhibits cell adhesion) and Fibronectin (increase cell attachment and proliferation) compete for absorption on the biomaterial surface. The anti-adhesive protein Albumin is the first to be absorbed on hydrophobic materials, bonding Fibronectin at lower rate. Due to the faster arrival rate of proteins on hydrophobic surface, adhesive proteins do not unfold completely, driving to low interaction sites between cells and polymer surface showing a round shape.
- Hydrophilic surface: The anti-adhesive protein Albumin is not adsorbed on hydrophilic surfaces allowing more bounding sites for Fibronectin with good affinity on hydrophilic surfaces. The highly solvated hydrophilic surface at initial stage limits protein arrival and allowed protein rearrangement and spreading over the surface promoting cell adhesion and proliferation with better cytoskeleton spreading.

5 Conclusions

5.1 First chapter – Study of the improvement of PCL thermal and mechanical properties through the addition of HA and HNTs

In a first stage, the mechanical and thermal properties of PCL were studied by modifying the additivation percentage of HA and HNTs. This preliminary study allowed to understand the synergic effect between the polymeric matrix and the functional groups present on the additives chemical structure. Accordingly, the first objective proposed in this thesis was fulfilled by establishing the additivation threshold and optimizing the additivation rate. In this way, a 20 wt.% of HA was kept constant while the percentage of HNTs varied from 2.5 wt.% to 7.5 wt.%. The optimal HNTs percentage was determined after mechanical and thermal tests: the materials that showed the best properties were those with 5 and 7.5 wt.% of HNTs. Although both materials show similar thermal and mechanical properties, a 7.5 wt.% of HNTs was established as the optimum percentage, rather than 5%, because of a higher percentage of HNTs to be loaded with a selected drug. In general terms, a noticeable improvement of mechanical properties was achieved with the simultaneous addition of the two fillers. Shore D Hardness increased 10.3% with the addition of the two fillers simultaneously. Flexural modulus improved as the HNTs percentage increased, reaching values of up to 112.3% in samples with 20% of HA and 7.5% of HNTs with a flexural modulus of 886.8 MPa. Young's Modulus was observed to increase up to 109.3% with the addition of the two fillers reaching its greatest value of 449.6 MPa. Dynamic Mechanical Analysis indicates that the addition of HA and HNTs as fillers entails an enhancement of the storage modulus being again the hybrid loaded with 7.5% HNTs the material that shows the highest value. Regarding the impact test different results are obtained as a function of the added filler, the addition of fillers provokes a lower toughness of samples, however, in samples with HNTs but not HA, the absorbed energy was greater.

After investigating the additivation effect on the mechanical and thermal properties of the PCL, the second objective proposed in this thesis was accomplished through HNTs functionalization with curcumin before their mixture with PCL and HA in the optimal proportion previously established (PCL 20 wt.% of HA and 7.5 wt.% of HNTs). HNTs were preferably functionalized with curcumin in an acetone saturated solution because its solubility in this solvent is greater than in others like ethanol or water, and subsequently rinsed in water, dried, mixed and injected with PCL and HA to be mechanically and thermally tested. The results showed that functionalization of HNTs

with curcumin entailed a reduction of the mechanical properties of the hybrids. SEM images suggest that the functionalization process provokes the formation of aggregates during the drying process, resulting in the generation of crack initiation sites that promote the failure of the material. Dispersion of functionalized HNTs should thus be further enhanced by using polar solvents followed by mechanical stirring and several extrusion processes prior to injection moulding to improve the mechanical properties of these nanohybrids. For curcumin release rate, a general slowing tendency was observed over time after an initial burst. No changes were observed between the samples additivated directly with curcumin and samples loaded with additivated HNTs, suggesting that most of the curcumin is not effectively loaded inside the nanotubes but coating their surfaces.

5.2 Second chapter - Study of the influence of the addition of HA and HNTs on the morphological properties of PCL- and PHEMA-based polymers

After the preliminary study on the effect of inorganic fillers into a polyester matrix, the results were transferred to the followings chapters, were polymers with different nature were studied. Thus, the third objective of this thesis was addressed. Consequently, morphological properties were studied and compared among different pairs of polymers and nanocomposites with similar chemical natures but different hydrophobicity. On the one hand, the hydrophobic polyester PCL was modified by its blending with PLA at a ratio of 1:1 wt.%. On the other hand, the hydrophilic acrylate PHEMA was copolymerized with EMA at a ratio of 1:1 wt.%. These polymers were used as neat resins and combined with HA nanoparticles and HNTs.

Surface and transversal section EDS mapping images were obtained to assess the distribution of the fillers throughout the samples. The surfaces and transversal section showed in all cases a homogeneous distribution of HA. However, HNTs are distributed in a dissimilar way, depending on their composition showing big aggregates in P(HEMA-co-EMA) copolymer and the PHEMA homopolymer.

PCL based hybrids did not efficiently induce any apatite growth, however, Polymethacrylate based hybrids induced the formation of a hydroxyapatite layer. Comparing neat polymers (especially PCL and PCL/PLA blend) with materials additivated with HA and HNTs, nucleation efficiency increases with the addition of the fillers. A greater bioactivity is seen for P(HEMA-co-EMA) with respect to PHEMA due to its less hydrophilic character which increases the number of nucleation sites for the Ca-P per surface unit.

Materials based on PCL did not show visual morphological changes after 12 weeks of degradation in PBS at 37°C, fact that coincided with the overall slow rate of mass loss and its associated gradual decrease of Young Modulus. As opposed, blends of PCL/PLA showed acute morphological changes after degradation in PBS at 37°C, with a maximum rate of mass loss of 41% after 12 weeks for samples with the two fillers. Decrease in mechanical properties was directly correlated to mass loss.

An overall conclusion can be discerned: polymers with moderately hydrophilic character induce a higher rate of hydroxyapatite nucleation and a faster degradation rate. However, HNTs tends to form big aggregates when the hydrophilic character increases, driving to crack initiation sites and failure of the material.

5.3 Third chapter - Influence of the hydrophobic–hydrophilic nature of PCL- and PHEMA-based polymers and their nanocomposites on their *in vitro* biological development

In this chapter, the fourth objective of the thesis was approached and the *in vitro* biological development of the different pair of polymers was studied regarding its hydrophobicity character. Cell viability, proliferation, and morphology were monitored on the two pairs of polymers after varying the polymer's chemical surface by blending hydrophilic and hydrophobic polymers, or copolymerizing monomers of opposite natures, and/or loading the polymer matrix with nanoparticles such as HA or HNTs. To this end, the polyesters PCL, PCL/PLA and the polyacrylates PHEMA and P(HEMA-co-EMA) were used alone and loaded with HA and HNTs.

The surface wettability was determined by water contact angle measurements locating PCL at the hydrophobic end, with a contact angle of 105° and PHEMA at the hydrophilic end, with a contact angle of 59.7°. The addition of HA and HNTs clearly improved surface wettability on PCL (mean contact angle value decreased around 22%). This effect was hardly observed in the less hydrophobic PCL/PLA mixture. The addition of HA and HNTs in PHEMA increased its surface wettability (mean contact angle value decreased around 18%), but that of P(HEMA-co-EMA) remained constant. In summary, it appears that the addition of HA and HNT increased the wettability of neat extreme samples (PCL and PHEMA), but not that of their balanced combinations (PCL/PLA and P(HEMA-co-EMA)).

An improvement in cell viability with the addition of HA and HNTs was observed in PCL/PLA and P(HEMA-co-EMA) based samples. This was due to the generation of new reactive sites with Ca^{2+} and PO_4^{3-} groups present in HA, and silanol groups (Si-OH)

located at the surfaces of HNTs. On moderately hydrophobic polyesters (PCL/PLA, PCL/PLA HA 20, and PCL/PLA HA 20 HNTs 7.5), at the initial stages, cells tended to proliferate and showed a round shape. Interactions occurred primarily between them or with the extracellular matrix, resulting in a monolayer of cells with few bonding sites with the polymer surface. On the contrary, on hydrophilic acrylates (P(HEMA-co-EMA), P(HEMA-co-EMA) HA 20, and P(HEMA-co-EMA) HA20 HNTs 7.5)) cell proliferation was found at longer periods, with cells exhibiting a flatter shape and establishing contacts with the polymer surface.

On neat P(HEMA-co-EMA) materials isolated cells well adhered to the surface and spreading their cytoskeleton with a flat surface were observed. However, on PCL/PLA surfaces, cells aggregated in clusters, showing a rounded shape. Similar results were observed for moderately hydrophilic surfaces (P(HEMA-co-EMA) HA20 and P(HEMA-co-EMA) HA20 HNTs7.5)) which showed a better cytoskeleton spreading than moderately hydrophobic ones (PCL/PLA HA20, PCL/PLA HA20 HNTs7.5). Competitive absorption and water steric hindrance support a plausible explanation for cell behaviour on polymer surfaces of different wettability.

Initially, fibronectin and albumin seemed to compete for absorption on the biomaterial surface depending on the arrival rate, size, and affinity to the biomaterial surface. In moderately hydrophobic surfaces (PCL, PCL/PLA), the non-adhesive protein albumin adhered more easily to the surface than fibronectin, due to its shorter size and suitable hydrophobic affinity. Although fibronectin also bonded, it did so at a lower rate, thus promoting cell adhesion. Hence, hydrophilic surfaces (PHEMA, P(HEMA-co-EMA)) were highly solvated, obstructing protein approach and absorption, and hence, cell adhesion. Nevertheless, after long cell culture periods, the fibronectin's slow initial absorption with good affinity on hydrophilic surfaces allowed a protein rearrangement and spreading over the surface promoting cell adhesion and proliferation.

6 List of contributions

Journal papers

Title: Improvement of mechanical and biological properties of Polycaprolactone loaded with Hydroxyapatite and Halloysite Nanotubes

Authors: Elena Torres, Vicent Fombuena, Ana Vallés-Lluch, Thomas Ellingham

Jornal: *Materials Science and Engineering C*, 2017, 75, 418-424

DOI: 10.1016/j.msec.2017.02.087

Title: Influence of the Hydrophobic-Hydrophilic Nature of Biomedical Polymers and Nanocomposites on In Vitro Biological Development

Authors: Elena Torres, Ana Vallés-Lluch, Vicent Fombuena, Brett Napiwocki, Turn Lih-Sheng

Jornal: *Macromolecular Materials and Engineering*, 2017, 302(12), 1700259-1700269

DOI: 10.1002/mame.201700259

Title: Enhanced hydrophobicity and reduced water transport properties in alkylalkoxysilane modified Poly(butylene terephthalate) using reactive extrusion.7

Authors: Marwa Kchaoua, Elena Torresc, Noëllie Yllaa, Marion Colellab, Fernande Da Cruz-Boissonb, Philippe Cassagnaua, Eliane Espuche, Véronique Bounor-Legaré.

Jornal: *Materials Chemistry and Physics*, 2018, 223, 597-606

DOI: 10.1016/j.matchemphys.2018.11.001

Congress Participation

Congress: 16th Annual International Polymer Colloquium, Madison, Wisconsin, 2016

Type of Participation: Poster

Title: Improvement of Mechanical and Biological Properties of Polycaprolactone Loaded with Hydroxyapatite and Halloysite Nanotubes.

Congress: VI Congreso I+D+i Campus de Alcoi. Creando sinergias, Alcoy, Spain, 2018

Type of Participation: Poster

Title: I+D De Nuevos Monofilamentos en Base a Biopolímeros Avanzados y de Altas Prestaciones. Desarrollo de Bio-materiales Destinados a Regeneración de Tejidos Vivos.

7 Figure Captions

Figure 1 Aliphatic polyesters typically used in Tissue Engineering.....	28
Figure 2 PLA stereoisomers: L-lactide (PLLA) on the left and D-lactide (PDLA) on the right.....	30
Figure 3 PLA Tacticity. Relative stereochemistry of adjacent PLA chiral centres.	30
Figure 4 Hydrolytic cleavage of ester bonds generating carboxylic acid end groups.....	34
Figure 5 Scheme of an halloysite nanotube [152].....	44
Figure 6 Halloysite nanotubes functionalization process with curcumin proposed by Abdullayev and Lvov [1].....	60
Figure 7 Comparison of Differential Scanning Calorimetry curves for PCL-based hybrids showing the normalized heat flux vs. temperature for PCL-based hybrids.....	76
Figure 8 Comparison of TGA curves showing the mass loss (%) vs. temperature for PCL-based hybrids.....	78
Figure 9 Dynamical Mechanical Thermal Analysis curves (storage modulus) for PCL-based hybrids.....	80
Figure 10 Comparison of mechanical properties of the different nanohybrids and PCL as control. —▲—DMA (MPa), —◆—Young's modulus (MPa), —■— Flexural modulus (MPa), —●— Shore D Hardness (secondary axis).	90
Figure 11 Normalized mass loss vs. temperature of halloysite nanotubes functionalized with curcumin using three different solvents (ethanol, acetone or water). The thermograms for HNTs and curcumin are given for comparison.	92
Figure 12. SEM images of PCL, PLA HA20 HNTs7.5 and PCL HA20 HNTs7.5 + curcumin samples, the last two showing HNTs aggregates.	96
Figure 13 Curcumin delivery rate measurements presented as cumulative concentration vs time for HNTs loaded with curcumin and dispersed in PBS, PCL aditivated with HNTs loaded with curcumin, and PCL aditivated with curcumin.	97
Figure 14 Representation of Mechanical properties for PCL/PLA based hybrids. On the left Young modulus and standard deviation of PCL/PLA based hybrids. On the right, Flexural modulus and standard deviation of PCL/PLA based hybrids.....	99
Figure 15 Energy-dispersive X-ray spectroscopy (EDS) for copolymers samples loaded with HA and HNTs (PCL HA20 HNTs7.5, PCL/PLA HA20 HNTs7.5, PHEMA HA20 HNTs7.5, PHEMA-co-EMA HA20 HNTs7.5)	101
Figure 16 Left: Results of degradation % mass loss over 4, 8 and 12 weeks for PCL based materials. Right: Results of degradation Young Modulus over 4, 8 and 12 weeks for PCL based materials	113
Figure 17 Left: Results of degradation % mass loss over 4, 8 and 12 weeks for PCL/PLA based materials. Right: Results of Young Modulus following 4, 8 and 12 weeks of degradation for PCL/PLA based materials.	114
Figure 18 MTS Cell viability results comparing first the raw polymers, secondly the addition of HA, and third the addition of HA and HNTs. A) Cell viability at initial stage and B) Cell viability at long periods of cell culture.	117

Figure 19 Immunocytochemistry images for raw PCL/PLA and P(HEMA-co-EMA) samples (scale bar 25 μm). Comparison of cell attachment and spreading depending on the surface hydrophobicity after 3 days of culture. Vinculin staining for focal adhesions is shown in white in the top row for the two materials, together with DAPI staining of the nuclei. Phalloidin staining of the actin cytoskeleton is shown in the bottom row in red. (DAPI staining in blue, vinculin in white in the top row, and phalloidin in red in the bottom row.) 123

Figure 20 Immunocytochemistry images (scale bar 25 μm) comparing moderately hydrophobic (PCL/PLA) and hydrophilic P(HEMA-co-EMA) surfaces loaded with HA and HNTs at day 3 of culture (DAPI staining in blue and phalloidin in red). 124

Figure 21 Competitive protein absorption between fibronectin and albumin at the initial stages and over longer culture periods. 128

Figure 22 Solvation effect. (A) Solvation on hydrophilic surfaces induces a 1 nm layer of water, delaying protein approach, and hence, absorption. (B) On hydrophobic surfaces, the layer of water is restricted to ions. 129

8 Table Captions

Table 1 PCL thermal, mechanical properties and degradation rate.....	28
Table 2 PLA thermal, mechanical properties and degradation rate.....	29
Table 3 Crystallinity, elongation and thermal properties of the different PLA stereoisomers.	30
Table 4 PGA thermal, mechanical properties and degradation rate.	31
Table 5 PHB thermal, mechanical properties and degradation rate.	32
Table 6 Comparison among PCL, PLA, PGA and PHB polyesters regarding crystallinity, hydrophobicity and degradation rate.	36
Table 7 PCL/HA/HNTs mass percent composition of injected mixtures.	54
Table 8 Extrusion and injection moulding parameters.	55
Table 9 Test conditions used in the Differential Scanning Calorimetry (DSC).	56
Table 10 Sample identification for the curcumin delivery rate evaluation.....	62
Table 11 Weight percentages of the reactants used for sample preparation.	64
Table 12 Materials selected for the biological study.	67
Table 13 Weight percentages of the polyester polymers and inorganic fillers used for samples preparation for biological studies.....	67
Table 14 Weight percentages of the acrylates polymers and inorganic fillers used for samples preparation for biological studies.....	68
Table 15 Differential Scanning Calorimetry results for PCL-based hybrids. Samples with a mass between 6.0 g and 9.5 g were used for the analysis. Enthalpy (ΔH (J/g)) is given as the integral area of the melting transition, melting (T_m) and decomposition temperature (T_d) is expressed in $^{\circ}\text{C}$	76
Table 16 Thermogravimetric Analysis results for PCL-based hybrids. Samples with a mass between 6.0 g and 9.5 g were used for the analysis. Mass loss (%) and mass residual ratio (%) were studied in a range of temperature of 200 $^{\circ}\text{C}$	77
Table 17 VICAT tests results and heat deflection temperatures (HDT) for PCL-based hybrids. VICAT analysis show results for two replicates of each sample, while HDT analysis show only one replicate for each sample.	79
Table 18 Shore D Hardness results for PCL-based hybrids. Values represented for 5 replicates of each sample indicating the average value (\bar{x}) and standard deviations (s).	81
Table 19 Impact Charpy analysis results for PCL-based hybrids. Values represented for 5 replicates of each sample indicating the average value (\bar{x}) and standard deviations (s).....	82
Table 20 Impact Charpy SEM failure surface morphology for PCL-based hybrids.....	83
Table 21 Flexural analysis results for PCL-based hybrids. Five replicates of each sample were studied, the mean value (\bar{x}) and standard deviation s are indicated.	88
Table 22 Tensile analysis results for PCL-based hybrids. Five replicates of each sample were studied, the mean value (\bar{x}) and standard deviation s are indicated.	89

Table 23. Comparison of the curcumin loading efficiency in HNTs using SEM images to evaluate the diameter of the loaded nanotubes with curcumin using water, ethanol or acetone as a solvent.	93
Table 24. Mechanical properties of PCL, PCL HA20 HNTs7.5 and PCL HA20 HNTs7.5+curcumin samples. Values represented for 5 replicates of each sample indicating the average value (\bar{x}) and standard deviations (s).	95
Table 25. Thermal properties of PCL, PCL HA20 HNTs7.5 and PCL HA20 HNTs7.5+curcumin samples, where $T_{m,onset}$ is the temperature at the melting onset, $T_{m,peak}$ is the temperature at the peak maximum, and Δh_m is the heat adsorbed per mass unit.	95
Table 26 Mechanical properties for PCL/PLA based hybrids. Young and Flexural moduli mean value for 5 replicates of each sample and the standard deviation.	100
Table 27 SEM and EDS images taken for hydroxyapatite nucleation analysis. 5000 magnification pictures are shown, and formation of hydroxyapatite cauliflowers can be observed in the surface of some materials. The Ca/P ratio was calculated in order to verify the hydroxyapatite layer formation.....	103
Table 28 Degradation results for PCL- and PCL/PLA-based materials. % mass loss, Young modulus (MPa) and % of Young modulus upkeep over a period of 4, 8 and 12 weeks.	111
Table 29 Contact angle results of raw polymers (PCL, PCL/PLA, PHEMA, P(HEMA-co-EMA)) compared with those loaded with HA, and HA and HNTs. \bar{x} and s stand for average contact angle and standard deviation, respectively.	116
Table 30 MTS Cell viability results divided into three different groups of materials according to their inorganic loading: in the first group, raw polymers PCL, PCL/PLA, PHEMA, and P(HEMA-co-EMA) are compared; in the second and third groups, HA or HA and HNTs are incorporated and compared.....	118
Table 31 SEM images (400 X) of the polymers showing the highest absorbance values in MTS assays: PCL/PLA, P(HEMA-co-EMA), raw and loaded with HA or HA and HNTs, after 3 and 14 days of culture.	119
Table 32 Influence of HNTs loaded with curcumin incorporated to the PCL matrix. Cell viability of samples aditivated with curcumin.....	121
Table 33 Albumin and Fibronectin competitive absorption on PLA (moderately hydrophobic) and PHB (hydrophobic), measuring five replicates of each sample and obtaining the mean value and standard deviation.	126

9 References

- [1] D. Williams, "On the nature of biomaterials," *Biomaterials*, vol. 30, no. 30, pp. 5897-5909, Oct 2009, doi: 10.1016/j.biomaterials.2009.07.027.
- [2] D. Williams, "Definition in Biomaterial," presented at the Consensus Conference on Definitions in Biomaterials Science, Chester, England, 1986.
- [3] S. Gautam, C. F. Chou, A. K. Dinda, P. D. Potdar, and N. C. Mishra, "Surface modification of nanofibrous polycaprolactone/gelatin composite scaffold by collagen type I grafting for skin tissue engineering," *Materials Science & Engineering C-Materials for Biological Applications*, vol. 34, pp. 402-409, Jan 2014, doi: 10.1016/j.msec.2013.09.043.
- [4] F. Groeber, M. Holeiter, M. Hampel, S. Hinderer, and K. Schenke-Layland, "Skin tissue engineering - In vivo and in vitro applications," *Advanced Drug Delivery Reviews*, vol. 63, no. 4-5, pp. 352-366, Apr 2011, doi: 10.1016/j.addr.2011.01.005.
- [5] W. J. Li *et al.*, "A three-dimensional nanofibrous scaffold for cartilage tissue engineering using human mesenchymal stem cells," *Biomaterials*, vol. 26, no. 6, pp. 599-609, Feb 2005, doi: 10.1016/j.biomaterials.2004.03.005.
- [6] A. I. Rodrigues, M. E. Gomes, I. B. Leonor, and R. L. Reis, "Bioactive starch-based scaffolds and human adipose stem cells are a good combination for bone tissue engineering," *Acta Biomaterialia*, vol. 8, no. 10, pp. 3765-3776, Oct 2012, doi: 10.1016/j.actbio.2012.05.025.
- [7] X. M. Li, Q. L. Feng, W. J. Wang, and F. Z. Cui, "Chemical characteristics and cytocompatibility of collagen-based scaffold reinforced by chitin fibers for bone tissue engineering," *Journal of Biomedical Materials Research Part B-Applied Biomaterials*, vol. 77B, no. 2, pp. 219-226, May 2006, doi: 10.1002/jbm.b.30425.
- [8] S. Sahoo, L. T. Ang, J. C. H. Goh, and S. L. Toh, "Bioactive nanofibers for fibroblastic differentiation of mesenchymal precursor cells for ligament/tendon tissue engineering applications," *Differentiation*, vol. 79, no. 2, pp. 102-110, Feb 2010, doi: 10.1016/j.diff.2009.11.001.
- [9] J. A. Hu, X. A. Sun, H. Y. Ma, C. Q. Xie, Y. E. Chen, and P. X. Ma, "Porous nanofibrous PLLA scaffolds for vascular tissue engineering," *Biomaterials*, vol. 31, no. 31, pp. 7971-7977, Nov 2010, doi: 10.1016/j.biomaterials.2010.07.028.
- [10] A. Hasan *et al.*, "Electrospun scaffolds for tissue engineering of vascular grafts," *Acta Biomaterialia*, vol. 10, no. 1, pp. 11-25, Jan 2014, doi: 10.1016/j.actbio.2013.08.022.
- [11] L. Ghasemi-Mobarakeh, M. P. Prabhakaran, M. Morshed, M. H. Nasr-Esfahani, and S. Ramakrishna, "Electrospun poly(epsilon-caprolactone)/gelatin nanofibrous scaffolds for nerve tissue engineering," *Biomaterials*, vol. 29, no. 34, pp. 4532-4539, Dec 2008, doi: 10.1016/j.biomaterials.2008.08.007.
- [12] M. A. Pattison, S. Wurster, T. J. Webster, and K. M. Haberstroh, "Three-dimensional, nano-structured PLGA scaffolds for bladder tissue replacement applications," *Biomaterials*, vol. 26, no. 15, pp. 2491-2500, May 2005, doi: 10.1016/j.biomaterials.2004.07.011.

- [13] F. Chen *et al.*, "Preparation and characterization of oxidized alginate covalently cross-linked galactosylated chitosan scaffold for liver tissue engineering," *Materials Science & Engineering C-Materials for Biological Applications*, vol. 32, no. 2, pp. 310-320, Mar 2012, doi: 10.1016/j.msec.2011.10.034.
- [14] H. Y. Tian, Z. H. Tang, X. L. Zhuang, X. S. Chen, and X. B. Jing, "Biodegradable synthetic polymers: Preparation, functionalization and biomedical application," *Progress in Polymer Science*, vol. 37, no. 2, pp. 237-280, Feb 2012, doi: 10.1016/j.progpolymsci.2011.06.004.
- [15] L. S. Nair and C. T. Laurencin, "Biodegradable polymers as biomaterials," *Progress in Polymer Science*, vol. 32, no. 8-9, pp. 762-798, Aug-Sep 2007, doi: 10.1016/j.progpolymsci.2007.05.017.
- [16] D. W. Hutmacher, "Scaffolds in tissue engineering bone and cartilage," *Biomaterials*, vol. 21, no. 24, pp. 2529-2543, Dec 2000, doi: 10.1016/s0142-9612(00)00121-6.
- [17] E. Torres, A. Valles-Lluch, V. Fombuena, B. Napiwocki, and T. Lih-Sheng, "Influence of the Hydrophobic-Hydrophilic Nature of Biomedical Polymers and Nanocomposites on In Vitro Biological Development," *Macromolecular Materials and Engineering*, vol. 302, no. 12, Dec 2017, Art no. 1700259, doi: 10.1002/mame.201700259.
- [18] A. Butscher, M. Bohner, S. Hofmann, L. Gauckler, and R. Mueller, "Structural and material approaches to bone tissue engineering in powder-based three-dimensional printing," *Acta Biomaterialia*, vol. 7, no. 3, pp. 907-920, Mar 2011, doi: 10.1016/j.actbio.2010.09.039.
- [19] X. Li *et al.*, "3D-Printed Biopolymers for Tissue Engineering Application," *International Journal of Polymer Science*, 2014 2014, Art no. 829145, doi: 10.1155/2014/829145.
- [20] Y. Ikada, "Challenges in tissue engineering," *Journal of the Royal Society Interface*, vol. 3, no. 10, pp. 589-601, Oct 22 2006, doi: 10.1098/rsif.2006.0124.
- [21] U. Meyer, Meyer, Th., Handschel, J., Wiesmann, H.P., *Fundamentals of Tissue Engineering and Regenerative Medicine*. Springer, 2009.
- [22] F. Barrere, T. A. Mahmood, K. de Groot, and C. A. van Blitterswijk, "Advanced biomaterials for skeletal tissue regeneration: Instructive and smart functions," *Materials Science & Engineering R-Reports*, vol. 59, no. 1-6, pp. 38-71, Feb 29 2008, doi: 10.1016/j.mser.2007.12.001.
- [23] J. C. Fricain *et al.*, "A nano-hydroxyapatite - Pullulan/dextran polysaccharide composite macroporous material for bone tissue engineering," *Biomaterials*, vol. 34, no. 12, pp. 2947-2959, Apr 2013, doi: 10.1016/j.biomaterials.2013.01.049.
- [24] Y. Noyama, T. Miura, T. Ishimoto, T. Itaya, M. Niinomi, and T. Nakano, "Bone Loss and Reduced Bone Quality of the Human Femur after Total Hip Arthroplasty under Stress-Shielding Effects by Titanium-Based Implant," *Materials Transactions*, vol. 53, no. 3, pp. 565-570, Mar 2012, doi: 10.2320/matertrans.M2011358.

- [25] J. P. Temple *et al.*, "Engineering anatomically shaped vascularized bone grafts with hASCs and 3D-printed PCL scaffolds," *Journal of Biomedical Materials Research Part A*, vol. 102, no. 12, pp. 4317-4325, Dec 2014, doi: 10.1002/jbm.a.35107.
- [26] A. S. Brydone, D. Meek, and S. Maclaine, "Bone grafting, orthopaedic biomaterials, and the clinical need for bone engineering," *Proceedings of the Institution of Mechanical Engineers Part H-Journal of Engineering in Medicine*, vol. 224, no. H12, pp. 1329-1343, 2010, doi: 10.1243/09544119jeim770.
- [27] J. M. Piitulainen, T. Kauko, K. M. J. Aitasalo, V. Vuorinen, P. K. Vallittu, and J. P. Posti, "Outcomes of Cranioplasty with Synthetic Materials and Autologous Bone Grafts," *World Neurosurgery*, vol. 83, no. 5, pp. 708-714, May 2015, doi: 10.1016/j.wneu.2015.01.014.
- [28] S. Honeybul and K. M. Ho, "How "Successful" Is Calvarial Reconstruction Using Frozen Autologous Bone?," *Plastic and Reconstructive Surgery*, vol. 130, no. 5, pp. 1110-1117, Nov 2012, doi: 10.1097/PRS.0b013e318267d4de.
- [29] K. D. Martin *et al.*, "Autologous bone flap cranioplasty following decompressive craniectomy is combined with a high complication rate in pediatric traumatic brain injury patients," *Acta Neurochirurgica*, vol. 156, no. 4, pp. 813-824, Apr 2014, doi: 10.1007/s00701-014-2021-0.
- [30] K. J. Lowry *et al.*, "Polycaprolactone/glass bioabsorbable implant in a rabbit humerus fracture model," *Journal of Biomedical Materials Research*, vol. 36, no. 4, pp. 536-541, Sep 15 1997.
- [31] T. J. Corden, I. A. Jones, C. D. Rudd, P. Christian, S. Downes, and K. E. McDougall, "Physical and biocompatibility properties of poly-epsilon-caprolactone produced using in situ polymerisation: a novel manufacturing technique for long-fibre composite materials," *Biomaterials*, vol. 21, no. 7, pp. 713-724, Apr 2000, doi: 10.1016/s0142-9612(99)00236-7.
- [32] L. Onal, S. Cozien-Cazuc, I. A. Jones, and C. Rudd, "Water absorption properties of phosphate glass fiber-reinforced poly-epsilon-caprolactone composites for craniofacial bone repair," *Journal of Applied Polymer Science*, vol. 107, no. 6, pp. 3750-3755, Mar 15 2008, doi: 10.1002/app.27518.
- [33] I. Ahmed, A. J. Parsons, G. Palmer, J. C. Knowles, G. S. Walkers, and C. D. Rudd, "Weight loss, ion release and initial mechanical properties of a binary calcium phosphate glass fibre/PCL composite," *Acta Biomaterialia*, vol. 4, no. 5, pp. 1307-1314, Sep 2008, doi: 10.1016/j.actbio.2008.03.018.
- [34] J. E. Gough, P. Christian, C. A. Scotchford, C. D. Rudd, and I. A. Jones, "Synthesis, degradation, and in vitro cell responses of sodium phosphate glasses for craniofacial bone repair," *Journal of Biomedical Materials Research*, vol. 59, no. 3, pp. 481-489, Mar 5 2002, doi: 10.1002/jbm.10020.
- [35] J. E. Gough, P. Christian, J. Unsworth, M. P. Evans, C. A. Scotchford, and I. A. Jones, "Controlled degradation and macrophage responses of a fluoride-treated polycaprolactone," *Journal of Biomedical Materials Research Part A*, vol. 69A, no. 1, pp. 17-25, Apr 1 2004, doi: 10.1002/jbm.a.20072.

- [36] R. R. M. Bos, F. R. Rozema, G. Boering, A. J. Nijenhuis, A. J. Pennings, and A. B. Verwey, "Bio-Absorbable Plates and Screws for Internal-Fixation of Mandibular Fractures - A Study in 6 Dogs," *International Journal of Oral and Maxillofacial Surgery*, vol. 18, no. 6, pp. 365-369, Dec 1989, doi: 10.1016/s0901-5027(89)80035-9.
- [37] K. C. Yerit *et al.*, "Fixation of mandibular fractures with biodegradable plates and screws," *Oral Surgery Oral Medicine Oral Pathology Oral Radiology and Endodontics*, vol. 94, no. 3, pp. 294-300, Sep 2002, doi: 10.1067/moe.2002.122833.
- [38] N. R. Boeree, J. Dove, J. J. Cooper, J. C. Knowles, and G. W. Hastings, "Development of A Degradable Composite for Orthopedic Use - Mechanical Evaluation of an Hydroxyapatite Polyhydroxybutyrate Composite-Material," *Biomaterials*, vol. 14, no. 10, pp. 793-796, Aug 1993, doi: 10.1016/0142-9612(93)90046-5.
- [39] E. Torres, V. Fombuena, A. Valles-Lluch, and T. Ellingham, "Improvement of mechanical and biological properties of Polycaprolactone loaded with Hydroxyapatite and Halloysite nanotubes," *Materials Science & Engineering C-Materials for Biological Applications*, vol. 75, pp. 418-424, Jun 2017, doi: 10.1016/j.msec.2017.02.087.
- [40] S. Bose, M. Roy, and A. Bandyopadhyay, "Recent advances in bone tissue engineering scaffolds," *Trends in Biotechnology*, vol. 30, no. 10, pp. 546-554, Oct 2012, doi: 10.1016/j.tibtech.2012.07.005.
- [41] K. Tuzlakoglu, N. Bolgen, A. J. Salgado, M. E. Gomes, E. Piskin, and R. L. Reis, "Nano- and micro-fiber combined scaffolds: A new architecture for bone tissue engineering," *Journal of Materials Science-Materials in Medicine*, vol. 16, no. 12, pp. 1099-1104, Dec 2005, doi: 10.1007/s10856-005-4713-8.
- [42] R. Scaffaro, F. Lopresti, L. Botta, S. Rigogliuso, and G. Gherzi, "Preparation of three-layered porous PLA/PEG scaffold: relationship between morphology, mechanical behavior and cell permeability," *Journal of the Mechanical Behavior of Biomedical Materials*, vol. 54, pp. 8-20, Feb 2016, doi: 10.1016/j.jmbbm.2015.08.033.
- [43] N. Ignjatovic, V. Wu, Z. Ajdukovic, T. Mihajilov-Krstev, V. Uskokovic, and D. Uskokovic, "Chitosan-PLGA polymer blends as coatings for hydroxyapatite nanoparticles and their effect on antimicrobial properties, osteoconductivity and regeneration of osseous tissues," *Materials Science & Engineering C-Materials for Biological Applications*, vol. 60, pp. 357-364, Mar 2016, doi: 10.1016/j.msec.2015.11.061.
- [44] L. Meinel *et al.*, "Bone tissue engineering using human mesenchymal stem cells: Effects of scaffold material and medium flow," *Annals of Biomedical Engineering*, vol. 32, no. 1, pp. 112-122, Jan 2004, doi: 10.1023/B:ABME.0000007796.48329.b4.
- [45] K. E. Washington, R. N. Kularatne, V. Karmegam, M. C. Biewer, and M. C. Stefan, "Recent advances in aliphatic polyesters for drug delivery applications," *Wiley Interdisciplinary Reviews-Nanomedicine and Nanobiotechnology*, vol. 9, no. 4, Jul-Aug 2017, Art no. UNSP e1446, doi: 10.1002/wnan.1446.
- [46] R. S. Bezwada *et al.*, "Monocryl(R) Suture, a New Ultra-Pliable Absorbable Monofilament Suture," *Biomaterials*, vol. 16, no. 15, pp. 1141-1148, Oct 1995, doi: 10.1016/0142-9612(95)93577-z.

- [47] A. P. Pego *et al.*, "In vivo behavior of poly(1,3-trimethylene carbonate) and copolymers of 1,3-trimethylene carbonate with D,L-lactide or epsilon-caprolactone: Degradation and tissue response," *Journal of Biomedical Materials Research Part A*, vol. 67A, no. 3, pp. 1044-1054, Dec 1 2003, doi: 10.1002/jbm.a.10121.
- [48] F. J. Van Natta, J. W. Hill, and W. H. Carothers, "Studies of polymerization and ring formation XXIII epsilon-Caprolactone and its polymers," *Journal of the American Chemical Society*, vol. 56, pp. 455-457, Jan-Jun 1934, doi: 10.1021/ja01317a053.
- [49] M. A. Woodruff and D. W. Hutmacher, "The return of a forgotten polymer-Polycaprolactone in the 21st century," *Progress in Polymer Science*, vol. 35, no. 10, pp. 1217-1256, Oct 2010, doi: 10.1016/j.progpolymsci.2010.04.002.
- [50] S. J. Hollister, "Porous scaffold design for tissue engineering," *Nature Materials*, vol. 4, no. 7, pp. 518-524, Jul 2005, doi: 10.1038/nmat1421.
- [51] J. R. Sarasua, A. L. Arraiza, P. Balerdi, and I. Maiza, "Crystallinity and mechanical properties of optically pure polylactides and their blends," *Polymer Engineering and Science*, vol. 45, no. 5, pp. 745-753, May 2005, doi: 10.1002/pen.20331.
- [52] M. I. Sabir, X. X. Xu, and L. Li, "A review on biodegradable polymeric materials for bone tissue engineering applications," *Journal of Materials Science*, vol. 44, no. 21, pp. 5713-5724, Nov 2009, doi: 10.1007/s10853-009-3770-7.
- [53] J. Rich, T. Jaakkola, T. Tirri, T. Narhi, A. Yli-Urpo, and J. Seppala, "In vitro evaluation of poly(epsilon-caprolactone-co-DL-lactide)/bioactive glass composites," *Biomaterials*, vol. 23, no. 10, pp. 2143-2150, May 2002, Art no. Pii s0142-9612(01)00345-3, doi: 10.1016/s0142-9612(01)00345-3.
- [54] H. Tsuji and Y. Ikada, "Blends of aliphatic polyesters .2. Hydrolysis of solution-cast blends from poly(L-lactide) and poly(epsilon-caprolactone) in phosphate-buffered solution," *Journal of Applied Polymer Science*, vol. 67, no. 3, pp. 405-415, Jan 18 1998.
- [55] R. E. Drumright, P. R. Gruber, and D. E. Henton, "Polylactic acid technology," *Advanced Materials*, vol. 12, no. 23, pp. 1841-1846, Dec 1 2000, doi: 10.1002/1521-4095(200012)12:23<1841::aid-adma1841>3.0.co;2-e.
- [56] J. K. Oh, "Polylactide (PLA)-based amphiphilic block copolymers: synthesis, self-assembly, and biomedical applications," *Soft Matter*, vol. 7, no. 11, pp. 5096-5108, 2011, doi: 10.1039/c0sm01539c.
- [57] Y. Ikada, K. Jamshidi, H. Tsuji, and S. H. Hyon, "Stereocomplex Formation Between Enantiomeric Poly(Lactides)," (in English), *Macromolecules*, Letter vol. 20, no. 4, pp. 904-906, Apr 1987, doi: 10.1021/ma00170a034.
- [58] J. C. Middleton and A. J. Tipton, "Synthetic biodegradable polymers as orthopedic devices," *Biomaterials*, vol. 21, no. 23, pp. 2335-2346, Dec 2000, doi: 10.1016/s0142-9612(00)00101-0.
- [59] T. Patricio, M. Domingos, A. Gloria, U. D'Amora, J. F. Coelho, and P. J. Bartolo, "Fabrication and characterisation of PCL and PCL/PLA scaffolds for tissue engineering,"

- Rapid Prototyping Journal*, vol. 20, no. 2, pp. 145-156, 2014 2014, doi: 10.1108/rpj-04-2012-0037.
- [60] O. S. Manoukian *et al.*, 2018.
- [61] K. Rezwani, Q. Z. Chen, J. J. Blaker, and A. R. Boccaccini, "Biodegradable and bioactive porous polymer/inorganic composite scaffolds for bone tissue engineering," *Biomaterials*, vol. 27, no. 18, pp. 3413-3431, Jun 2006, doi: 10.1016/j.biomaterials.2006.01.039.
- [62] A. C. Vieira, J. C. Vieira, R. M. Guedes, and A. T. Marques, "Degradation and Viscoelastic Properties of PLA-PCL, PGA-PCL, PDO and PGA Fibres," Patent 1-2, 2010. [Online]. Available: <Go to ISI>://WOS:000280763200125
- [63] S. Vainionpää, "Biodegradation of Polyglycolic Acid in Bone Tissue - An Experimental Study on Rabbits," *Archives of Orthopaedic and Trauma Surgery*, vol. 104, no. 6, pp. 333-338, 1986, doi: 10.1007/bf00454425.
- [64] C. Doyle, E. T. Tanner, and W. Bonfield, "Invitro and Invivo Evaluation of Polyhydroxybutyrate and of Polyhydroxybutyrate Reinforced With Hydroxyapatite," *Biomaterials*, vol. 12, no. 9, pp. 841-847, Nov 1991, doi: 10.1016/0142-9612(91)90072-i.
- [65] E. I. Shishatskaya, I. A. Khlusov, and T. G. Volova, "A hybrid PHB-hydroxyapatite composite for biomedical application: production, in vitro and in vivo investigation," *Journal of Biomaterials Science-Polymer Edition*, vol. 17, no. 5, pp. 481-498, 2006, doi: 10.1163/156856206776986242.
- [66] B. Zhang, R. Carlson, and F. Srienc, "Engineering the monomer composition of polyhydroxyalkanoates synthesized in *Saccharomyces cerevisiae*," *Applied and Environmental Microbiology*, vol. 72, no. 1, pp. 536-543, Jan 2006, doi: 10.1128/aem.72.1.536-543.2006.
- [67] Z. A. Raza, S. Abid, and I. M. Banat, "Polyhydroxyalkanoates: Characteristics, production, recent developments and applications," *International Biodeterioration & Biodegradation*, vol. 126, pp. 45-56, Jan 2018, doi: 10.1016/j.ibiod.2017.10.001.
- [68] G. Q. Chen and Q. Wu, "The application of polyhydroxyalkanoates as tissue engineering materials," *Biomaterials*, vol. 26, no. 33, pp. 6565-6578, Nov 2005, doi: 10.1016/j.biomaterials.2005.04.036.
- [69] M. Meischel *et al.*, "Adhesive strength of bone-implant interfaces and in-vivo degradation of PHB composites for load-bearing applications," *Journal of the Mechanical Behavior of Biomedical Materials*, vol. 53, pp. 104-118, Jan 2016, doi: 10.1016/j.jmbbm.2015.08.004.
- [70] M. Vert, "Aliphatic polyesters: Great degradable polymers that cannot do everything," *Biomacromolecules*, vol. 6, no. 2, pp. 538-546, Mar-Apr 2005, doi: 10.1021/bm0494702.
- [71] J. D. Badia, O. Gil-Casten, and A. Ribes-Greus, "Long-term properties and end-of-life of polymers from renewable resources," *Polymer Degradation and Stability*, vol. 137, pp. 35-57, Mar 2017, doi: 10.1016/j.polymdegradstab.2017.01.002.

- [72] C. G. Pitt, M. M. Gratzl, G. L. Kimmel, J. Surles, and A. Schindler, "ALIPHATIC POLYESTERS .2. THE DEGRADATION OF POLY(DL-LACTIDE), POLY(EPSILON-CAPROLACTONE), AND THEIR COPOLYMERS INVIVO," *Biomaterials*, vol. 2, no. 4, pp. 215-220, 1981 1981.
- [73] S. M. Li, H. Garreau, and M. Vert, "Structure Property Relationships In The Case of the Degradation of Massive Aliphatic Poly-(Alpha-Hydroxy Acids) In Aqueous-Media .1. Poly(DL-Lactic Acid)," *Journal of Materials Science-Materials in Medicine*, vol. 1, no. 3, pp. 123-130, Oct 1990, doi: 10.1007/bf00700871.
- [74] F. Von Burkersroda, L. Schedl, and A. Gopferich, "Why degradable polymers undergo surface erosion or bulk erosion," *Biomaterials*, vol. 23, no. 21, pp. 4221-4231, Nov 2002, Art no. Pii s0142-9612(02)00170-9, doi: 10.1016/s0142-9612(02)00170-9.
- [75] I. Kyrikou and D. Briassoulis, "Biodegradation of agricultural plastic films: A critical review," *Journal of Polymers and the Environment*, vol. 15, no. 2, pp. 125-150, Apr 2007, doi: 10.1007/s10924-007-0053-8.
- [76] N. Lucas, C. Bienaime, C. Belloy, M. Queneudec, F. Silvestre, and J. E. Nava-Saucedo, "Polymer biodegradation: Mechanisms and estimation techniques," *Chemosphere*, vol. 73, no. 4, pp. 429-442, Sep 2008, doi: 10.1016/j.chemosphere.2008.06.064.
- [77] K. H. Lee, H. Y. Kim, M. S. Khil, Y. M. Ra, and D. R. Lee, "Characterization of nano-structured poly(epsilon-caprolactone) nonwoven mats via electrospinning," *Polymer*, vol. 44, no. 4, pp. 1287-1294, Feb 2003, Art no. Pii s0032-3861(02)00820-0, doi: 10.1016/s0032-3861(02)00820-0.
- [78] H. F. Sun, L. Mei, C. X. Song, X. M. Cui, and P. Y. Wang, "The in vivo degradation, absorption and excretion of PCL-based implant," *Biomaterials*, vol. 27, no. 9, pp. 1735-1740, Mar 2006, doi: 10.1016/j.biomaterials.2005.09.019.
- [79] S. M. Li, H. Garreau, and M. Vert, "Structure-Property Relationships in the Case of the Degradation of Massive Poly(Alpha-Hydroxy Acids) in Aqueous-Media .3. Influence of the Morphology of Poly(L-Lactic Acid)," *Journal of Materials Science-Materials in Medicine*, vol. 1, no. 4, pp. 198-206, Nov 1990, doi: 10.1007/bf00701077.
- [80] H. Kweon *et al.*, "A novel degradable polycaprolactone networks for tissue engineering," *Biomaterials*, vol. 24, no. 5, pp. 801-808, Feb 2003, Art no. Pii s0142-9612(02)00370-8, doi: 10.1016/s0142-9612(02)00370-8.
- [81] A. P. Pego, A. A. Poot, D. W. Grijpma, and J. Feijen, "Copolymers of trimethylene carbonate and epsilon-caprolactone for porous nerve guides: Synthesis and properties," *Journal of Biomaterials Science-Polymer Edition*, vol. 12, no. 1, pp. 35-53, 2001 2001.
- [82] A. P. Pego, A. A. Poot, D. W. Grijpma, and J. Feijen, "In vitro degradation of trimethylene carbonate based (Co)polymers," *Macromolecular Bioscience*, vol. 2, no. 9, pp. 411-419, Dec 30 2002, doi: 10.1002/mabi.200290000.
- [83] H. Pistner, D. R. Bendix, J. Muhling, and J. F. Reuther, "Poly(L-Lactide) - a Long-Term Degradation Study Invivo 3. Analytical Characterization," *Biomaterials*, vol. 14, no. 4, pp. 291-298, Mar 1993, doi: 10.1016/0142-9612(93)90121-h.

- [84] S. C. Woodward, P. S. Brewer, F. Moatamed, A. Schindler, and C. G. Pitt, "The Intracellular Degradation of Poly(Epsilon-Caprolactone)," *Journal of Biomedical Materials Research*, vol. 19, no. 4, pp. 437-444, 1985 1985, doi: 10.1002/jbm.820190408.
- [85] S. Franz, S. Rammelt, D. Scharnweber, and J. C. Simon, "Immune responses to implants - A review of the implications for the design of immunomodulatory biomaterials," *Biomaterials*, vol. 32, no. 28, pp. 6692-6709, Oct 2011, doi: 10.1016/j.biomaterials.2011.05.078.
- [86] C. X. F. Lam, D. W. Hutmacher, J. T. Schantz, M. A. Woodruff, and S. H. Teoh, "Evaluation of polycaprolactone scaffold degradation for 6 months in vitro and in vivo," *Journal of Biomedical Materials Research Part A*, vol. 90A, no. 3, pp. 906-919, Sep 2009, doi: 10.1002/jbm.a.32052.
- [87] J. M. Anderson, A. Rodriguez, and D. T. Chang, "Foreign body reaction to biomaterials," *Seminars in Immunology*, vol. 20, no. 2, pp. 86-100, Apr 2008, doi: 10.1016/j.smim.2007.11.004.
- [88] M. Hakkarainen, A. Högglund, K. Odellius, and A. C. Albertsson, "Tuning the release rate of acidic degradation products through macromolecular design of caprolactone-based copolymers," *Journal of the American Chemical Society*, vol. 129, no. 19, pp. 6308-6312, May 2007, doi: 10.1021/ja0702871.
- [89] N. A. Peppas and R. Langer, "New Challenges In Biomaterials," *Science*, vol. 263, no. 5154, pp. 1715-1720, Mar 1994, doi: 10.1126/science.8134835.
- [90] W. Heidemann *et al.*, "Degradation of poly(D,L)lactide implants of calciumphosphates with or without addition in vivo," *Biomaterials*, vol. 22, no. 17, pp. 2371-2381, Sep 2001, doi: 10.1016/s0142-9612(00)00424-5.
- [91] A. Marcos-Fernandez, G. A. Abraham, J. L. Valentin, and J. San Roman, "Synthesis and characterization of biodegradable non-toxic poly(ester-urethane-urea)s based on poly(epsilon-caprolactone) and amino acid derivatives," *Polymer*, vol. 47, no. 3, pp. 785-798, Jan 2006, doi: 10.1016/j.polymer.2005.12.007.
- [92] A. Kulkarni, J. Reiche, K. Kratz, H. Kamusewitz, I. M. Sokolov, and A. Lendlein, "Enzymatic chain scission kinetics of Poly(epsilon-caprolactone) monolayers," *Langmuir*, vol. 23, no. 24, pp. 12202-12207, Nov 2007, doi: 10.1021/la701523e.
- [93] O. Bostman, U. Paivarinta, E. Partio, J. Vasenius, M. Manninen, and P. Rokkanen, "Degradation and Tissue Replacement of an Absorbable Polyglycolide Screw in the Fixation of Rabbit Femoral Osteotomies," *Journal of Bone and Joint Surgery-American Volume*, vol. 74A, no. 7, pp. 1021-1031, Aug 1992.
- [94] M. J. Manninen and T. Pohjonen, "Intramedullary Nailing of the Cortical Bone Osteotomies in Rabbits with Self-Reinforced Poly-L-Lactide Rods Manufactured by The Fibrillation Method," *Biomaterials*, vol. 14, no. 4, pp. 305-312, Mar 1993, doi: 10.1016/0142-9612(93)90123-j.
- [95] P. A. Gunatillake and R. Adhikari, "Biodegradable synthetic polymers for tissue engineering," *European cells & materials*, vol. 5, pp. 1-16, 2003 May 2003.

- [96] K. Ceonzo, A. Gaynor, L. Shaffer, K. Kojima, C. A. Vacanti, and G. L. Stahl, "Polyglycolic acid-induced inflammation: Role of hydrolysis and resulting complement activation," *Tissue Engineering*, vol. 12, no. 2, pp. 301-308, Feb 2006, doi: 10.1089/ten.2006.12.301.
- [97] S. Gogolewski, M. Jovanovic, S. M. Perren, J. G. Dillon, and M. K. Hughes, "Tissue-Response and in-Vivo Degradation of Selected Polyhydroxyacids - Polylactides (PLA), Poly(3-Hydroxybutyrate) (PHB), and Poly(3-Hydroxybutyrate-Co-3-Hydroxyvalerate) (PHB/VA)," *Journal of Biomedical Materials Research*, vol. 27, no. 9, pp. 1135-1148, Sep 1993, doi: 10.1002/jbm.820270904.
- [98] C. S. K. Reddy, R. Ghai, Rashmi, and V. C. Kalia, "Polyhydroxyalkanoates: an overview," *Bioresource Technology*, vol. 87, no. 2, pp. 137-146, Apr 2003, Art no. Pii s0960-8524(02)00212-2, doi: 10.1016/s0960-8524(02)00212-2.
- [99] A. Atlic *et al.*, "Continuous production of poly(R -3-hydroxybutyrate) by *Cupriavidus necator* in a multistage bioreactor cascade," *Applied Microbiology and Biotechnology*, vol. 91, no. 2, pp. 295-304, Jul 2011, doi: 10.1007/s00253-011-3260-0.
- [100] O. Wichterle and D. Lim, "Hydrophilic Gels for Biological Use," *Nature*, vol. 185, no. 4706, pp. 117-118, 1960, doi: 10.1038/185117a0.
- [101] A. S. Hoffman, "Hydrogels for biomedical applications," *Advanced Drug Delivery Reviews*, vol. 64, pp. 18-23, Dec 2012, doi: 10.1016/j.addr.2012.09.010.
- [102] J. S. Belkas, C. A. Munro, M. S. Shoichet, M. Johnston, and R. Midha, "Long-term in vivo biomechanical properties and biocompatibility of poly(2-hydroxyethyl methacrylate-co-methyl methacrylate) nerve conduits," *Biomaterials*, vol. 26, no. 14, pp. 1741-1749, May 2005, doi: 10.1016/j.biomaterials.2004.05.031.
- [103] R. Jeyanthi and K. P. Rao, "Invivo Biocompatibility Of Collagen Poly(Hydroxyethyl Methacrylate) Hydrogels," *Biomaterials*, vol. 11, no. 4, pp. 238-243, May 1990, doi: 10.1016/0142-9612(90)90004-a.
- [104] K. Smetana, J. Sulc, Z. Krcova, and S. Pitrova, "Intraocular Biocompatibility of Hydroxyethyl Methacrylate And Methacrylic-Acid Copolymer Partially Hydrolyzed Poly(2-Hydroxyethyl Methacrylate)," *Journal of Biomedical Materials Research*, vol. 21, no. 10, pp. 1247-1253, Oct 1987, doi: 10.1002/jbm.820211007.
- [105] J. Venkatesan and S. K. Kim, "Nano-Hydroxyapatite Composite Biomaterials for Bone Tissue Engineering-A Review," *Journal of Biomedical Nanotechnology*, vol. 10, no. 10, pp. 3124-3140, Oct 2014, doi: 10.1166/jbn.2014.1893.
- [106] V. Vergaro *et al.*, "Cytocompatibility and Uptake of Halloysite Clay Nanotubes," *Biomacromolecules*, vol. 11, no. 3, pp. 820-826, Mar 2010, doi: 10.1021/bm9014446.
- [107] **A. Ospovat, "Dictionary of Scientific Biography," in *Dictionary of Scientific Biography*, A. G. Werner, Gillespie, and CC., Eds., ed, 1970-1990.**
- [108] J. J. Berzelius, "Ueber basische phosphorsaure kalkerde," *Ann Chem Pharmac* vol. 53, p. 286, 1845.

- [109] W.-Y. Choi, H.-E. Kim, and Y.-H. Koh, "Production, mechanical properties and in vitro biocompatibility of highly aligned porous poly(epsilon-caprolactone) (PCL)/hydroxyapatite (HA) scaffolds," *Journal of Porous Materials*, vol. 20, no. 4, pp. 701-708, Aug 2013, doi: 10.1007/s10934-012-9644-4.
- [110] M. G. Yeo and G. H. Kim, "Preparation and Characterization of 3D Composite Scaffolds Based on Rapid-Prototyped PCL/beta-TCP Struts and Electrospun PCL Coated with Collagen and HA for Bone Regeneration," *Chemistry of Materials*, vol. 24, no. 5, pp. 903-913, Mar 13 2012, doi: 10.1021/cm201119q.
- [111] A. Salerno, S. Zeppetelli, E. Di Maio, S. Iannace, and P. A. Netti, "Design of Bimodal PCL and PCL-HA Nanocomposite Scaffolds by Two Step Depressurization During Solid-state Supercritical CO₂ Foaming," *Macromolecular Rapid Communications*, vol. 32, no. 15, pp. 1150-1156, Aug 3 2011, doi: 10.1002/marc.201100119.
- [112] I. T. Jackson and R. Yavuzer, "Hydroxyapatite cement: an alternative for craniofacial skeletal contour refinements," *British Journal of Plastic Surgery*, vol. 53, no. 1, pp. 24-29, Jan 2000, doi: 10.1054/bjps.1999.3236.
- [113] L. Miller, A. B. Guerra, R. S. Bidros, C. Trahan, R. Baratta, and S. E. Metzinger, "A comparison of resistance to fracture among four commercially available forms of hydroxyapatite cement," *Annals of Plastic Surgery*, vol. 55, no. 1, pp. 87-92, Jul 2005, doi: 10.1097/01.sap.0000162510.05196.c6.
- [114] E. E. Lawson, B. W. Barry, A. C. Williams, and H. G. M. Edwards, "Biomedical applications of Raman spectroscopy," *Journal of Raman Spectroscopy*, vol. 28, no. 2-3, pp. 111-117, Feb-Mar 1997, doi: 10.1002/(sici)1097-4555(199702)28:2/3<111::aid-jrs87>3.0.co;2-z.
- [115] K. J. MacKelvie, H. A. McKay, M. A. Petit, and R. W. Schutz, "Familial relationship in proximal femur bone mineral density is related to child's stage of maturity," *Journal of Bone and Mineral Research*, vol. 14, pp. S228-S228, Sep 1999.
- [116] D. F. Scott and W. L. Jaffe, "Host-bone response to porous-coated cobalt-chrome and hydroxyapatite-coated titanium femoral components in hip arthroplasty - Dual-energy x-ray absorptiometry analysis of paired bilateral cases at 5 to 7 years," *Journal of Arthroplasty*, vol. 11, no. 4, pp. 429-437, Jun 1996, doi: 10.1016/s0883-5403(96)80033-7.
- [117] H. M. Kim, T. Himeno, M. Kawashita, T. Kokubo, and T. Nakamura, "The mechanism of biomineralization of bone-like apatite on synthetic hydroxyapatite: an in vitro assessment," *Journal of the Royal Society Interface*, vol. 1, no. 1, pp. 17-22, Nov 22 2004, doi: 10.1098/rsif.2004.0003.
- [118] C. Loty, J. M. Sautier, H. Boulekbache, T. Kokubo, H. M. Kim, and N. Forest, "In vitro bone formation on a bone-like apatite layer prepared by a biomimetic process on a bioactive glass-ceramic," *Journal of Biomedical Materials Research*, vol. 49, no. 4, pp. 423-434, Mar 2000, doi: 10.1002/(sici)1097-4636(20000315)49:4<423::aid-jbm1>3.3.co;2-z.
- [119] A. V. Lluch, G. G. Ferrer, and M. M. Pradas, "Biomimetic apatite coating on P(EMA-co-HEA)/SiO₂ hybrid nanocomposites," *Polymer*, vol. 50, no. 13, pp. 2874-2884, Jun 2009, doi: 10.1016/j.polymer.2009.04.022.

- [120] H. Takadama, H. M. Kim, F. Miyaji, T. Kokubo, and T. Nakamura, "Mechanism of apatite formation induced by silanol groups - TEM observation," *Journal of the Ceramic Society of Japan*, vol. 108, no. 2, pp. 118-121, Feb 2000, doi: 10.2109/jcersj.108.1254_118.
- [121] A. L. Oliveira, J. F. Mano, and R. L. Reis, "Nature-inspired calcium phosphate coatings: present status and novel advances in the science of mimicry," *Current Opinion in Solid State & Materials Science*, vol. 7, no. 4-5, pp. 309-318, Aug-Oct 2003, doi: 10.1016/j.cossms.2003.10.009.
- [122] Zainuddin, D. J. T. Hill, A. K. Whittaker, and T. V. Chirila, "In-vitro study of the spontaneous calcification of PHEMA-based hydrogels in simulated body fluid," *Journal of Materials Science-Materials in Medicine*, vol. 17, no. 12, pp. 1245-1254, Dec 2006, doi: 10.1007/s10856-006-0598-4.
- [123] T. Jesionowski, J. Zdarta, and B. Krajewska, "Enzyme immobilization by adsorption: a review," *Adsorption-Journal of the International Adsorption Society*, vol. 20, no. 5-6, pp. 801-821, Aug 2014, doi: 10.1007/s10450-014-9623-y.
- [124] P. Roach, D. Eglin, K. Rohde, and C. C. Perry, "Modern biomaterials: a review-bulk properties and implications of surface modifications," *Journal of Materials Science-Materials in Medicine*, vol. 18, no. 7, pp. 1263-1277, Jul 2007, doi: 10.1007/s10856-006-0064-3.
- [125] P. V. Azzopardi, J. O'Young, G. Lajoie, M. Karttunen, H. A. Goldberg, and G. K. Hunter, "Roles of Electrostatics and Conformation in Protein-Crystal Interactions," *Plos One*, vol. 5, no. 2, Feb 19 2010, Art no. e9330, doi: 10.1371/journal.pone.0009330.
- [126] B. Feng, J. Y. Chen, and X. D. Zhang, "Interaction of calcium and phosphate in apatite coating on titanium with serum albumin," *Biomaterials*, vol. 23, no. 12, pp. 2499-2507, Jun 2002, Art no. Pii s0142-9612(01)00384-2, doi: 10.1016/s0142-9612(01)00384-2.
- [127] J.-W. Shen, T. Wu, Q. Wang, and H.-H. Pan, "Molecular simulation of protein adsorption and desorption on hydroxyapatite surfaces," *Biomaterials*, vol. 29, no. 5, pp. 513-532, Feb 2008, doi: 10.1016/j.biomaterials.2007.10.016.
- [128] H. Zhou, T. Wu, X. Dong, Q. Wang, and J. Shen, "Adsorption mechanism of BMP-7 on hydroxyapatite (001) surfaces," *Biochemical and Biophysical Research Communications*, vol. 361, no. 1, pp. 91-96, Sep 14 2007, doi: 10.1016/j.bbrc.2007.06.169.
- [129] L. W. Lin, L. Chow, and Y. Leng, "Study of hydroxyapatite osteoinductivity with an osteogenic differentiation of mesenchymal stem cells," *Journal of Biomedical Materials Research Part A*, vol. 89A, no. 2, pp. 326-335, May 2009, doi: 10.1002/jbm.a.31994.
- [130] B. Q. Chen and K. Sun, "Mechanical and dynamic viscoelastic properties of hydroxyapatite reinforced poly(epsilon-caprolactone)," *Polymer Testing*, vol. 24, no. 8, pp. 978-982, Dec 2005, doi: 10.1016/j.polymertesting.2005.07.013.
- [131] S. J. Heo *et al.*, "Fabrication and characterization of novel nano- and micro-HA/PCL composite scaffolds using a modified rapid prototyping process," *Journal of Biomedical Materials Research Part A*, vol. 89A, no. 1, pp. 108-116, Apr 2009, doi: 10.1002/jbm.a.31726.

- [132] Z. K. Hong *et al.*, "Nano-composite of poly(L-lactide) and surface grafted hydroxyapatite: Mechanical properties and biocompatibility," *Biomaterials*, vol. 26, no. 32, pp. 6296-6304, Nov 2005, doi: 10.1016/j.biomaterials.2005.04.018.
- [133] C. Y. Zhang, H. Lu, Z. Zhuang, X. P. Wang, and Q. F. Fang, "Nano-hydroxyapatite/poly(L-lactic acid) composite synthesized by a modified in situ precipitation: preparation and properties," *Journal of Materials Science-Materials in Medicine*, vol. 21, no. 12, pp. 3077-3083, Dec 2010, doi: 10.1007/s10856-010-4161-y.
- [134] A. Ronca, L. Ambrosio, and D. W. Grijpma, "Preparation of designed poly(D,L-lactide)/nanosized hydroxyapatite composite structures by stereolithography," *Acta Biomaterialia*, vol. 9, no. 4, pp. 5989-5996, Apr 2013, doi: 10.1016/j.actbio.2012.12.004.
- [135] A. Abdal-haya, F. A. Sheikh, and J. K. Lim, "Air jet spinning of hydroxyapatite/poly(lactic acid) hybrid nanocomposite membrane mats for bone tissue engineering," *Colloids and Surfaces B-Biointerfaces*, vol. 102, pp. 635-643, Feb 2013, doi: 10.1016/j.colsurfb.2012.09.017.
- [136] J. Song *et al.*, "Elastomeric high-mineral content hydrogel-hydroxyapatite composites for orthopedic applications," *Journal of Biomedical Materials Research Part A*, vol. 89A, no. 4, pp. 1098-1107, Jun 15 2009, doi: 10.1002/jbm.a.32110.
- [137] J. Huang *et al.*, "Development of nano-sized hydroxyapatite reinforced composites for tissue engineering scaffolds," *Journal of Materials Science-Materials in Medicine*, vol. 18, no. 11, pp. 2151-2157, Nov 2007, doi: 10.1007/s10856-007-3201-8.
- [138] J. A. Juhasz, S. M. Best, and W. Bonfield, "Preparation of novel bioactive nano-calcium phosphate-hydrogel composites," *Science and Technology of Advanced Materials*, vol. 11, no. 1, Feb 2010, Art no. 014103, doi: 10.1088/1468-6996/11/1/014103.
- [139] Y. M. Lvov, D. G. Shchukin, H. Mohwald, and R. R. Price, "Halloysite clay nanotubes for controlled release of protective agents," *Acs Nano*, vol. 2, no. 5, pp. 814-820, May 2008, doi: 10.1021/nn800259q.
- [140] Y. Lvov, R. Price, B. Gaber, and I. Ichinose, "Thin film nanofabrication via layer-by-layer adsorption of tubule halloysite, spherical silica, proteins and polycations," *Colloids and Surfaces a-Physicochemical and Engineering Aspects*, vol. 198, pp. 375-382, Feb 18 2002, Art no. Pii s0927-7757(01)00970-0, doi: 10.1016/s0927-7757(01)00970-0.
- [141] E. Abdullayev and Y. Lvov, "Halloysite clay nanotubes as a ceramic "skeleton" for functional biopolymer composites with sustained drug release," *Journal of Materials Chemistry B*, vol. 1, no. 23, pp. 2894-2903, 2013 2013, doi: 10.1039/c3tb20059k.
- [142] K.-S. Lee and Y.-W. Chang, "Thermal, mechanical, and rheological properties of poly(epsilon-caprolactone)/halloysite nanotube nanocomposites," *Journal of Applied Polymer Science*, vol. 128, no. 5, pp. 2807-2816, Jun 5 2013, doi: 10.1002/app.38457.
- [143] M. Liu, B. Guo, M. Du, Y. Lei, and D. Jia, "Natural inorganic nanotubes reinforced epoxy resin nanocomposites," *Journal of Polymer Research*, vol. 15, no. 3, pp. 205-212, Jun 2008, doi: 10.1007/s10965-007-9160-4.

- [144] K. Prashantha, M. F. Lacrampe, and P. Krawczak, "Processing and characterization of halloysite nanotubes filled polypropylene nanocomposites based on a masterbatch route: effect of halloysites treatment on structural and mechanical properties," *Express Polymer Letters*, vol. 5, no. 4, pp. 295-307, Apr 2011, doi: 10.3144/expresspolymlett.2011.30.
- [145] R. T. De Silva, P. Pasbakhsh, K. L. Goh, S. P. Chai, and J. Chen, "Synthesis and characterisation of poly (lactic acid)/halloysite bionanocomposite films," *Journal of Composite Materials*, vol. 48, no. 30, pp. 3705-3717, Dec 2014, doi: 10.1177/0021998313513046.
- [146] G. Stoclet *et al.*, "Elaboration of poly(lactic acid)/halloysite nanocomposites by means of water assisted extrusion: structure, mechanical properties and fire performance," *Rsc Advances*, vol. 4, no. 101, pp. 57553-57563, 2014 2014, doi: 10.1039/c4ra06845a.
- [147] K. Prashantha, B. Lecouvet, M. Sclavons, M. F. Lacrampe, and P. Krawczak, "Poly(lactic acid)/halloysite nanotubes nanocomposites: Structure, thermal, and mechanical properties as a function of halloysite treatment," *Journal of Applied Polymer Science*, vol. 128, no. 3, pp. 1895-1903, May 5 2013, doi: 10.1002/app.38358.
- [148] G. Gorrasi, R. Pantani, M. Murariu, and P. Dubois, "PLA/Halloysite Nanocomposite Films: Water Vapor Barrier Properties and Specific Key Characteristics," *Macromolecular Materials and Engineering*, vol. 299, no. 1, pp. 104-115, Jan 2014, doi: 10.1002/mame.201200424.
- [149] M. Liu, Y. Zhang, and C. Zhou, "Nanocomposites of halloysite and polylactide," *Applied Clay Science*, vol. 75-76, pp. 52-59, May 2013, doi: 10.1016/j.clay.2013.02.019.
- [150] J. Matusik, E. Stodolak, and K. Bahranowski, "Synthesis of polylactide/clay composites using structurally different kaolinites and kaolinite nanotubes," *Applied Clay Science*, vol. 51, no. 1-2, pp. 102-109, Jan 2011, doi: 10.1016/j.clay.2010.11.010.
- [151] S. Zhou *et al.*, "Hydrogen bonding interaction of poly(D,L-lactide)/hydroxyapatite nanocomposites," *Chemistry of Materials*, vol. 19, no. 2, pp. 247-253, Jan 23 2007, doi: 10.1021/cm0619398.
- [152] E. Abdullayev and Y. Lvov, "Clay nanotubes for corrosion inhibitor encapsulation: release control with end stoppers," *Journal of Materials Chemistry*, vol. 20, no. 32, pp. 6681-6687, 2010 2010, doi: 10.1039/c0jm00810a.
- [153] D. Rawtani and Y. K. Agrawal, "Multifarious Applications of Halloysite Nanotubes: A Review," *Reviews on Advanced Materials Science*, vol. 30, no. 3, pp. 282-295, Jun 2012.
- [154] Ruiz-Hitzky, A. E., and L. K., Y., W. London, Ed. *Halloysite Nanotubes, a novel substrate for the Controlled Delivery of Bioactive molecules. in Bio-Inorganic Hybrid Nanomaterials*. Berlin, 2007.
- [155] R. Price and B. Gaber, "Controlled Release of Active Agents Using Inorganic Tubules," United States of America, 1997.

- [156] R. R. Price, B. P. Gaber, and Y. Lvov, "In-vitro release characteristics of tetracycline HCl, khellin and nicotinamide adenine dinucleotide from halloysite; a cylindrical mineral," *Journal of Microencapsulation*, vol. 18, no. 6, pp. 713-722, Nov-Dec 2001.
- [157] D. G. Shchukin, G. B. Sukhorukov, R. R. Price, and Y. M. Lvov, "Halloysite nanotubes as biomimetic nanoreactors," *Small*, vol. 1, no. 5, pp. 510-513, May 2005, doi: 10.1002/smll.200400120.
- [158] S. Y. Lee and S. J. Kim, "Adsorption of naphthalene by HDTMA modified kaolinite and halloysite," *Applied Clay Science*, vol. 22, no. 1-2, pp. 55-63, Nov 2002, Art no. Pii s0169-1317(02)00113-8, doi: 10.1016/s0169-1317(02)00113-8.
- [159] C. Viseras, C. Aguzzi, P. Cerezo, and M. C. Bedmar, "Biopolymer-clay nanocomposites for controlled drug delivery," *Materials Science and Technology*, vol. 24, no. 9, pp. 1020-1026, Sep 2008, doi: 10.1179/174328408x341708.
- [160] S. Mellouk *et al.*, "Intercalation of halloysite from Djebel Debagh (Algeria) and adsorption of copper ions," *Applied Clay Science*, vol. 44, no. 3-4, pp. 230-236, May 2009, doi: 10.1016/j.clay.2009.02.008.
- [161] E. Joussein, S. Petit, J. Churchman, B. Theng, D. Righi, and B. Delvaux, "Halloysite clay minerals - A review," *Clay Minerals*, vol. 40, no. 4, pp. 383-426, Dec 2005, doi: 10.1180/0009855054040180.
- [162] R. M. Carr, N. Chaikum, and N. Patterson, "Intercalation of Salts in Halloysite," *Clays and Clay Minerals*, vol. 26, no. 2, pp. 144-152, 1978 1978, doi: 10.1346/ccmn.1978.0260210.
- [163] R. L. Frost and J. Kristof, "Intercalation of halloysite: A Raman spectroscopic study," *Clays and Clay Minerals*, vol. 45, no. 4, pp. 551-563, Aug 1997, doi: 10.1346/ccmn.1997.0450407.
- [164] E. Joussein, S. Petit, and B. Delvaux, "Behavior of halloysite clay under formamide treatment," *Applied Clay Science*, vol. 35, no. 1-2, pp. 17-24, Jan 2007, doi: 10.1016/j.clay.2006.07.002.
- [165] S. Hillier and P. C. Ryan, "Identification of halloysite (7 angstrom) by ethylene glycol solvation: the 'MacEwan effect'," *Clay Minerals*, vol. 37, no. 3, pp. 487-496, Sep 2002, doi: 10.1180/0009855023730047.
- [166] S. R. Levis and P. B. Deasy, "Characterisation of halloysite for use as a microtubular drug delivery system," *International Journal of Pharmaceutics*, vol. 243, no. 1-2, pp. 125-134, Aug 28 2002, Art no. Pii s0378-5173(02)00274-0, doi: 10.1016/s0378-5173(02)00274-0.
- [167] E. Epstein, "The Anomaly of Silicon in Plant Biology," *Proceedings of the National Academy of Sciences of the United States of America*, vol. 91, no. 1, pp. 11-17, Jan 4 1994, doi: 10.1073/pnas.91.1.11.
- [168] W. Y. Zhou, B. Guo, M. Liu, R. Liao, A. B. M. Rabie, and D. Jia, "Poly(vinyl alcohol)/Halloysite nanotubes bionanocomposite films: Properties and in vitro osteoblasts and fibroblasts response," *Journal of Biomedical Materials Research Part A*, vol. 93A, no. 4, pp. 1574-1587, Jun 15 2010, doi: 10.1002/jbm.a.32656.

- [169] W. Xue, A. Bandyopadhyay, and S. Bose, "Mesoporous calcium silicate for controlled release of bovine serum albumin protein," *Acta Biomaterialia*, vol. 5, no. 5, pp. 1686-1696, Jun 2009, doi: 10.1016/j.actbio.2009.01.012.
- [170] M. Vallet-Regi, A. Ramila, R. P. del Real, and J. Perez-Pariente, "A new property of MCM-41: Drug delivery system," *Chemistry of Materials*, vol. 13, no. 2, pp. 308-311, Feb 2001, doi: 10.1021/cm0011559.
- [171] R. A. Sharma, A. J. Gescher, and W. P. Steward, "Curcumin: The story so far," *European Journal of Cancer*, vol. 41, no. 13, pp. 1955-1968, Sep 2005, doi: 10.1016/j.ejca.2005.05.009.
- [172] A. Goel, A. B. Kunnumakkara, and B. B. Aggarwal, "Curcumin as "Curecumin": From kitchen to clinic," *Biochemical Pharmacology*, vol. 75, no. 4, pp. 787-809, Feb 15 2008, doi: 10.1016/j.bcp.2007.08.016.
- [173] M. M. Y. Chan, H. I. Huang, M. R. Fenton, and D. Fong, "In vivo inhibition of nitric oxide synthase gene expression by curcumin, a cancer preventive natural product with anti-inflammatory properties," *Biochemical Pharmacology*, vol. 55, no. 12, pp. 1955-1962, Jun 15 1998, doi: 10.1016/s0006-2952(98)00114-2.
- [174] A. Khar, A. M. Ali, B. V. V. Pardhasaradhi, Z. Begum, and R. Anjum, "Antitumor activity of curcumin is mediated through the induction of apoptosis in AK-5 tumor cells," *Febs Letters*, vol. 445, no. 1, pp. 165-168, Feb 19 1999, doi: 10.1016/s0014-5793(99)00114-3.
- [175] B. B. Aggarwal, A. Kumar, and A. C. Bharti, "Anticancer potential of curcumin: Preclinical and clinical studies," *Anticancer Research*, vol. 23, no. 1A, pp. 363-398, Jan-Feb 2003.
- [176] P. Anand *et al.*, "Cancer is a Preventable Disease that Requires Major Lifestyle Changes," *Pharmaceutical Research*, vol. 25, no. 9, pp. 2097-2116, Sep 2008, doi: 10.1007/s11095-008-9661-9.
- [177] R. Yang, S. Zhang, D. Kong, X. Gao, Y. Zhao, and Z. Wang, "Biodegradable Polymer-Curcumin Conjugate Micelles Enhance the Loading and Delivery of Low-Potency Curcumin," *Pharmaceutical Research*, vol. 29, no. 12, pp. 3512-3525, Dec 2012, doi: 10.1007/s11095-012-0848-8.
- [178] S. M. Zhang *et al.*, "Fabrication and characterization of biodegradable nanospheres containing curcumin," Patent 1-2, 2007. [Online]. Available: <Go to ISI>://WOS:000244739900182
- [179] S. Bisht *et al.*, "Polymeric nanoparticle-encapsulated curcumin ("nanocurcumin"): a novel strategy for human cancer therapy," *Journal of nanobiotechnology*, vol. 5, pp. 3-3, 2007 Apr 2007, doi: 10.1186/1477-3155-5-3.
- [180] V. Kumar, S. A. Lewis, S. Mutalik, D. B. Shenoy, Venkatesh, and N. Udupa, "Biodegradable microspheres of curcumin for treatment of inflammation," *Indian journal of physiology and pharmacology*, vol. 46, no. 2, pp. 209-17, 2002-Apr 2002.

- [181] K. Sou, S. Inenaga, S. Takeoka, and E. Tsuchida, "Loading of curcumin into macrophages using lipid-based nanoparticles," *International Journal of Pharmaceutics*, vol. 352, no. 1-2, pp. 287-293, Mar 20 2008, doi: 10.1016/j.ijpharm.2007.10.033.
- [182] E. Abdullayev and Y. Lvov, "Halloysite Clay Nanotubes for Controlled Release of Protective Agents," *Journal of Nanoscience and Nanotechnology*, vol. 11, no. 11, pp. 10007-10026, Nov 2011, doi: 10.1166/jnn.2011.5724.
- [183] Y. Lvov, A. Aerov, and R. Fakhrullin, "Clay nanotube encapsulation for functional biocomposites," *Advances in Colloid and Interface Science*, vol. 207, pp. 189-198, May 2014, doi: 10.1016/j.cis.2013.10.006.
- [184] T. Kokubo and H. Takadama, "How useful is SBF in predicting in vivo bone bioactivity?," *Biomaterials*, vol. 27, no. 15, pp. 2907-2915, May 2006, doi: 10.1016/j.biomaterials.2006.01.017.
- [185] Y. Abe, T. Kokubo, and T. Yamamuro, "Apatite Coating on Ceramics, Metals and Polymers Utilizing a Biological Process," *Journal of Materials Science-Materials in Medicine*, vol. 1, no. 4, pp. 233-238, Nov 1990, doi: 10.1007/bf00701082.
- [186] M. Ranjbar-Mohammadi and S. H. Bahrami, "Development of nanofibrous scaffolds containing gum tragacanth/poly (epsilon-caprolactone) for application as skin scaffolds," *Materials Science & Engineering C-Materials for Biological Applications*, vol. 48, pp. 71-79, Mar 1 2015, doi: 10.1016/j.msec.2014.10.020.
- [187] R. Khiari, Z. Marrakchi, M. N. Belgacem, E. Mauret, and F. Mhenni, "New lignocellulosic fibres-reinforced composite materials: A stepforward in the valorisation of the *Posidonia oceanica* balls," *Composites Science and Technology*, vol. 71, no. 16, pp. 1867-1872, Nov 14 2011, doi: 10.1016/j.compscitech.2011.08.022.
- [188] P. E. Sanchez-Jimenez, L. A. Perez-Maqueda, A. Perejon, and J. M. Criado, "Nanoclay Nucleation Effect in the Thermal Stabilization of a Polymer Nanocomposite: A Kinetic Mechanism Change," *Journal of Physical Chemistry C*, vol. 116, no. 21, pp. 11797-11807, May 31 2012, doi: 10.1021/jp302466p.
- [189] D. Milovac, G. Gallego Ferrer, M. Ivankovic, and H. Ivankovic, "PCL-coated hydroxyapatite scaffold derived from cuttlefish bone: Morphology, mechanical properties and bioactivity," *Materials Science & Engineering C-Materials for Biological Applications*, vol. 34, pp. 437-445, Jan 1 2014, doi: 10.1016/j.msec.2013.09.036.
- [190] B. Ferrero, V. Fombuena, O. Fenollar, T. Boronat, and R. Balart, "Development of Natural Fiber-Reinforced Plastics (NFRP) Based on Biobased Polyethylene and Waste Fibers from *Posidonia oceanica* Seaweed," vol. 36, pp. 1378-1385doi: DOI 10.1002/pc.23042.
- [191] F. Yahiaoui, F. Benhacine, H. Ferfera-Harrar, A. Habi, A. S. Hadj-Hamou, and Y. Grohens, "Development of antimicrobial PCL/nanoclay nanocomposite films with enhanced mechanical and water vapor barrier properties for packaging applications," *Polymer Bulletin*, vol. 72, no. 2, pp. 235-254, Feb 2015, doi: 10.1007/s00289-014-1269-0.
- [192] H. Lun, J. Ouyang, and H. Yang, "Natural halloysite nanotubes modified as an aspirin carrier," *Rsc Advances*, vol. 4, no. 83, pp. 44197-44202, 2014 2014, doi: 10.1039/c4ra09006c.

- [193] H. Schmitt, N. Creton, K. Prashantha, J. Soulestin, M. F. Lacrampe, and P. Krawczak, "Melt-Blended Halloysite Nanotubes/Wheat Starch Nanocomposites as Drug Delivery System," *Polymer Engineering and Science*, vol. 55, no. 3, pp. 573-580, Mar 2015, doi: 10.1002/pen.23919.
- [194] A. Kamoun, A. Jelidi, and M. Chaabouni, "Evaluation of the performance of sulfonated esparto grass lignin as a plasticizer-water reducer for cement," *Cement and Concrete Research*, vol. 33, no. 7, pp. 995-1003, Jul 2003, doi: 10.1016/s0008-8846(02)01098-0.
- [195] J. Mohammadi-Rovshandeh, P. Pouresmaeel-Selakjani, B. Kaffashi, A. Hassani, and A. Bahmeyi, "Effect of Lignin Removal on Mechanical, Thermal, and Morphological Properties of Polylactide/Starch/Rice Husk Blend Used in Food Packaging," *Journal of Applied Polymer Science*, vol. 131, no. 22, Nov 15 2014, Art no. 41095, doi: 10.1002/app.41095.
- [196] M. R. Rahman, M. N. Islam, M. M. Huque, S. Hamdan, and A. Ahmed, "Effect of Chemical Treatment on Rice Husk (RH) Reinforced Polyethylene (PE) Composites," *Bioresources*, vol. 5, no. 2, pp. 854-869, 2010 2010.
- [197] F. I. Altuna, L. H. Esposito, R. A. Ruseckaite, and P. M. Stefani, "Thermal and Mechanical Properties of Anhydride-Cured Epoxy Resins with Different Contents of Biobased Epoxidized Soybean Oil," *Journal of Applied Polymer Science*, vol. 120, no. 2, pp. 789-798, Apr 15 2011, doi: 10.1002/app.33097.
- [198] B. Ferrero, T. Boronat, R. Moriana, O. Fenollar, and R. Balart, "Green Composites Based on Wheat Gluten Matrix and Posidonia Oceanica Waste Fibers as Reinforcements," *Polymer Composites*, vol. 34, no. 10, pp. 1663-1669, Oct 2013, doi: 10.1002/pc.22567.
- [199] L. F. Charles, M. T. Shaw, J. R. Olson, and M. Wei, "Fabrication and mechanical properties of PLLA/PCL/HA composites via a biomimetic, dip coating, and hot compression procedure," *Journal of Materials Science-Materials in Medicine*, vol. 21, no. 6, pp. 1845-1854, Jun 2010, doi: 10.1007/s10856-010-4051-3.
- [200] R. B. Ashman and J. Y. Rho, "Elastic-Modulus of Trabecular Bone Material," *Journal of Biomechanics*, vol. 21, no. 3, pp. 177-181, 1988 1988, doi: 10.1016/0021-9290(88)90167-4.
- [201] D. T. Reilly, A. H. Burstein, and V. H. Frankel, "Elastic-Modulus for Bone," *Journal of Biomechanics*, vol. 7, no. 3, pp. 271-&, 1974 1974, doi: 10.1016/0021-9290(74)90018-9.
- [202] J. Y. Rho, L. Kuhn-Spearing, and P. Zioupos, "Mechanical properties and the hierarchical structure of bone," *Medical Engineering & Physics*, vol. 20, no. 2, pp. 92-102, Mar 1998, doi: 10.1016/s1350-4533(98)00007-1.
- [203] P. K. Zysset, X. E. Guo, C. E. Hoffler, K. E. Moore, and S. A. Goldstein, "Elastic modulus and hardness of cortical and trabecular bone lamellae measured by nanoindentation in the human femur," *Journal of Biomechanics*, vol. 32, no. 10, pp. 1005-1012, Oct 1999, doi: 10.1016/s0021-9290(99)00111-6.
- [204] Z. Chen *et al.*, "Thermal degradation kinetics study of curcumin with nonlinear methods," *Food Chemistry*, vol. 155, pp. 81-86, Jul 15 2014, doi: 10.1016/j.foodchem.2014.01.034.

- [205] F. Jasim and T. Talib, "Some Observations on the Thermal-Behavior of Curcumin Under Air and Argon Atmospheres," *Journal of Thermal Analysis*, vol. 38, no. 11, pp. 2549-2552, Nov 1992, doi: 10.1007/bf01974631.
- [206] E. Ruiz-Hitzky, K. Ariga, and Y. M. Lvov, *Halloysite Nanotubes a Novel Substrate for the Controlled Delivery of Bioactive Molecules*, in *Bio-Inorganic Hybrid Nanomaterials*. Berlin, London: Eduardo Ruiz-Hitzky, Katsuhiko Ariga and Yuri M. Lvov, 2008, pp. 440-478.
- [207] P. Yuan *et al.*, "Changes in Structure, Morphology, Porosity, and Surface Activity of Mesoporous Halloysite Nanotubes under Heating," *Clays and Clay Minerals*, vol. 60, no. 6, pp. 561-573, Dec 2012, doi: 10.1346/ccmn.2012.0600602.
- [208] M. E. Smith, G. Neal, M. B. Trigg, and J. Drennan, "Structural Characterization of the Thermal Transformation of Halloysite by Solid-State NMR," *Applied Magnetic Resonance*, vol. 4, no. 1-2, pp. 157-170, 1993 1993.
- [209] S. Riela *et al.*, "Development and characterization of co-loaded curcumin/triazole-halloysite systems and evaluation of their potential anticancer activity," *International Journal of Pharmaceutics*, vol. 475, no. 1-2, pp. 613-623, Nov 20 2014, doi: 10.1016/j.ijpharm.2014.09.019.
- [210] L. Wang *et al.*, "Encapsulation of curcumin within poly(amidoamine) dendrimers for delivery to cancer cells," *Journal of Materials Science-Materials in Medicine*, vol. 24, no. 9, pp. 2137-2144, Sep 2013, doi: 10.1007/s10856-013-4969-3.
- [211] A. Fernandez, M. Muniesa, and J. Gonzalez, "Characterisation and Processing of Reinforced PA 6 with Halloysite Nanotubes (HNT) for Injection Molding," *Strojniski Vestnik-Journal of Mechanical Engineering*, vol. 59, no. 3, pp. 183-192, Mar 2013, doi: 10.5545/sv-jme.2012.417.
- [212] M. Liu, B. Guo, M. Du, and D. Jia, "Drying induced aggregation of halloysite nanotubes in polyvinyl alcohol/halloysite nanotubes solution and its effect on properties of composite film," *Applied Physics a-Materials Science & Processing*, vol. 88, no. 2, pp. 391-395, Aug 2007, doi: 10.1007/s00339-007-3995-8.
- [213] H. Ismail, P. Pasbakhsh, M. N. A. Fauzi, and A. Abu Bakar, "Morphological, thermal and tensile properties of halloysite nanotubes filled ethylene propylene diene monomer (EPDM) nanocomposites," *Polymer Testing*, vol. 27, no. 7, pp. 841-850, Oct 2008, doi: 10.1016/j.polymertesting.2008.06.007.
- [214] Y. Ye, H. Chen, J. Wu, and C. M. Chan, "Interlaminar properties of carbon fiber composites with halloysite nanotube-toughened epoxy matrix," *Composites Science and Technology*, vol. 71, no. 5, pp. 717-723, Mar 22 2011, doi: 10.1016/j.compscitech.2011.01.018.
- [215] U. A. Handge, K. Hedicke-Hoechstoeetter, and V. Altstaedt, "Composites of polyamide 6 and silicate nanotubes of the mineral halloysite: Influence of molecular weight on thermal, mechanical and rheological properties," *Polymer*, vol. 51, no. 12, pp. 2690-2699, May 28 2010, doi: 10.1016/j.polymer.2010.04.041.

- [216] M. Liu, Z. Jia, D. Jia, and C. Zhou, "Recent advance in research on halloysite nanotubes-polymer nanocomposite," *Progress in Polymer Science*, vol. 39, no. 8, pp. 1498-1525, Aug 2014, doi: 10.1016/j.progpolymsci.2014.04.004.
- [217] S. A. Hutchens, R. S. Benson, B. R. Evans, H. M. O'Neill, and C. J. Rawn, "Biomimetic synthesis of calcium-deficient hydroxyapatite in a natural hydrogel," *Biomaterials*, vol. 27, no. 26, pp. 4661-4670, Sep 2006, doi: 10.1016/j.biomaterials.2006.04.032.
- [218] A. L. Oliveira, P. B. Malafaya, and R. L. Reis, "Sodium silicate gel as a precursor for the in vitro nucleation and growth of a bone-like apatite coating in compact and porous polymeric structures," *Biomaterials*, vol. 24, no. 15, pp. 2575-2584, Jul 2003, doi: 10.1016/s0142-9612(03)00060-7.
- [219] K. Zhang, H. W. Yan, D. C. Bell, A. Stein, and L. F. Francis, "Effects of materials parameters on mineralization and degradation of sol-gel bioactive glasses with 3D-ordered macroporous structures," *Journal of Biomedical Materials Research Part A*, vol. 66A, no. 4, pp. 860-869, Sep 2003, doi: 10.1002/jbm.a.10093.
- [220] H. M. Kim *et al.*, "Composition and structure of the apatite formed on PET substrates in SBF modified with various ionic activity products," *Journal of Biomedical Materials Research*, vol. 46, no. 2, pp. 228-235, Aug 1999, doi: 10.1002/(sici)1097-4636(199908)46:2<228::aid-jbm12>3.0.co;2-j.
- [221] H. Y. Li, Y. F. Chen, and Y. S. Xie, "Photo-crosslinking polymerization to prepare polyanhydride/needle-like hydroxyapatite biodegradable nanocomposite for orthopedic application," *Materials Letters*, vol. 57, no. 19, pp. 2848-2854, Jun 2003, doi: 10.1016/s0167-577x(02)01386-1.
- [222] A. C. Albertsson and I. K. Varma, "Aliphatic polyesters: Synthesis, properties and applications," (in English), *Degradable Aliphatic Polyesters*, Review vol. 157, pp. 1-40, 2002.
- [223] J. G. Merrell, S. W. McLaughlin, L. Tie, C. T. Laurencin, A. F. Chen, and L. S. Nair, "Curcumin-loaded poly(epsilon-caprolactone) nanofibres: Diabetic wound dressing with anti-oxidant and anti-inflammatory properties," *Clinical and Experimental Pharmacology and Physiology*, vol. 36, no. 12, pp. 1149-1156, Dec 2009, doi: 10.1111/j.1440-1681.2009.05216.x.
- [224] L. Xue and H. P. Greisler, "Biomaterials in the development and future of vascular grafts," *Journal of Vascular Surgery*, vol. 37, no. 2, pp. 472-480, Feb 2003, doi: 10.1067/mva.2003.88.
- [225] Y. Tamada and Y. Ikada, "Effect of Preadsorbed Proteinso Cell-Adhesion to Polymer Surfaces," *Journal of Colloid and Interface Science*, vol. 155, no. 2, pp. 334-339, Feb 1993, doi: 10.1006/jcis.1993.1044.
- [226] T. A. Horbett, "THE ROLE OF ADSORBED PROTEINS IN ANIMAL-CELL ADHESION," *Colloids and Surfaces B-Biointerfaces*, vol. 2, no. 1-3, pp. 225-240, Mar 1994, doi: 10.1016/0927-7765(94)80037-5.

- [227] F. Grinnell, M. Feld, and D. Minter, "Fibroblast Adhesion to Fibrinogen and Fibrin Substrata - Requirement for Cold-Insoluble Globulin (Plasma Fibronectin)," (in English), *Cell*, Article vol. 19, no. 2, pp. 517-525, 1980, doi: 10.1016/0092-8674(80)90526-7.
- [228] Y. Z. Yang, R. Cavin, and J. L. Ong, "Protein adsorption on titanium surfaces and their effect on osteoblast attachment," (in English), *Journal of Biomedical Materials Research Part A*, Article vol. 67A, no. 1, pp. 344-349, Oct 2003, doi: 10.1002/jbm.a.10578.
- [229] W. Dessau, J. Sasse, R. Timpl, F. Jilek, and K. Vondermark, "Synthesis and Extracellular Deposition of Fibronectin in Chondrocyte Cultures - Response to Removal of Extracellular Cartilage Matrix," (in English), *Journal of Cell Biology*, Article vol. 79, no. 2, pp. 342-355, 1978, doi: 10.1083/jcb.79.2.342.
- [230] S. Ayad, R. P. Boot-Handford, M. J. Humphries, K. E. Kadler, and C. A. Shuttleworth, *The extracellular matrix facts Book*. San Diego, California: Academic Press, Harcourt Brace and Company, 1994.
- [231] E. Ruoslahti and J. C. Reed, "Anchorage Dependence, Integrins, and Apoptosis," *Cell*, vol. 77, no. 4, pp. 477-478, May 1994, doi: 10.1016/0092-8674(94)90209-7.
- [232] R. O. Hynes, "Integrins - Versatility, Modulation, and Signaling in Cell-Adhesion," *Cell*, vol. 69, no. 1, pp. 11-25, Apr 1992, doi: 10.1016/0092-8674(92)90115-s.
- [233] W. Norde, "Adsorption of Proteins From Solution at the Solid-Liquid Interface," *Advances in Colloid and Interface Science*, vol. 25, no. 4, pp. 267-340, Sep 1986, doi: 10.1016/0001-8686(86)80012-4.
- [234] D. T. H. Wassell, R. C. Hall, and G. Embery, "Adsorption of Bovine Serum-Albumin Onto Hydroxyapatite," *Biomaterials*, vol. 16, no. 9, pp. 697-702, Jun 1995, doi: 10.1016/0142-9612(95)99697-k.
- [235] C. Liao, Y. Xie, and J. Zhou, "Computer simulations of fibronectin adsorption on hydroxyapatite surfaces," *Rsc Advances*, vol. 4, no. 30, pp. 15759-15769, 2014 2014, doi: 10.1039/c3ra47381c.
- [236] Y. L. Liu, P. Layrolle, J. de Bruijn, C. van Blitterswijk, and K. de Groot, "Biomimetic coprecipitation of calcium phosphate and bovine serum albumin on titanium alloy," *Journal of Biomedical Materials Research*, vol. 57, no. 3, pp. 327-335, Dec 5 2001, doi: 10.1002/1097-4636(20011205)57:3<327::aid-jbm1175>3.0.co;2-j.
- [237] M. Zelzer, D. Albutt, M. R. Alexander, and N. A. Russell, "The Role of Albumin and Fibronectin in the Adhesion of Fibroblasts to Plasma Polymer Surfaces," *Plasma Processes and Polymers*, vol. 9, no. 2, pp. 149-156, Feb 2012, doi: 10.1002/ppap.201100054.
- [238] P. Q. Ying, Y. Yu, G. Jin, and Z. L. Tao, "Competitive protein adsorption studied with atomic force microscopy and imaging ellipsometry," *Colloids and Surfaces B-Biointerfaces*, vol. 32, no. 1, pp. 1-10, Oct 2003, doi: 10.1016/s0927-7765(02)00133-9.
- [239] J. H. Wei, T. Igarashi, N. Okumori, T. Maetani, B. L. Liu, and M. Yoshinari, "Influence of surface wettability on competitive protein adsorption and initial attachment of

- osteoblasts," *Biomedical Materials*, vol. 4, no. 4, Aug 2009, Art no. 045002, doi: 10.1088/1748-6041/4/4/045002.
- [240] C. R. Nuttelman, D. J. Mortisen, S. M. Henry, and K. S. Anseth, "Attachment of fibronectin to poly(vinyl alcohol) hydrogels promotes NIH3T3 cell adhesion, proliferation, and migration," *Journal of Biomedical Materials Research*, vol. 57, no. 2, pp. 217-223, Nov 2001, doi: 10.1002/1097-4636(200111)57:2<217::aid-jbm1161>3.0.co;2-i.
- [241] D. J. Iuliano, S. S. Saavedra, and G. A. Truskey, "Effect of the Conformation and Orientation of Adsorbed Fibronectin on Endothelial-Cell Spreading and the Strength of Adhesion," *Journal of Biomedical Materials Research*, vol. 27, no. 8, pp. 1103-1113, Aug 1993, doi: 10.1002/jbm.820270816.
- [242] F. Grinnell and M. K. Feld, "Adsorption Characteristics of Plasma Fibronectin in Relationship to Biological-Activity," *Journal of Biomedical Materials Research*, vol. 15, no. 3, pp. 363-381, 1981, doi: 10.1002/jbm.820150308.
- [243] J. Fripiat, J. Cases, M. Francois, and M. Letellier, "Thermodynamic and Microdynamic Behavior of Water in Clay Suspensions and Gels," *Journal of Colloid and Interface Science*, vol. 89, no. 2, pp. 378-400, 1982, doi: 10.1016/0021-9797(82)90191-6.
- [244] C. F. Wertz and M. M. Santore, "Effect of surface hydrophobicity on adsorption and relaxation kinetics of albumin and fibrinogen: Single-species and competitive behavior," *Langmuir*, vol. 17, no. 10, pp. 3006-3016, May 15 2001, doi: 10.1021/la0017781.

